

**ISTANBUL TECHNICAL UNIVERSITY ★ GRADUATE SCHOOL OF SCIENCE**  
**ENGINEERING AND TECHNOLOGY**

**EVALUATION OF CHANGES IN SWELLING PRESSURE  
CHARACTERISTICS OF CLAYS EXPOSED TO FREEZE-THAW CYCLES**



**M.Sc. THESIS**

**Efe ASLAN**

**Department of Civil Engineering**

**Soil Mechanics and Geotechnical Engineering Programme**

**JUNE 2019**



**ISTANBUL TECHNICAL UNIVERSITY ★ GRADUATE SCHOOL OF SCIENCE**  
**ENGINEERING AND TECHNOLOGY**

**EVALUATION OF CHANGES IN SWELLING PRESSURE  
CHARACTERISTICS OF CLAYS EXPOSED TO FREEZE-THAW CYCLES**

**M.Sc. THESIS**

**Efe ASLAN  
(501161310)**

**Department of Civil Engineering**

**Soil Mechanics and Geotechnical Engineering Programme**

**Thesis Advisor: Prof. Dr. Aykut ŞENOL**

**JUNE 2019**



**İSTANBUL TEKNİK ÜNİVERSİTESİ ★ FEN BİLİMLERİ ENSTİTÜSÜ**

**DONMA ÇÖZÜLME ÇEVİRİMLERİNE MARUZ KALMIŞ KİLLERDE ŞİŞME  
BASINCINDAKİ DEĞİŞİMLERİN BELİRLENMESİ**

**YÜKSEK LİSANS TEZİ**

**Efe ASLAN  
(501161310)**

**İnşaat Mühendisliği Anabilim Dalı**

**Zemin Mekaniği ve Geoteknik Mühendisliği Programı**

**Tez Danışmanı: Prof. Dr. Aykut ŞENOL**

**HAZİRAN 2019**



Efe ASLAN, a M.Sc. student of ITU Graduate School of Science Engineering and Technology student ID 501161310, successfully defended the thesis entitled “EVALUATION OF CHANGES IN SWELLING PRESSURE CHARACTERISTICS OF CLAYS EXPOSED TO FREEZE-THAW CYCLES”, which he prepared after fulfilling the requirements specified in the associated legislations, before the jury whose signatures are below.

**Thesis Advisor :**    **Prof. Dr. Aykut ŞENOL**    .....

Istanbul Technical University

**Jury Members :**    **Prof. Dr. Recep İYİSAN**    .....

Istanbul Technical University

**Prof. Dr. Feyza ÇİNİCİOĞLU**    .....

Özyeğin University

**Date of Submission : 3 MAY 2019**

**Date of Defense : 13 JUNE 2019**







*To my family,*



## **FOREWORD**

In this study, it is aimed to determine the swelling pressures of the soils and behavior characteristics after freeze-thaw cycles. For this purpose, laboratory tests were conducted to determine the swelling pressures of different clay samples before and after the freeze-thaw cycles. The aim of this study is to investigate the relationships between the engineering parameters obtained from the experiments and the geotechnical properties of the samples.

This is a great opportunity for me to express my deepest appreciation to Prof. Dr. Aykut ŞENOL. As a supervisor, he always provides helpful advice, constructive criticism and inspiring encouragement. He is not only a supervisor who guides my research, but also an individual who shares his experiences in academia and life. This master's thesis would not be possible without his knowledge, expertise, comments, gracious support and guidance.

I owe a deep sense of gratitude to Dr. Aslı Y. DAYIOĞLU, for her collaborative efforts on helping with my first publication, for providing me with materials, for inspiring and encouraging me upon difficulties, for criticizing and improving my technical writing skills and giving her very kind guidance on the topic of my research.

I would like to thank to all I.T.U Soil Mechanics Laboratory staff for their valuable support they gave during my experiments. Also, I am thankful to the Istanbul Technical University Scientific Research Office (BAP) for their financial support of this research.

Finally I express my sincere thanks to my parents for their moral and financial support. This thesis is dedicated to them. I would never have accomplished without their support, love, patience and faith in me.

May 2019

Efe ASLAN  
(Civil Engineer)



## TABLE OF CONTENTS

	<u>Page</u>
<b>FOREWORD</b> .....	<b>ix</b>
<b>TABLE OF CONTENTS</b> .....	<b>xi</b>
<b>ABBREVIATIONS</b> .....	<b>xiii</b>
<b>SYMBOLS</b> .....	<b>xv</b>
<b>LIST OF TABLES</b> .....	<b>xvii</b>
<b>LIST OF FIGURES</b> .....	<b>xix</b>
<b>SUMMARY</b> .....	<b>xxiii</b>
<b>ÖZET</b> .....	<b>xxvii</b>
<b>1. INTRODUCTION</b> .....	<b>1</b>
1.1 Purpose of Thesis .....	2
1.2 Scope of Thesis .....	2
<b>2. SWELLING BEHAVIOR OF CLAY SOILS</b> .....	<b>5</b>
2.1 Clay Minerology .....	5
2.2 Classification of Clay Minerals.....	6
2.2.1 Kaolinite group .....	10
2.2.2 Smectite (montmorillonite) group.....	11
2.2.3 Illite group.....	13
2.2.4 Chlorite group .....	14
2.3 Mechanism of Swelling.....	16
2.3.1 Diffuse double layer.....	17
2.3.2 Factors affecting swelling behavior of soil .....	19
2.4 Identification of Expansive Soils .....	21
2.4.1 Mineralogical and chemical identification methods .....	23
2.4.1.1 X-ray diffraction (XRD) .....	24
2.4.1.2 Differential thermal analysis (DTA) .....	25
2.4.1.3 Dye adsorption .....	25
2.4.1.4 Scanning electron microscope (SEM).....	25
2.4.1.5 Cation exchange capacity (CEC) .....	26
2.4.1.6 Specific surface area (SSA) .....	28
2.4.1.7 Total potassium (TP).....	28
2.4.2 Direct methods (oedometer tests) .....	28
2.4.2.1 Method A .....	31
2.4.2.2 Method B.....	31
2.4.2.3 Method C.....	32
2.4.3 Indirect methods.....	33
2.4.3.1 Classification based on index properties tests.....	33
2.4.3.2 Free swell tests .....	38
2.4.3.3 Potential volume change (PVC).....	40
2.4.3.4 Expansion index (EI) test .....	41
2.4.3.5 Standard absorption moisture content (SAMC).....	43
2.4.3.6 Coefficient of linear extensibility (COLE) .....	44
2.5 Empirical Swell Prediction Methods.....	44

<b>3. THE EFFECTS OF FREEZE-THAW CYCLES ON SOIL .....</b>	<b>47</b>
3.1 Frozen Soils .....	47
3.1.1 Seasonally frozen soils .....	47
3.1.2 Active zone.....	49
3.1.3 Permanently frozen soils (permafrost) .....	52
3.1.3.1 Ice wedges .....	52
3.1.3.2 Pingos .....	53
3.2 Freezing Process .....	54
3.3 Thawing Process.....	56
3.4 Frost Action .....	57
3.5 Frost Susceptibility of Soils.....	57
3.6 Effects of the Freeze-Thaw Cycles on Geotechnical Properties .....	60
3.6.1 Freeze-thaw effects on permeability .....	60
3.6.2 Freeze-thaw effects on void ratio .....	62
3.6.3 Freeze-thaw effects on Atterberg limits .....	63
3.6.4 Freeze-thaw effects on consolidation.....	65
3.6.5 Freeze-thaw effects on unconfined compressive strength.....	66
3.6.6 Freeze-thaw effects on swelling pressure.....	69
<b>4. EXPERIMENTAL RESEARCH.....</b>	<b>71</b>
4.1 Purpose .....	71
4.2 Laboratory Experiments .....	72
4.2.1 Sieve analysis and hydrometer tests.....	72
4.2.2 Consistency (Atterberg) limit tests.....	73
4.2.3 Specific gravity test.....	75
4.2.4 Modified Harvard miniature compaction test .....	75
4.2.5 Freeze–Thaw Cycle Experiments.....	78
4.2.6 Swelling pressure tests .....	78
4.3 Material Selection.....	79
4.3.1 CH <sub>3</sub> (Na Bentonite) .....	80
4.3.2 CH <sub>4</sub> (Ca Bentonite) .....	82
4.3.3 CH <sub>5</sub> .....	83
4.3.4 CH <sub>6</sub> .....	85
4.3.5 CL <sub>1</sub> .....	86
4.4 Evaluation of Laboratory Experiments .....	88
4.4.1 Swelling pressure tests before freeze-thaw cycles .....	89
4.4.2 Relationships between engineering properties and swelling pressure .....	93
4.4.3 Swelling pressure tests after freeze-thaw cycles .....	96
4.4.3.1 CH <sub>3</sub> results .....	97
4.4.3.2 CH <sub>4</sub> results .....	99
4.4.3.3 CH <sub>5</sub> results .....	100
4.4.3.4 CH <sub>6</sub> results .....	102
4.4.3.5 CL <sub>1</sub> results .....	103
4.4.4 Relationships between engineering properties and $\sigma_s$ after F-T cycles...	105
4.4.5 Relationship between void ratio and swelling pressure after F-T cycles	108
<b>5. CONCLUSIONS AND RECOMMENDATIONS .....</b>	<b>111</b>
<b>REFERENCES .....</b>	<b>117</b>
<b>APPENDICES .....</b>	<b>125</b>
APPENDIX A .....	126
<b>CURRICULUM VITAE .....</b>	<b>131</b>

## **ABBREVIATIONS**

<b>AASHTO</b>	: American Association of State Highway and Transportation Officials
<b>ASTM</b>	: American Society for Testing and Materials
<b>CBR</b>	: California Bearing Ratio
<b>CEC</b>	: Cation Exchange Capacity
<b>COLE</b>	: Coefficient of Linear Extensibility
<b>DTA</b>	: Differential Thermal Analysis
<b>EI</b>	: Expansion Index
<b>F-T</b>	: Freeze – Thaw
<b>FSI</b>	: Free Swell Index
<b>LE</b>	: Linear Extensibility
<b>MFSI</b>	: Modified Free Swell Index
<b>MBT</b>	: Methylene Blue Test
<b>MBV</b>	: Methylene Blue Value
<b>SAMC</b>	: Standard Absorption Moisture Content
<b>SEM</b>	: Scanning Electron Microscope
<b>SSA</b>	: Specific Surface Area
<b>PVC</b>	: Potential Volume Change
<b>TP</b>	: Total Potassium
<b>USCS</b>	: Unified Soil Classification System
<b>XRD</b>	: X-ray Diffraction





## SYMBOLS

<b>A</b>	: Activity
<b>Å</b>	: Angstrom
<b>C</b>	: Celcius
<b>c<sub>u</sub></b>	: Undrained shear strength
<b>c<sub>v</sub></b>	: Coefficient of consolidation
<b>D</b>	: Diameter
<b>D<sub>10</sub></b>	: Effective pore diameter
<b>E</b>	: Modulus of elasticity
<b>e</b>	: Void ratio
<b>F</b>	: Fahrenheit
<b>h</b>	: Height
<b>h<sub>c</sub></b>	: Maximum capillary rise
<b>IS</b>	: Shrinkage index
<b>LL</b>	: Liquid limit
<b>LI</b>	: Liquidity index
<b>LS</b>	: Linear shrinkage
<b>mEq/100 g</b>	: Milliequivalents per 100 grams of clay
<b>N</b>	: Standard Proctor test blow numbers
<b>°</b>	: Degree
<b>PL</b>	: Plastic limit
<b>PI</b>	: Plasticity index
<b>PI<sub>w</sub></b>	: Weighted plasticity index
<b>S</b>	: Swelling potential
<b>SL</b>	: Shrinkage limit
<b>SI</b>	: Swell index
<b>q</b>	: Surcharge load
<b>q<sub>u</sub></b>	: Unconfined compression strength
<b>V<sub>o</sub></b>	: Volume of dry soil
<b>w</b>	: Water content
<b>w<sub>opt</sub></b>	: Optimum water content

$\mu_{nat}$	: Soil suction at natural moisture content
$\gamma_d$	: Dry unit weight of soil
$\gamma_{dmax}$	: Maximum dry unit weight of soil
$\varepsilon$	: Strain
$\sigma_s$	: Swelling pressure
$\Delta h$	: Percentage of swell



## LIST OF TABLES

	<u>Page</u>
<b>Table 2.1</b> : Typical problems caused by the clay minerals (Stadler, 1973). .....	15
<b>Table 2.2</b> : Effects of the soil properties on the swelling potential (Nelson and Miller, 1992). .....	19
<b>Table 2.3</b> : Effects of the environmental conditions on the swelling potential (Nelson and Miller, 1992). .....	20
<b>Table 2.4</b> : Effects of the stress conditions on the swelling potential (Nelson and Miller, 1992). .....	21
<b>Table 2.5</b> : Laboratory tests used for the identification of expansive soils (Nelson and Miller, 1992). .....	22
<b>Table 2.6</b> : Typical Values of CEC, SSA, and TP for Clay Minerals (Mitchell and Soga 2005). .....	27
<b>Table 2.7</b> : Swell prediction tests using oedometers (Nelson et al. 1995). .....	29
<b>Table 2.8</b> : Expansive soil classification based on colloid content, plasticity index and shrinkage limit (Holtz and Gibbs, 1956).....	34
<b>Table 2.9</b> : Expansive soil classification based on shrinkage limit or linear shrinkage (Altmeyer, 1955).....	34
<b>Table 2.10</b> : Relationship between plasticity index and degree of expansion (Chen, 1988). .....	34
<b>Table 2.11</b> : Expansive soil classification based on liquid limit, plasticity index and in-situ suction (Snethen et al. 1977). .....	35
<b>Table 2.12</b> : Typical values of activities for various clay minerals zone (Nelson and Miller, 1992). .....	36
<b>Table 2.13</b> : Expansion potential based on free swell index (Nelson et al., 2015). ..	40
<b>Table 2.14</b> : Typical values of free swell for clay minerals (Grim, 1968; Shamburger et al., 1975). .....	40
<b>Table 2.15</b> : The soil expansivity classification based on MFSI (Sridharan et al., 1986). .....	40
<b>Table 2.16</b> : Swelling potential according to PVC values (Nelson and Miller, 1992). .....	41
<b>Table 2.17</b> : Classification of the expansive soils regarding the expansion index (ASTM, 2011).....	42
<b>Table 2.18</b> : Proposed expansive soil classification based on oedometer percent expansion (Sridharan and Prakash, 2000). .....	42
<b>Table 2.19</b> : Classification standard for expansive soils (Yao et al., 2004). .....	43
<b>Table 2.20</b> : Common LE/Clay values of clay minerals (Nelson et al. 1995). .....	44
<b>Table 2.21</b> : Empirical methods to identify behavior of swelling mechanism (Nelson et al., 2015). .....	45
<b>Table 3.1</b> : U.S. Army Corps of Engineers frost design soil classification system (Johnson et al., 1986). .....	58
<b>Table 3.2</b> : Frost-susceptibility classification for the lab. tests (Johnson et al., 1986). .....	60

**Table 4.1** : Comparison of laboratory compaction tests..... **78**

**Table 4.2** : The results of index tests for all samples. .... **88**

**Table A.1** : Swelling pressure and normalized  $\sigma_s/\sigma_0$  results of CH<sub>3</sub> after F-T cycles.  
..... **126**

**Table A.2** : Swelling pressure and normalized  $\sigma_s/\sigma_0$  results of CH<sub>4</sub> after F-T cycles.  
..... **127**

**Table A.3** : Swelling pressure and normalized  $\sigma_s/\sigma_0$  results of CH<sub>5</sub> after F-T cycles.  
..... **128**

**Table A.4** : Swelling pressure and normalized  $\sigma_s/\sigma_0$  results of CH<sub>6</sub> after F-T cycles.  
..... **129**

**Table A.5** : Swelling pressure and normalized  $\sigma_s/\sigma_0$  results of CL<sub>1</sub> after F-T cycles.  
..... **130**



## LIST OF FIGURES

	<u>Page</u>
<b>Figure 2.1</b> : (a) Single octahedral unit and (b) The sheet structure of the octahedral units (Grim, 1968). .....	6
<b>Figure 2.2</b> : Structural scheme of soil minerals based on tetrahedral and octahedral sheets (Schulze, 2002). .....	7
<b>Figure 2.3</b> : (a) Sketch of double chains of silica tetrahedrons and (b) Projected on the plane of the base of the tetrahedrons (Grim, 1968). .....	8
<b>Figure 2.4</b> : Effect of the cation size on cation migration into a clay interlayer (Civan, 2015). .....	8
<b>Figure 2.5</b> : Classification of silicates (Bailey, 1980; Rieder et al., 1998). .....	9
<b>Figure 2.6</b> : Schematic diagrams of the structure: (a) kaolinite; (b) illite and (c) montmorillonite (Nelson et al., 2015). .....	10
<b>Figure 2.7</b> : Schematic diagram of the structure of kaolinite (Mitchell and Soga, 2005). .....	11
<b>Figure 2.8</b> : Expansion of the calcium and sodium montmorillonites by hydration (Civan, 2015). .....	12
<b>Figure 2.9</b> : Schematic diagram of the structure of montmorillonite (Mitchell and Soga, 2005). .....	13
<b>Figure 2.10</b> : Schematic diagram of the structure of illite (Mitchell and Soga, 2005). .....	14
<b>Figure 2.11</b> : Schematic diagram of the structure of chlorite (Mitchell and Soga, 2005). .....	14
<b>Figure 2.12</b> : Scanning electron microscopic photos of typical clay minerals (a) kaolinite, (b) illite, (c) montmorillonite (Tovey, 1971). .....	15
<b>Figure 2.13</b> : The schematic drawing of swelling mechanism (www.geology.arkansas.gov). .....	16
<b>Figure 2.14</b> : Model of swelling process for montmorillonite (Likos, 2004). .....	17
<b>Figure 2.15</b> : Distributions of ions adjacent to a clay surface according to the concept of the diffuse double layer (Mitchell and Soga, 2005). .....	18
<b>Figure 2.16</b> : X-ray generation by electron displacement (Mitchell and Soga, 2005). .....	24
<b>Figure 2.17</b> : Geometrical display of X-ray diffraction (Mitchell and Soga, 2005). .....	24
<b>Figure 2.18</b> : SEM images of kaolinite in order of increasing magnification (Velasco, 2013). .....	26
<b>Figure 2.19</b> : Expansion potential as indicated by clay activity and $CEA_c$ (Nelson et al., 2015). .....	27
<b>Figure 2.20</b> : Deformation versus vertical stress, method A (ASTM, 2014). .....	31
<b>Figure 2.21</b> : Deformation versus vertical stress, method B (ASTM, 2014). .....	32
<b>Figure 2.22</b> : Deformation versus vertical stress, method C (ASTM, 2014). .....	32
<b>Figure 2.23</b> : Plasticity characteristics of clay minerals (Holtz et al., 2011). .....	35

<b>Figure 2.24</b> : Classification chart based on activity and percentage of clay (Seed et al., 1962). .....	<b>36</b>
<b>Figure 2.25</b> : Classification chart based on plasticity index and clay content (Skempton, 1953). .....	<b>37</b>
<b>Figure 2.26</b> : Classification chart based on weighted plasticity index and clay content (Van der Merwe, 1964). .....	<b>37</b>
<b>Figure 2.27</b> : Classification chart based on plasticity index and liquid limit (Dakshanamurthy and Raman, 1973). .....	<b>38</b>
<b>Figure 2.28</b> : PVC apparatus and swell index versus PVC (Lambe, 1960). .....	<b>41</b>
<b>Figure 3.1</b> : Sinusoidal fluctuations of surface and ground temperatures (Andersland and Ladanyi, 2004). .....	<b>48</b>
<b>Figure 3.2</b> : Conceptual temperature attenuation with depth (Andersland and Ladanyi, 2004). .....	<b>48</b>
<b>Figure 3.3</b> : Water content profile in the active zone (Nelson and Miller, 1992). ....	<b>49</b>
<b>Figure 3.4</b> : Seasonal water content profiles in Colorado (Hamberg, 1985). .....	<b>50</b>
<b>Figure 3.5</b> : Determination of active zone depth (Das, 2015). .....	<b>51</b>
<b>Figure 3.6</b> : Seasonal ground freezing beneath a pavement structure (Andersland and Ladanyi, 2004). .....	<b>51</b>
<b>Figure 3.7</b> : Typical profile of permafrost in cold regions (Brown et al., 1981). .....	<b>52</b>
<b>Figure 3.8</b> : Schematic of ice-wedge evolution (Lachenbruch, 1963). .....	<b>53</b>
<b>Figure 3.9</b> : A typical example of pingo which located in Canada (Mackay, 1973). .....	<b>54</b>
<b>Figure 3.10</b> : Schematic drawings of pingo growth (Mackay, 1992). .....	<b>54</b>
<b>Figure 3.11</b> : Ice formation in soils: a) closed system; b) open system; c) pea gravel layer changes upper part of specimen into a closed system (Terzaghi, 1952). .....	<b>55</b>
<b>Figure 3.12</b> : Relation between volume and pressure for a frozen soil subjected to thawing (Andersland and Ladanyi, 1994). .....	<b>56</b>
<b>Figure 3.13</b> : Schematic of freezing test equipment (Johnson et al., 1986). .....	<b>59</b>
<b>Figure 3.14</b> : Relationship of hydraulic permeability and overburden pressure for unfrozen samples and subjected to F-T cycles (Othman and Benson, 1993). .....	<b>61</b>
<b>Figure 3.15</b> : Residual void ratio in terms of freeze-thaw (Viklander, 1998). .....	<b>62</b>
<b>Figure 3.16</b> : Relationship between volumetric strain and number of freeze-thaw cycles (Eigenbrod, 1996). .....	<b>63</b>
<b>Figure 3.17</b> : Plastic limit vs. number of freeze-thaw cycles of naturally structured soils (Dagesse, 2015). .....	<b>64</b>
<b>Figure 3.18</b> : a) Liquid limit vs. number of freeze-thaw cycles of naturally structured soils, b) Liquid limit vs. number of freeze-thaw cycles of unstructured soils (Dagesse, 2015). .....	<b>64</b>
<b>Figure 3.19</b> : Relationship of the consolidation coefficient and freeze-thaw cycles (Paudel and Wang, 2010). .....	<b>65</b>
<b>Figure 3.20</b> : Unconfined compression strength change with freeze and thaw effect (Dayioglu, 2015). .....	<b>68</b>
<b>Figure 3.21</b> : Strength behavior of CH <sub>1</sub> clay and lime mixtures after different freeze-thaw cycles (Ciftliklioglu, 2018). .....	<b>69</b>
<b>Figure 3.22</b> : Swelling pressure results of bentonite affected by five repetitive freeze- thaw cycles (Schatz and Martikainen, 2010). .....	<b>70</b>
<b>Figure 3.23</b> : Swelling pressure change with freeze and thaw effect (Dayioglu, 2015). .....	<b>70</b>
<b>Figure 4.1</b> : Hydrometer analysis tools. ....	<b>72</b>

<b>Figure 4.2</b> : Casagrande liquid limit apparatus. ....	<b>73</b>
<b>Figure 4.3</b> : Modified Harvard miniature compaction test apparatus. ....	<b>76</b>
<b>Figure 4.4</b> : Calibration results of modified harvard compaction test (CH <sub>4</sub> ). ....	<b>77</b>
<b>Figure 4.5</b> : Oedometers in the I.T.U laboratories. ....	<b>79</b>
<b>Figure 4.6</b> : Ca bentonite and natural soil samples. ....	<b>80</b>
<b>Figure 4.7</b> : Grain size distribution and classification of CH <sub>3</sub> . ....	<b>81</b>
<b>Figure 4.8</b> : Compaction test results of CH <sub>3</sub> . ....	<b>81</b>
<b>Figure 4.9</b> : Grain size distribution and classification of CH <sub>4</sub> . ....	<b>82</b>
<b>Figure 4.10</b> : Compaction test results of CH <sub>4</sub> . ....	<b>83</b>
<b>Figure 4.11</b> : Grain size distribution and classification of CH <sub>5</sub> . ....	<b>84</b>
<b>Figure 4.12</b> : Compaction test results of CH <sub>5</sub> . ....	<b>84</b>
<b>Figure 4.13</b> : Grain size distribution and classification of CH <sub>6</sub> . ....	<b>85</b>
<b>Figure 4.14</b> : Compaction test results of CH <sub>6</sub> . ....	<b>86</b>
<b>Figure 4.15</b> : Grain size distribution and classification of CL <sub>1</sub> . ....	<b>87</b>
<b>Figure 4.16</b> : Compaction test results of CL <sub>1</sub> . ....	<b>87</b>
<b>Figure 4.17</b> : Prepared soil samples. ....	<b>89</b>
<b>Figure 4.18</b> : a) Sample prepared for the swelling pressure test; b) one-dimensional oedometer swelling pressure test setup. ....	<b>90</b>
<b>Figure 4.19</b> : Swelling pressure results of CH <sub>3</sub> samples which are not subjected to the freeze-thaw. ....	<b>91</b>
<b>Figure 4.20</b> : Swelling pressure results of CH <sub>4</sub> samples which are not subjected to the freeze-thaw. ....	<b>91</b>
<b>Figure 4.21</b> : Swelling pressure results of CH <sub>5</sub> samples which are not subjected to the freeze-thaw. ....	<b>92</b>
<b>Figure 4.22</b> : Swelling pressure results of CH <sub>6</sub> samples which are not subjected to the freeze-thaw. ....	<b>92</b>
<b>Figure 4.23</b> : Swelling pressure results of CL <sub>1</sub> samples which are not subjected to the freeze-thaw. ....	<b>93</b>
<b>Figure 4.24</b> : $\sigma_s$ – LL (%) relationship of samples which are not subjected to the F-T cycles. ....	<b>94</b>
<b>Figure 4.25</b> : $\sigma_s$ – PI (%) relationship of samples which are not subjected to the F-T cycles. ....	<b>94</b>
<b>Figure 4.26</b> : $\sigma_s$ – activity relationship of samples which are not subjected to the F-T cycles. ....	<b>95</b>
<b>Figure 4.27</b> : $\sigma_s$ – $W_{opt.}$ (%) relationship of samples which are not subjected to the F-T cycles. ....	<b>95</b>
<b>Figure 4.28</b> : $\sigma_s$ – $\gamma_{dmax}$ relationship of samples which are not subjected to the F-T cycles. ....	<b>96</b>
<b>Figure 4.29</b> : a) samples exposed to freezing; b) thawing samples in desiccator. ....	<b>97</b>
<b>Figure 4.30</b> : Physical appearance of CH <sub>3</sub> clay after 1, 3, 15 and 20 F-T cycles. ....	<b>98</b>
<b>Figure 4.31</b> : Swelling pressure results of CH <sub>3</sub> samples after F-T cycles. ....	<b>98</b>
<b>Figure 4.32</b> : Physical appearance of CH <sub>4</sub> clay after 3, 5, 10 and 15 F-T cycles. ....	<b>99</b>
<b>Figure 4.33</b> : Swelling pressure results of CH <sub>4</sub> samples after F-T cycles. ....	<b>100</b>
<b>Figure 4.34</b> : Physical appearance of CH <sub>5</sub> clay after 3, 5, 10 and 15 F-T cycles. ....	<b>101</b>
<b>Figure 4.35</b> : Swelling pressure results of CH <sub>5</sub> samples after F-T cycles. ....	<b>101</b>
<b>Figure 4.36</b> : Physical appearance of CH <sub>6</sub> clay after 3, 5, 10 and 15 F-T cycles. ....	<b>102</b>
<b>Figure 4.37</b> : Swelling pressure results of CH <sub>6</sub> samples after F-T cycles. ....	<b>103</b>
<b>Figure 4.38</b> : Swelling pressure results of CL <sub>1</sub> samples after F-T cycles. ....	<b>104</b>
<b>Figure 4.39</b> : Physical appearance of CL <sub>1</sub> clay after 3, 5, 7 and 15 F-T cycles. ....	<b>104</b>
<b>Figure 4.40</b> : $\sigma_s$ – LL (%) relationships after F-T cycles. ....	<b>105</b>

<b>Figure 4.41</b> : $\sigma_s - PI$ (%) relationships after F-T cycles. ....	<b>106</b>
<b>Figure 4.42</b> : $\sigma_s - W_{opt.}$ (%) relationships after F-T cycles. ....	<b>106</b>
<b>Figure 4.43</b> : $\sigma_s - \gamma_{dry}$ (kN/m <sup>3</sup> ) relationships after F-T cycles. ....	<b>107</b>
<b>Figure 4.44</b> : All $\sigma_s$ results according to F-T cycles. ....	<b>107</b>
<b>Figure 4.45</b> : Void ratios of CH <sub>3</sub> according to the F-T cycles. ....	<b>108</b>
<b>Figure 4.46</b> : Void ratios of CH <sub>4</sub> according to the F-T cycles. ....	<b>109</b>
<b>Figure 4.47</b> : Void ratios of CH <sub>5</sub> according to the F-T cycles. ....	<b>109</b>
<b>Figure 4.48</b> : Void ratios of CH <sub>6</sub> according to the F-T cycles. ....	<b>110</b>
<b>Figure 4.49</b> : Void ratios of CL <sub>1</sub> according to the F-T cycles. ....	<b>110</b>





## **EVALUATION OF CHANGES IN SWELLING PRESSURE CHARACTERISTICS OF CLAYS EXPOSED TO FREEZE-THAW CYCLES**

### **SUMMARY**

The soils that located in cold climatic regions are exposed to periodic freeze-thaw cycles. The mechanical properties of the soils in these regions are subject to significant changes due to the ice lenses formed between the soil particles during freezing process and the excess amount of water that occurs during the thawing process. Changes in the geotechnical engineering parameters such as bearing capacity, settlement and swelling potential of the soils under the effect of freeze-thaw should be considered in the design section of projects. Especially, the deformations occurring on the structures built on clayey soils with high swelling potential constitute an important part. The determination of the potential of swelling on clayey soils that susceptible to swell in cold regions will prevent deformations and damages that may be created on structures, road structures, motorways, sidewalks and substructures to be constructed or to be built on the clay layer. Thereby, the safety will be increased and the maintenance costs will be reduced in the risk regions where damages may occur.

Within the scope of the master thesis, it is aimed to determine the parameters affecting the swelling pressure of clay soils which are exposed to freezing-thawing cycles. In order to investigate the short and long-term swelling characteristics of soil samples, clayey soils with different plasticity behaviors and different mineralogical characteristics were subjected to varying freeze and thaw cycles, and swelling pressure tests before and after freeze-thawing process were carried out on specimens obtained from these soils. Swelling pressure tests were performed after 0, 1, 3, 5, 7, 10, 15, 20 and 25 F-T cycles of specimens were completed. The relationship between swelling pressures determined by experiments, soil index and mineralogical properties were investigated. The variation of swelling pressure of clay samples was investigated with respect to liquid limit, plastic limit, plasticity index, maximum dry unit volume weight, optimum water content and void ratio. According to the results of the laboratory tests obtained; an increase in swelling pressure was observed as the liquid limit and the plasticity index values of the soils increased. After exposed to freeze-thaw cycling, the swelling pressure values of the soils follow the decreasing trend and stabilize after a while. The void ratios of the soils have increased after exposure to freeze-thaw cycles. The volume of water in the sample expands due to freezing process. This physical process may be caused by ice lenses which formed in frozen soils. Ice lenses form through the horizontal lines. In the thawing process, these ice lenses melt and void ratio of the soil increases. The increasing void ratio and the segregation of the soil particles by irregular placement which causes the decomposition of flocculated soil structure may be reason for decrease in swelling pressure results.

The samples were prepared by using the Harvard miniature compaction apparatus at the maximum dry unit weight and optimum water content that obtained from compaction tests. 2 swelling pressure samples were prepared from the upper and lower parts of the samples. It is expected that the bottom part of the sample will have more

water content than the upper region due to the distribution of compaction energy. Therefore, the swelling pressure results will be different from each other. In order to inspect this phenomena, 2 bottom and 1 top sample prepared for each swelling pressure test. Under the guidance of C method of ASTM D-4546 standard, one-dimensional swelling tests were performed. As a result of the tests, the general tendency was determined as the swelling pressures obtained from the bottom samples were evaluated greater than the results of the top samples for all clay samples. . In accordance with the ASTM D560, the samples were freeze for 24 hours at the initial temperature ( $-23 \pm 2$  ° C). Then the samples removed from the refrigerant were allowed to dissolve in desiccators for 24 hours in laboratory conditions ( $23 \pm 2$  ° C). This 48 hours freeze-thaw process was determined as 1 freeze-thaw cycle and experiments were conducted by using these freeze-thaw cycles.

After the F-T cycles, the relationship between the swelling pressures and liquid limit, plasticity index, optimum water content, dry unit weight of soils was investigated. Samples with high liquid limit have more swelling pressures and have decreased with the increasing F-T cycles. The same swelling pressure behavior was observed with the increasing plasticity index and optimum water content values after the F-T cycles. On the contrary, considering the increasing dry unit weights of samples, it was determined that the  $\sigma_s$  followed a decreasing trend.

The results of the CH<sub>3</sub> swelling pressure tests indicates that the bottom swelling pressures are higher than the top swelling pressure results. With the increase in the number of freeze-thaw cycles, the loss of swelling pressure rate decreased until the 10<sup>th</sup> cycle and became stable for the bottom samples. For top samples, the results of the swelling pressure were stabilized after the 5<sup>th</sup> F-T cycle. After the 25<sup>th</sup> F-T cycle, an average 59% decrease in swelling pressure results was observed. The swelling pressure results of the CH<sub>4</sub> are followed by a decrease trend after being exposed to freeze-thaw cycles and become stabilized after the 10<sup>th</sup> F-T cycle for both top and bottom samples. After the 25<sup>th</sup> F-T cycle, an average 45% decrease in swelling pressure results was determined. In accordance with previous soil samples, the CH<sub>5</sub> bottom swelling pressures are higher than the top results after F-T cycles and decrease rate of swelling pressure reduced, becomes stable after the 1<sup>st</sup> F-T cycle. Top swelling behavior follows a steady trend after 10<sup>th</sup> F-T cycle. After the 25<sup>th</sup> F-T cycle, 44% decrease in swelling pressure results was observed in bottom results and 67% in top results. For CH<sub>6</sub> samples, small decreases were observed until the 10<sup>th</sup> cycle. After 10<sup>th</sup> F-T cycle, bottom swelling pressure values follow a steady trend. After the 25<sup>th</sup> F-T cycle, 67% decrease in swelling pressure results was observed in bottom results. For CL<sub>1</sub>, after 10<sup>th</sup> F-T cycle bottom swelling behavior follows a steady trend and for top samples it is determined in the 3<sup>rd</sup> F-T cycle. After the 25<sup>th</sup> F-T cycle, 53% decrease in swelling pressure was observed in bottom results and 80% in top results.

All swelling pressure test results were evaluated depending on the freeze-thaw cycles. It was observed that the swelling pressures in high plasticity clays decreased and became stable, whereas the observed decreases in low plasticity clay were not as high as the high plasticity clays and were stable with the increasing number of freeze-thaw cycles. It was determined that the rate of decrease in swelling pressures for high plasticity clays was higher than low plasticity clay sample. Compared to the Ca and Na bentonite results, sodium bentonite swelling pressures were found to be higher than the calcium bentonite swelling pressures and a greater swelling pressure decrease in sodium bentonite was observed as a result of the freeze-thaw experiments. In addition, the decrease in swelling pressure observed at the end of the 1<sup>st</sup> F-T cycle was more

than the calcium bentonite. When these results were examined, the effect of mineralogical properties on swelling pressure behavior was investigated.

The void ratios of the samples were investigated, and it is stated that with the increasing number of F-T cycles void ratios are increased. After the certain F-T cycle numbers, it was observed that the void ratios did not increase much and reached to the residual values. General behavior that observed from the results, the void ratios did not change much after the 10<sup>th</sup> F-T cycle and the increases in swelling pressures were stabilized accordingly. It was determined that the increase in the void ratio in high plasticity clays was higher than the low plasticity clay. This may be an explanatory reason for the difference in swelling behavior of soils.





## DONMA ÇÖZÜLME ÇEVİRİMLERİNE MARUZ KALMIŞ KİLLERDE ŞİŞME BASINCINDAKİ DEĞİŞİMLERİN BELİRLENMESİ

### ÖZET

Soğuk iklim bölgelerinde bulunan zeminler, periyodik donma-çözülme çevrimlerine maruz kalmaktadır. Bu bölgelerdeki zeminlerin mühendislik özellikleri, donma işlemi sırasında zemin daneleri arasında oluşan buz mercekleri ve çözülme işlemi sırasında oluşan su nedeniyle önemli değişikliklere uğrayabilmektedir. Donma-çözülme maruz kalan zeminlerin permeabilite, boşluk oranı, kıvam limitleri gibi fiziksel özellikleri ile konsolidasyon katsayısı, şişme basıncı ve serbest basınç mukavemeti gibi mühendislik özellikleri de olumsuz etkilenebilmektedir. Donma-çözülme etkisi altındaki zeminlerin taşıma kapasitesi, oturma ve şişme potansiyeli gibi geoteknik özelliklerindeki değişiklikler projelerin tasarım aşamasında dikkate alınmalıdır. Özellikle, yüksek şişme potansiyeline sahip killi zeminlerde inşa edilen veya edilecek yapılar üzerinde meydana gelecek deformasyonlar önemli bir problem teşkil etmektedir. Soğuk iklimin hakim olduğu bölgelerde şişme potansiyelinin belirlenmesi ile kil tabakası üzerine inşa edilecek yapılar, yol yapıları, otoyollar, kaldırımlarda meydana gelebilecek deformasyonlar ve hasarlar önlenecektir. Böylece, güvenlik artacak ve riskli bölgelerde oluşabilecek hasarların önüne geçip bakım maliyetleri azalacaktır.

Bu çalışma kapsamında donma-çözülme maruz kalmış killerde şişme basıncına etki eden faktörlerin belirlenmesi hedeflenmiştir. Zemin numunelerinin erken dönem ve uzun dönem şişme karakteristiklerinin incelenmesi amacıyla farklı plastisiteye sahip ve farklı mineralojik yapıdaki killi zeminler değişken donma-çözülme çevrimlerine maruz bırakılmış, bu zeminlere ait numuneler üzerinde donma-çözülme öncesi ve sonrası şişme basıncı deneyleri yapılmıştır. Deneyler sonucunda belirlenen şişme basınçları ile zeminin endeks özellikleri arasındaki ilişkiler incelenmiştir. Şişme basıncının, likit limit, plastik limit, plastisite indisi, maksimum kuru birim hacim ağırlık, optimum su muhtevası ve boşluk oranına bağlı olarak değişimi incelenmiştir.

İstanbul Teknik Üniversitesi Geoteknik Laboratuvarlarında, yüksek plastisiteli killerin ( $CH_3$ ,  $CH_4$ ,  $CH_5$  ve  $CH_6$ ) ve düşük plastisiteli kilin ( $CL_1$ ) donma-çözülme sonrasındaki şişme basıncı davranışı incelenmiştir. Bu amaçla, tez kapsamında kullanılan numunelerin sınıflandırılması için elek analizi, hidrometre deneyi ve kıvam limitleri gibi endeks deneyleri yapılmıştır. Sonrasında, Harvard minyatür kompaksiyon aletinde optimum su muhtevasında numuneler hazırlanmış ve hazırlanan bu numuneler üzerinde 9 adet donma-çözülme çevrimi uygulanmıştır. 0, 1, 3, 5, 7, 10, 15, 20 ve 25 çevrim sonunda tüm numuneler üzerinde şişme basıncı deneyleri yapılmış ve donma-çözülme maruz kalan numunelerin şişme basıncındaki değişimler incelenmiştir. Çalışmada kullanılan numunelerin plastisite indisi,  $PI = \%20-255$  aralığında, likit limiti,  $LL = \%36-296$  aralığında ve plastik limiti  $PL = \%16-41$  aralığında değişmektedir.

Sodyum bentonitin ( $CH_3$ ) kıvam limitleri belirlenmiştir. Likit limit,  $LL = \%296$ , plastik limit,  $PL = \%41$ , plastisite indisi,  $PI = \%255$  olarak belirlenmiştir. Modifiye Harvard

kompaksiyon deneyi sonucunda, optimum su muhtevası ( $W_{opt.}$ ) %37 ve  $\gamma_{kmaks.}$  11.60 kN/m<sup>3</sup> olarak belirlenmiştir. Kalsiyum bentonitin (CH<sub>4</sub>) kıvam limitleri belirlenmiştir. Likit limit, LL =%288, plastik limit, PL =%38, plastisite indisi, PI =%250 olarak belirlenmiştir. Modifiye Harvard kompaksiyon deneyi sonucunda, optimum su muhtevası ( $W_{opt.}$ ) %30 ve  $\gamma_{kurumaks.}$  12.40 kN/m<sup>3</sup> olarak belirlenmiştir. CH<sub>5</sub> için kıvam limitleri belirlenmiştir. Likit limit, LL =%68, plastik limit, PL =%20, plastisite indisi, PI =%48 olarak belirlenmiştir. Modifiye Harvard kompaksiyon deneyi sonucunda, optimum su muhtevası ( $W_{opt.}$ ) %22 ve  $\gamma_{kurumaks.}$  14.80 kN/m<sup>3</sup> olarak belirlenmiştir. CH<sub>6</sub> için kıvam limitleri belirlenmiştir. Likit limit, LL =%52, plastik limit, PL =%28, plastisite indisi, PI =%24 olarak belirlenmiştir. Modifiye Harvard kompaksiyon deneyi sonucunda, optimum su muhtevası ( $W_{opt.}$ ) %23 ve  $\gamma_{kmaks.}$  14.70 kN/m<sup>3</sup> olarak belirlenmiştir. CL<sub>1</sub> için kıvam limitleri belirlenmiştir. Likit limit, LL =%36, plastik limit, PL =%16, plastisite indisi, PI =%20 olarak belirlenmiştir. Modifiye Harvard kompaksiyon deneyi sonucunda, optimum su muhtevası ( $W_{opt.}$ ) %15 ve  $\gamma_{kmaks.}$  16 kN/m<sup>3</sup> olarak belirlenmiştir.

Proctor sıklığında oluşturulan numunelerin donma-çözülme çevrimlerine maruz kalmadan yapılan şişme deneyleri için numunelerin altından ve üstünden olmak üzere 2 adet örnek alınıp şişme deneylerinde kullanılmıştır. Yapılan deneyler sonucunda hazırlanan numunelerin altından ve üstünden elde edilen şişme basıncı sonuçlarında farklılıklar olduğu gözlenmiştir. Bu sebep ile hazırlanan numunelerin şişme basınçları, alt ve üst şişme basınçları olarak incelenmesine karar verilmiştir. ASTM D-4546 standardındaki C yöntemi kullanılarak tek boyutlu şişme basıncı deneyleri yapılmıştır.

Zemin numuneleri, ASTM D560 No.'lu Standart 'da belirtilmiş yönteme uygun kapalı bir sistemde yapılan donma ve çözülme çevrimlerine maruz bırakılmıştır. Numuneler 24 saat boyunca başlangıç sıcaklığı ( $-23 \pm 2^\circ C$ )'de soğutma işlemine tabii tutulmuştur. Daha sonra soğutucudan çıkartılan numuneler laboratuvar koşullarında ( $23 \pm 2^\circ C$ ) 24 saat boyunca desikatörlerde bekletilerek çözülmeye bırakılmıştır. Toplam 48 saat süren bu donma-çözülme işlemi 1 donma-çözülme çevrimi olarak belirlenmiş ve araştırma boyunca bu donma-çözülme çevrimleri kullanılarak deneylere devam edilmiştir. Numunelerin farklı donma-çözülme çevrimlerine göre şişme basıncı davranışlarını incelemek için araştırmanın başında belirlenmiş çevrimlere karşılık gelen şişme basınç deneyleri yapılmıştır.

Donma-çözülme çevrimlerine maruz kalmış zeminlerin şişme basınçları ile likit limiti, plastisite indeksi, optimum su muhtevası, kuru birim hacim ağırlık arasındaki ilişkiler incelenmiştir. Yapılan deneyler sonucunda, bütün zemin örneklerinde artan donma-çözülme çevrim sayısı ile şişme basınçlarının azaldığı gözlemlenmiştir. Artan likit limit değerleri ile ölçülen şişme basıncı değerleri artma eğiliminde olduğu belirlenmiştir. Aynı şişme basıncı davranışı, artan optimum su muhtevası ve plastisite indisi değerleri ile gözlemlenmiştir.

Tüm şişme basıncı deneyi sonuçları, donma-çözülme çevrimlerine bağlı olarak yüksek ve düşük plastisiteli killer için ayrı ayrı değerlendirilmiştir. Yapılan değerlendirmeler sonucunda yüksek plastisiteli killerde şişme basınçlarının artan donma-çözülme çevrimleri ile azaldığı ve belirli bir çevrim sayısından sonra stabil hale gelip fazla değişiklik göstermediği, düşük plastisiteli kilde gözlenen şişme basıncı azalışlarının ise yüksek plastisiteli killerdeki kadar belirgin olmadığı ve donma sayısının artmasıyla stabil hale geldiği gözlemlenmiştir. Yüksek plastisiteli killer için şişme basınçlarındaki azalma oranının, düşük plastisiteli kil numunesinden daha yüksek olduğu tespit edilmiştir. Sodyum bentonit (CH<sub>3</sub>) ve kalsiyum bentonit (CH<sub>4</sub>) şişme basıncı deney

sonuları karřılařtırıldıđında, sodyum bentonit řiřme basınları kalsiyum bentonit řiřme basınlarından daha fazla llmüřtür. Donma-özölme deneyleri sonucunda sodyum bentonit řiřme basıncı deđerlerinde kalsiyum řiřme basıncı deđerlerine göre daha büyük düşüř zlemlenmiřtir. Elde edilen sonulara göre, zeminlerin mineralojik farklılıkların řiřme basıncı davranıřına etkisi zlemlenmiřtir.

Son olarak, kullanılan numunelerin boşluk oranları arařtırılmıř ve řiřme basıncı davranıřları ile boşluk oranları arasında bir iliřki kurulması amalanmıřtır. Bu dođrultuda, numunelerin donma-özölme evrimleri sonrasında boşluk oranları belirlenmiřtir. Artan donma-özölme evrimleri ile boşluk oranlarının arttıđı zlenmiřtir. řiřme basınlarının stabil hale geldiđi donma-özölme evrimlerinden sonra, boşluk oranlarının ok fazla artmadıđı ve rezidüel deđerlere ulařtıđı zlemlenmiřtir. Yüksek plastisiteli killerin boşluk oranlarındaki artıřın, düşük plastisiteli kilden daha fazla olduđu tespit edilmiřtir. Plastisitenin boşluk oranlarındaki deđiřimi üzerine etkisi zlenmiřtir. Elde edilen bulgular, zeminlerin donma-özölme evrimlerinde sonra řiřme davranıřlarındaki farklar iin aıklayıcı bir unsur olabilir.







## **1. INTRODUCTION**

The problematic soils have become an important problem for the civil engineers. The climatic conditions are also an important factor that affects the geotechnical properties of the soil. Therefore, seasonal conditions should be examined in collapsible and expansive soils exposed to the harsh climatic conditions. The soils are exposed to periodic freeze-thaw cycles where cold climatic conditions are observed. The increase in the volume and the loss of bearing capacity due to freezing process in the cold regions are included in the research subjects of geotechnical engineering. Since an important part of the earth is composed of cold areas, the soil is affected negatively by the freezing and thawing process. Therefore, the effects and precautions of freezing on soils have been investigated by various researchers. Recurrent freeze-thaw cycles due to seasonal conditions in cold regions can be repeated at least twice a year and significantly alter the geotechnical properties of soil. The mechanical properties of the soil are subject to essential changes due to the ice lenses formed between the soil particles during freezing and the excess amount of water that occurs during the thawing process. Changes in the geotechnical engineering parameters such as bearing capacity, settlement, and swelling potential of the soils under the effect of freezing and thawing should be investigated. The deformations in the structures built on clayey soils with high swelling potential are an important part of them. By determining the potential of swelling on clayey soils in cold regions, the deformations and damages that may occur in the structures, road structures, motorways, sidewalks and substructures that built on the clay layer can be prevented. Thus, economic benefits will be provided and the cost of maintenance and repair will be reduced in the potential regions where the deformations will occur. The effects of soil type, grain size distribution, freezing rate, water content during freezing and freeze-thaw cycles on soil stability and soil structure were investigated. During the freezing process, water is known to expand by 9% by volume. Water forms into the ice crystals by freezing and increases the void ratio of the soil due to the volumetric increase and causes deformation. This freeze-thaw behavior in cold climatic zones will adversely affect the physical and mechanical

properties of the soil. For this reason, it is important to determine the swelling potential, swelling pressure. The mineralogical structure of clay layers is one of the most important factors affecting the volumetric change for the soil where swelling problem is observed. Expansive soils can be classified into different groups by regarding their physical properties, chemical composition and mineral content. Several field and laboratory tests can be applied to determine the swelling pressure of soil. Various methods are used by geotechnical engineers to determine and classify expansive soils.

### **1.1 Purpose of Thesis**

In this study, it is aimed to determine the swelling pressures of the soils and behavior characteristics after freeze-thaw cycles. For this purpose, laboratory tests were conducted to determine swelling pressures of different clay samples before and after the freeze-thaw cycles. The aim of this study is to investigate the relationships between the engineering parameters obtained from the experiments and the geotechnical properties of the samples.

Five different clay samples with different index properties were used to achieve this goal. For this purpose, index tests were performed on five different low and high plasticity clay samples. Then, compaction parameters were determined by using standard Proctor and Harvard miniature compaction test tools. Freeze-thaw tests were performed on these samples. Afterwards, one dimensional swelling pressure tests were carried out to investigate the changes of the swelling pressures of samples that freeze-thaw cycles would affect. In order to determine the swelling potential and swelling behavior after the freeze-thaw cycles, various correlations have been tried to be developed for practical purposes. After concluding the laboratory tests, the relationship between the swelling pressures and the index properties of the soils, including the liquid limit, plastic limit, plasticity index and void ratios were investigated.

### **1.2 Scope of Thesis**

Within the scope of the thesis, at Istanbul Technical University Soil Mechanics Laboratories, swelling pressure tests were performed on five different clay soils before

and after the freeze-thaw cycles to examine swelling behavior. In consideration of the findings obtained from the tests, it was aimed to correlate the engineering properties with the swelling pressures which will be altered due to effects of freeze-thaw cycles.

In the second part of the thesis study, the characteristics of clayey soils and swelling behaviors were discussed. In this section, the literature studies about the mineralogical properties of clays, the mechanism of swelling, the identification and classification of swelling soils are presented.

In the third chapter, literature researches about the effects of freezing and thawing cycles on the soil are mentioned. After the freeze-thaw process, previous scientific researches which focused on the changes in the physical and mechanical properties of soils are mentioned.

In the fourth chapter, the index properties of the materials which are used in this study is represented. After, the methods and preparation of the samples, freeze-thaw experiments and the effects of such climate changes on the swelling characteristics have been tested. The results of the experimental studies are shown in the last part of this chapter.

In the last section, the results obtained from the evaluation of the experimental studies are summarized.



## **2. SWELLING BEHAVIOR OF CLAY SOILS**

Expansive soils can be identified by their volumetric changes due to varying water conditions. Seasonal and regional conditions may constitute changes in the water content which is the main reason for expansive movements in the soils. These volumetric changes cause detrimental damages in every aspect of engineering structures.

### **2.1 Clay Minerology**

The term of soil is used by a geologist and by a civil engineer with different senses of applications. Civil engineers defines and divides into two categories which are rock and soils. Terzaghi and Peck (1948) stated, "Soil is a natural aggregate of mineral grains that can be separated by such gentle means as agitation in water." Regardless of particle-size distribution, composition, or organic content any loose material at the earth's crust, is soil to the engineer. The term clay is defines a particle-size to the engineer.

The definition of clay can be stated as in general; a natural, fine-grained material which develops plasticity when mixed with water. Silica, alumina, and water, mostly with appreciable amount of iron, alkalies, and alkaline earths are the main substances of clay (Grim, 1968).

The maximum size of particles is defined differently in various disciplines for the clay size grade. In soil investigations and in the terms of engineering applications, 2 microns as the upper limit of the clay particles size.

Clay minerals are responsible for many of the soil's most important and characteristic physical and chemical properties. Soil properties such as cation exchange, shrink and swell properties and practical considerations are all affected by minerals. Due to different structures of clay minerals, each one of them can be distinguished by observing their crystal structures.

Earth's crust is formed by only a few elements. O and Si cover the 75% of the checmical elements regarding their masses. However, oxygen consists of more than



Another structural unit is called tetrahedrons which are built from silicas can be defined . In these structures, a silicon atom is located at equal distance from four oxygen atoms or hydroxyls. The oxygen atoms are shared at the basal corners of the tetrahedral sheets. In many tetrahedral layers of the clay minerals, the substitution of  $\text{Si}^{4+}$  by  $\text{Al}^{3+}$  or  $\text{Fe}^{3+}$  take placed. The silica tetrahedral groups are configured to form a hexagonal structure (Grim,1968). Structural scheme of soil minerals based on tetrahedral and octahedral sheets are stated in the Figure 2.2. Demonstration of silica tetrahedrons and tetrahedrons which are displayed on the base plane are given in the Figure 2.3.

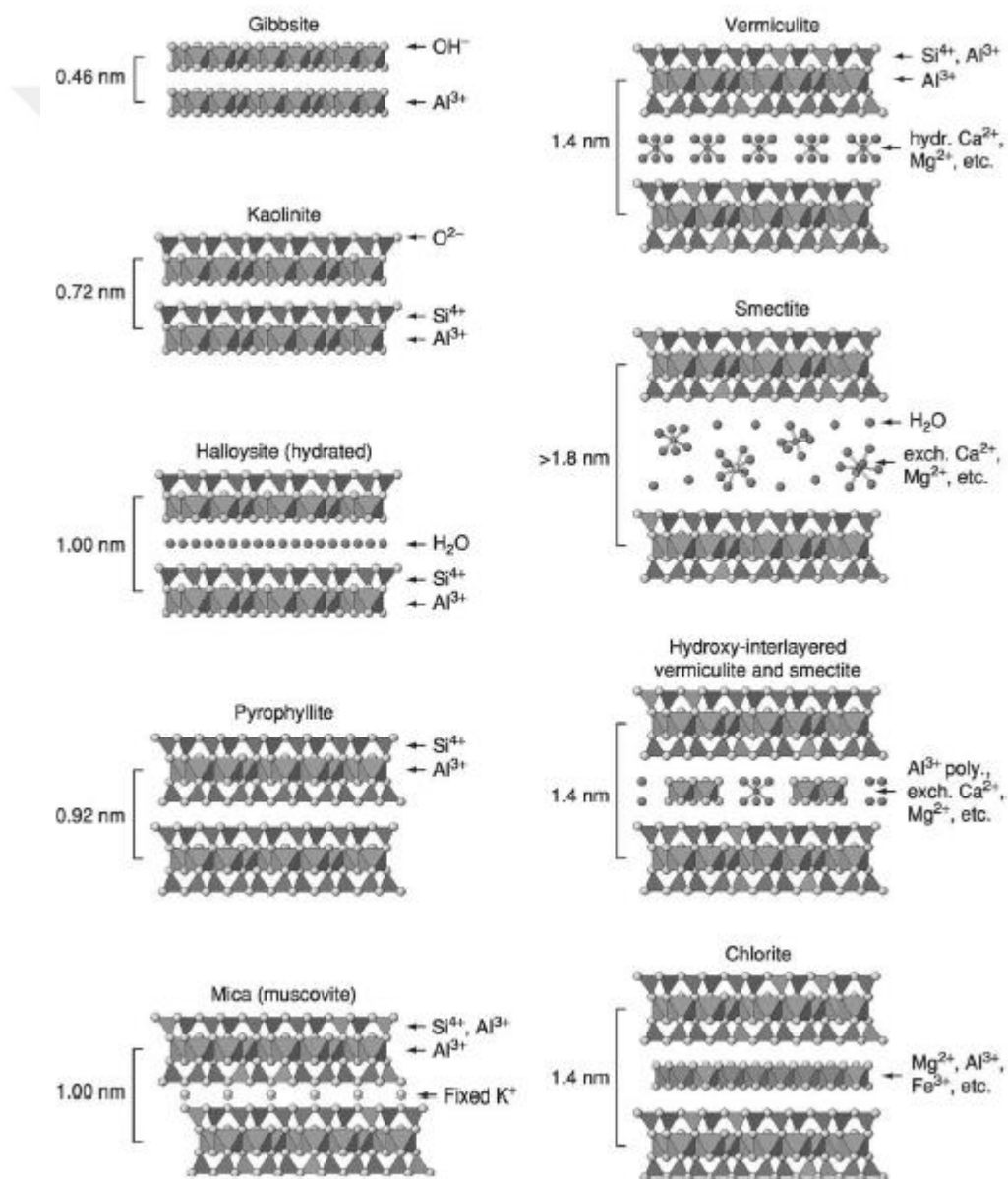


**Figure 2.2 :** Structural scheme of soil minerals based on tetrahedral and octahedral sheets (Schulze, 2002).

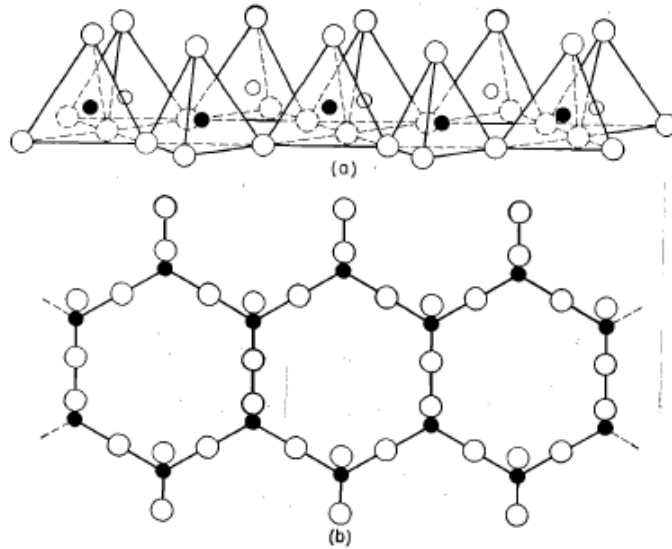


**Figure 2.3 :** (a) Sketch of double chains of silica tetrahedrons and (b) Projected on the plane of the base of the tetrahedrons (Grim, 1968).

Mungan (1989), stated that clay damage depends on;

- The type and the amount of the exchangeable cations, such as  $K^+$ ,  $Na^+$ ,  $Ca^{2+}$
- The layered structure which exists in the clay minerals.

By maintaining high concentrations of  $K^+$  cation in liquid solutions, clay damage can be prevented. Because of the small-sized  $K^+$  cation, it can penetrate the interlayers of the clay and hold the clay platelets together. Therefore clay platelets keep intact (Civan, 2015). The various metal ions are shown in terms of their relative effective hydrated sizes as shown in the Figure 2.4.

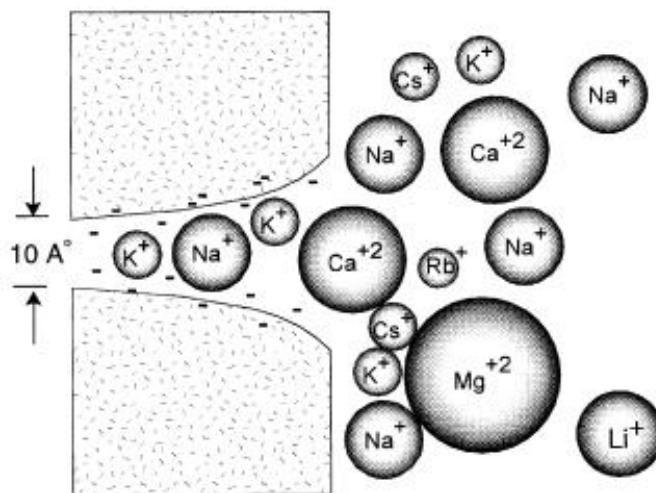


**Figure 2.4 :** Effect of the cation size on cation migration into a clay interlayer (Civan, 2015).



Many researchers such as Mungan (1965), Reed (1977), Kia et al. (1987) and Khilar and Fogler (1998) have contributed to identify the water sensitivity of clayey soils. From the most damaging to the least damaging cations can be ordered as  $H^+ > Na^+ > Ca^{++}$  (Reed, 1977). However, the order of replaceability of the common cations in clays from the most to the least replaceable cations determined by Grim (1968) as  $Li^+ > Na^+ > K^+ > Rb^+ > Cs^+ > Mg^{++} > Ca^{++} > Sr^{++} > Ba^{++} > H^+$ . Hughes (1951) stated that hydrogen replaces calcium in normal conditions, which in turn replace sodium. The firmness increases with the valence of the cation which are held in the clay structure, except of potassium in illites. Bailey (1980) and Rieder et al. (1998), classified the silicates which is indicated in the Figure 2.5. The swelling behavior of these different minerals depends on bonding between the sheets which is given in the Figure 2.6 that shows the schematic diagrams of kaolinite illite and montmorillonite structures, respectively.

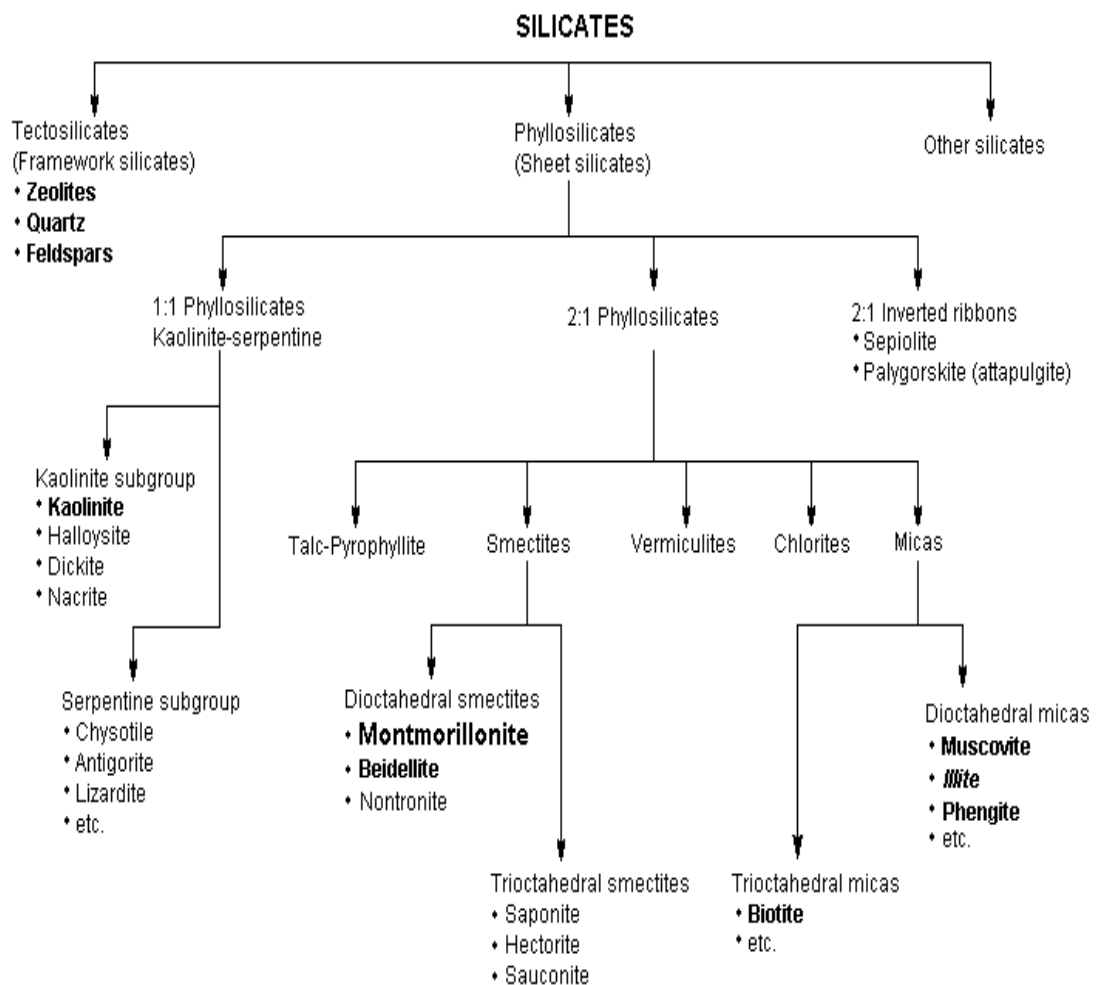


**Figure 2.5 :** Classification of silicates (Bailey, 1980; Rieder et al., 1998).

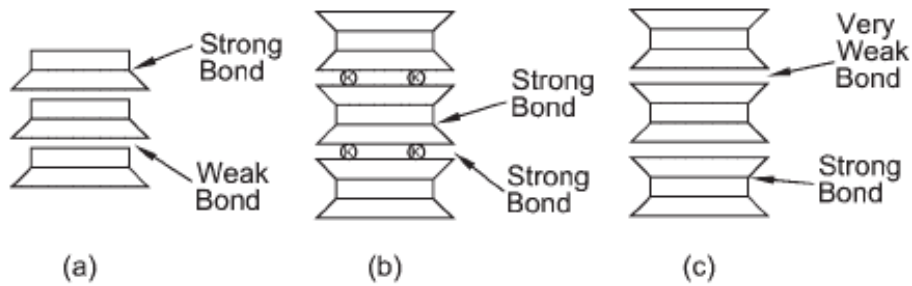


**Figure 2.6 :** Schematic diagrams of the structure: (a) kaolinite; (b) illite and (c) montmorillonite (Nelson et al., 2015).

Snethen et al. (1975), defined the combination of the octahedral and the tetrahedral sheets of the the clay minerals as follows;

1. One silica tetrahedral layer bonded to one aluminum octahedral layer is defined as 1:1 clays. To illustrate, kaolinite is the common mineral of 1:1 clays.
2. One octahedral layer bonded between two tetrahedral layers is stated as 2:1 clays. Illite and montmorillonite can be illustrated for this type of clay minerals.
3. Mixed-layer clays consist arrangements of the 1:1 or 2:1 clay minerals. It can be arranged by randomly or regularly. Chlorite and montmorillonite-chlorite can be given example for the these arrangements.

Kaolinite contains  $\text{Al}^{3+}$  in the octahedral sites and  $\text{Si}^{4+}$  in the tetrahedral sites. The 1:1 layer is electrically neutral and adjacent layers are held together by van der Waals bonds between the basal oxygens of the tetrahedral sheet and the hydroxyls of the octahedral sheet, which restricts expansion and limits the reactive area to external surfaces (Mitchell and Soga, 2005). The 1:1 layer has little or no permanent charge because of the low amount of substitution. Consequently, cation exchange capacities and surface areas are generally low.

### 2.2.1 Kaolinite group

The structure of kaolinite was suggested by Pauling (1930) and revised by Brindley et al. (1946). The structure is shaped of a single silica tetrahedral sheet and a single alumina octahedral sheet combined in a unit. The tips of the silica tetrahedrons and one of the layers of the octahedral sheet form a common layer as shown in the Figure 2.7.

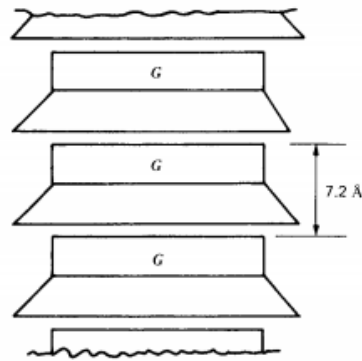


**Figure 2.7 :** Schematic diagram of the structure of kaolinite (Mitchell and Soga, 2005).

### 2.2.2 Smectite (montmorillonite) group

Smectite minerals are made of the combination of two silica tetrahedral sheet with central octahedral sheet which is indicated as a 2:1 layered mineral. Water molecules and cations occupy the space between the 2:1 layers. The tetrahedral and octahedral sheets are combined so that the tips of the tetrahedrons of each silica sheet and one of the hydroxyl layers of the octahedral sheet form a common layer (Grim, 1968). The major smectite minerals are Na-montmorillonite, Ca-montmorillonite, saponite (Mg-montmorillonite), nontronite (Fe-montmorillonite), hectorite (Li-montmorillonite), and beidellite (Al-montmorillonite).

The theoretical formula is  $(\text{OH})_4\text{Si}_8\text{Al}_4\text{O}_{20} \cdot n\text{H}_2\text{O}$  and the theoretical composition without the interlayer material is based on  $\text{SiO}_2$ , 66.7%;  $\text{Al}_2\text{O}_3$ , 28.3%; and  $\text{H}_2\text{O}$ , 5%. However, there is a significant amount of the substitution in the octahedral sheet and some in the tetrahedral sheets of montmorillonite. Because of the large amount of unbalanced substitution in the montmorillonite minerals, they have high cation exchange capacities which are in the range of 80 to 150 meq/100 g (Mitchell and Soga, 2005). Grim (1953), determined the order of replaceability of the common cations in clays from most to least exchangeable cations as,  $\text{Li}^+ > \text{Na}^+ > \text{K}^+ > \text{Rb}^+ > \text{Cs}^+ > \text{Ca}^{++} > \text{Sr}^{++} > \text{Ba}^{++} > \text{H}^+$ .

Na-montmorillonite tend to swell more than Ca-montmorillonite because the Ca cation is more strongly adsorbed than the Na cations (Civan, 2015). As a result, when these clays are in contact with water, Ca-montmorillonite structures maintains initial condition and keep close to each other, however the Na-montmorillonite swells and the structures are separated from each other. Thus, water can easily fill the gaps between the plates and form thicker water envelopes around the Na-montmorillonite

in comparison to the Ca-montmorillonite (Civan, 2015). Figure 2.8 shows the expansion of the calcium and sodium montmorillonites by hydration. A schematic diagram of the structure of montmorillonite is shown in the Figure 2.9.

Bentonite which is made of smectite group has the capacity of high swelling behavior. It is widely used for different purposes. Drilling mud and slurry walls are main usage areas of bentonite. The bentonite is expansive alteration product of volcanic ash. It has high liquid limit values than other clay soils in general. Commonly, it is used as a backfill during the construction of slurry trench walls, as a soil admixture for construction of seepage barriers and as a grout material. Stability problems in underground construction may be caused by the presence of montmorillonite (Brekke and Selmer-Olsen, 1965).

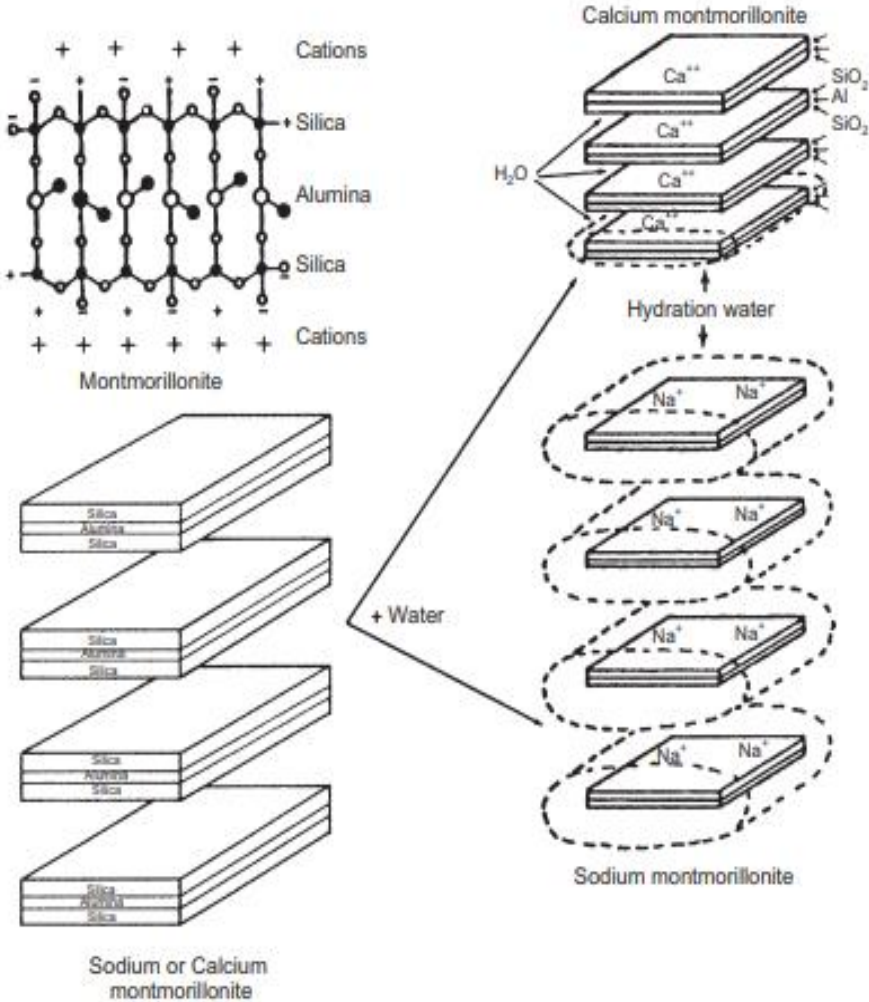


**Figure 2.8 :** Expansion of the calcium and sodium montmorillonites by hydration (Civan, 2015).

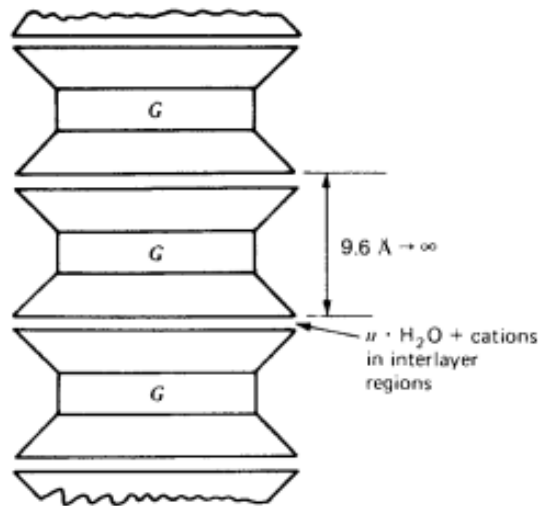


**Figure 2.9** : Schematic diagram of the structure of montmorillonite (Mitchell and Soga, 2005).

### 2.2.3 Illite group

Illite is a clay mineral which was named by Grim et al. (1937). The structure is a 2:1 layer in which the interlayer cation is potassium. The size, charge and coordination number of potassium fit in hexagonal ring of oxygens of the adjacent silica tetrahedral sheets. This gives the structure a strong interlocking bond which holds the layers together. Illite is the most commonly found clay mineral in soils encountered in engineering practice. The schematic diagram of the structure of illite is shown in Figure 2.10.

The structural formula is  $(\text{OH})_4\text{K}_2(\text{Si}_{16}\text{Al}_2)\text{Al}_4\text{O}_{20}$ . It is the threelayer silica–gibbsite–silica structure with the tips of all the tetrahedra pointing toward the center and common with octahedral sheet ions. One-fourth of the silicon positions are filled by aluminum, and the charge deficiency is balanced by potassium which located between the layers (Grim, 1968). Some illite may contain magnesium and iron in the octahedral sheet as well as aluminum (Marshall, 1965). The cation exchange capacity of illite is less than that of smectite, amounting to 10 to 40 meq/100 g. Values greater than 10 to 15 meq/100 g may be indicative of some expanding layers (Weaver and Pollard, 1973). The balancing cation is mainly potassium, and is mainly in the silica sheet and close to the surface of the unit layer rather than in the octahedral layer as in smectites (Grim, 1968). These differences from smectites produce a structure in which interlayer balancing cations are not easily exchanged and the unit layers are fixed in position and do not permit water to enter between them and produce expansion.

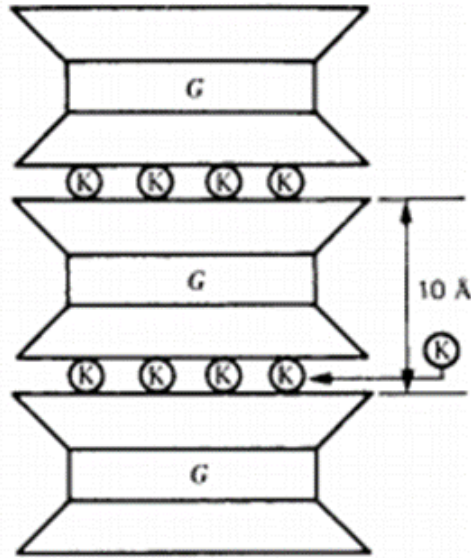


**Figure 2.10** : Schematic diagram of the structure of illite (Mitchell and Soga, 2005).

### 2.2.4 Chlorite group

The structure of chlorite was first suggested by Pauling (1930). The chlorite contains a 2:1 layer with an interlayer hydroxide sheet. In some references, they are referred to as 2:1:1 mineral. The structural formula is  $(\text{OH})_4(\text{SiAl})_8(\text{Mg}\cdot\text{Fe})_6\text{O}_{20}$ . The interlayer hydroxide sheet may have a positive charge. The schematic diagram of the structure of Chlorite is given in the Figure 2.11. In the Figure 2.12, scanning electron microscopic (S.E.M.) photos of the clay minerals are shown.

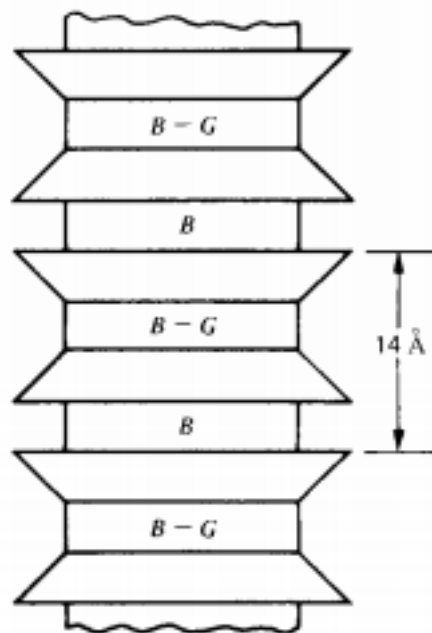
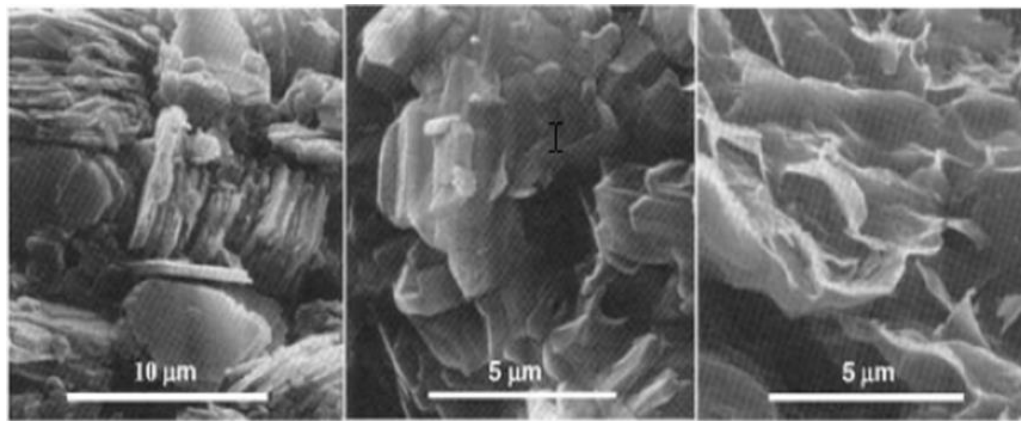


**Figure 2.11** : Schematic diagram of the structure of chlorite (Mitchell and Soga, 2005).



a) *Kaolinite*

b) *illite*

c) *montmorillonite*

**Figure 2.12** : Scanning electron microscopic photos of typical clay minerals (a) kaolinite, (b) illite, (c) montmorillonite (Tovey, 1971).

Stadler (1973) is stated the most essential problems caused by clay minerals related to the civil engineering which are given in the Table 2.1. Increasing surface area values cause to the susceptibility of expansion. Montmorillonite minerals sensitive to water which results in expansion and loss of microporosity.

**Table 2.1** : Typical problems caused by the clay minerals (Stadler, 1973).

Mineral	Chemical Elements	Surface area (m <sup>2</sup> /g)	Major reservoir Problems
Kaolinite	$Al_4[Si_4O_{10}](OH)_8$	20	Causes the loss of permeability and gathers around the pore throat
Chlorite	$(Mg, Al, Fe)_{12}[(Si, Al)_8O_{20}](OH)_{16}$	100	Susceptible to acids and forms $Fe(OH)_3$ which do not go through pore throats.
Illite	$(K_{1-1.5}Al_4[Si_{7-6.5}Al_{1-1.5}O_{20}](OH)_4)$	100	Tend to close the pore throats with other fine materials. Can be expandable clay with the leaching of potassium ions
Smectite (montmorillonite)	$(1/2Ca, Na)_{0.7}(Al, Mg, Fe)_4[(Si, Al)_8O_{20}] \cdot nH_2O$	700	Extremely water sensitive and expandable
Mixed-Layer	Illite-Smectite and Chlorite-Smectite	100-700	Breaks apart and closes the pores subsequently reduces the permeability.

### 2.3 Mechanism of Swelling

Generally, the swelling behavior is related to the existence of water in an expanding clay mineral. Permitting great amount of water in the clay structure, the configuration and water absorbing potential of clay minerals, resulting in the considerable swelling of soil (Patrick and Snethen, 1976). Many researchers have investigated the swelling mechanism of expansive soil through the years. (Grim 1968; Chen 1975; Snethen et al. 1975; Nelson and Miller 1992; Stavridakis 2006). The schematic drawing of swelling mechanism shown in the Fig. 2.13.

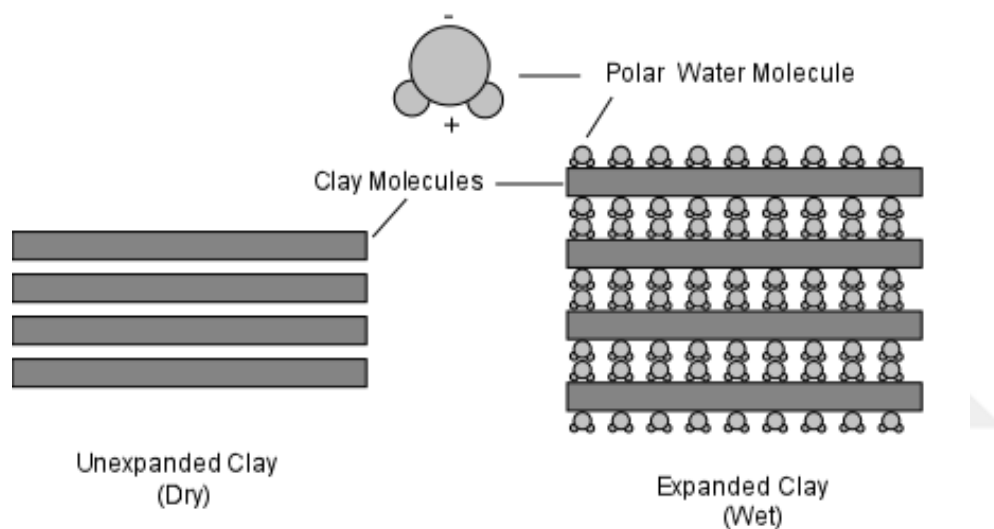


**Figure 2.13 :** The schematic drawing of swelling mechanism (www.geology.arkansas.gov).

The major reasons of the swelling potential of expansive soils are their mineralogy and the chemical structure of the soil. To illustrate, commonly the expansive soil problems occurs where soil has the montmorillonite mineral. Soils with a high percentage of swelling clay have a very high proximity for water partly because of their small size and their positive ions (Day et al., 1999). Generally, the expansive soil swells and sticks when it is wetted, and shrinks with formed of wide open cracks. The expansion depends on the class and amount of clay minerals, their exchangeable ions, electrolyte content of aqueous phase, and the internal structure in terms of mineralogy of clay layers. A general model of swelling process for montmorillonite is given in the Figure 2.14.



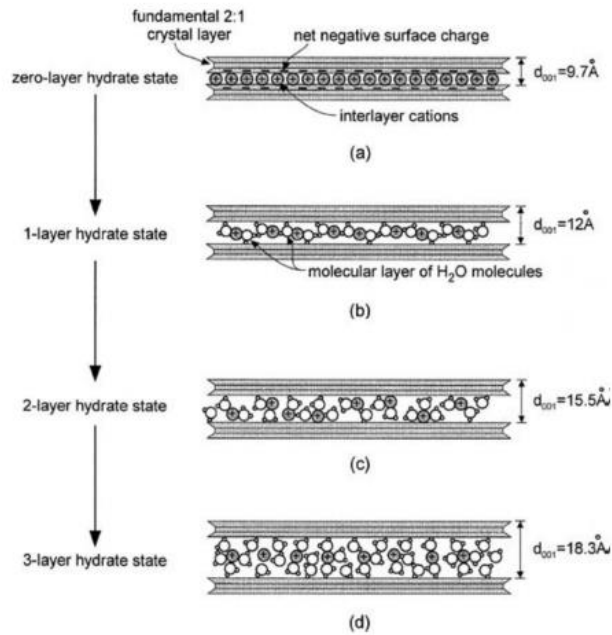


**Figure 2.14 :** Model of swelling process for montmorillonite (Likos, 2004).

Seed et al. (1962), expressed the swelling potential as the percentage of swell of a laterally confined sample which compacted to maximum density at optimum water content in the standard AASHTO compaction test under a 1 Psi surcharge load. Lambe et al (1969), used the swell index which determined as the the slope of the e-log p curve to measure the expansion characteristics of clay. The pressure increment from 1.0 to 0.1  $\text{kg/cm}^2$  was used. A standard method proposed by Holtz (1970), this method includes the oedometer for the tests. The procedure involves the testing of two similar samples, one for loaded and expanded test and the other for expanded and loaded test.

### 2.3.1 Diffuse double layer

Adsorbed cations are held on surfaces of negatively charged clay particles. When negatively charged clay surfaces are approached, cation concentration increases. Positive poles of the water dipoles configured towards the negative clay particle surfaces, this array diminishes with increasing distance from the surface. This increased concentration means that water molecules tend to diffuse toward the surface to equalize concentrations. In the Figure 2.15, distributions of ions adjacent to a clay surface is illustrated.

The charged clay surface and the distributed charge in soil solution are called as the diffuse double layer. Gouy (1910) and Chapman (1913), suggested a theory to analyze

the diffuse double layer. Verwey et al. (1948), focused on diffuse double layer in order to analyze the forces of interaction between particles and determination of the stability. This theory is called as DLVO Theory (Sposito, 1989). Sridharan and Jayadeva (1982), Greathouse et al. (1994) and Tripathy et al. (2004) have contributed to the better understanding of the behaviour of volumetric changes regarding the double layer repulsive forces.

The diffuse double layer theory gives helpful information about the ionic distributions adjacent to clay particles. Flocculation, deflocculation, swelling and the effects of pore water can be investigated. The DLVO theory provides investigations and evaluations related to swelling clay systems with monovalent ions such like Na-montmorillonite. Nonetheless, pH, ion size, particle interference, and forces are neglected in this theory to idealize the conditions.

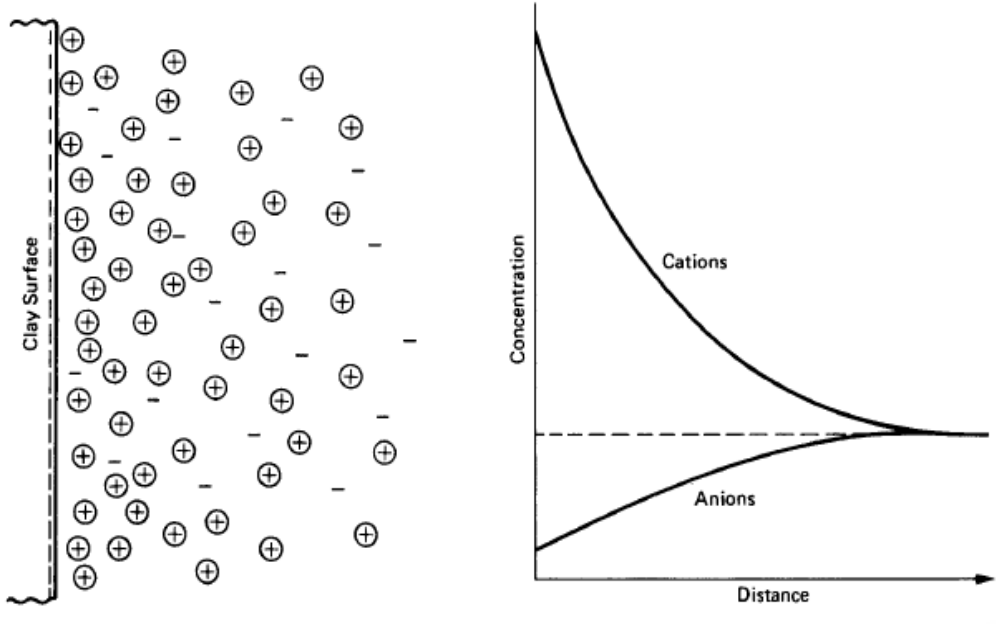


**Figure 2.15 :** Distributions of ions adjacent to a clay surface according to the concept of the diffuse double layer (Mitchell and Soga, 2005).

Mitchell (2005), stated that the thickness of diffuse double layer related with the valence, the concentration the dielectric constant and temperature of the medium. At the same concentration and constant surface charged solutions, a change in cation valence decreases the thickness of the double layer. The permittivity of the pore fluid called as the dielectric constant affects the diffuse layer thickness. In addition to that, diffuse layer thickness increases with the temperature (Mitchell and Soga, 2005).

### 2.3.2 Factors affecting swelling behavior of soil

Swelling behaviour of soil depends on various factors. Nelson and Miller (1992), categorized these factors into three different groups. The first and foremost, soil properties affect the swelling potential of the soil which consists of the clay mineralogy, soil-water chemistry, soil suction, plasticity, dry density, soil structure and fabrics of the soil. Table 2.2 indicates the effects of the soil properties on the swelling potential.

**Table 2.2 :** Effects of the soil properties on the swelling potential (Nelson and Miller, 1992).

<b>Factor</b>	<b>Description</b>	<b>References</b>
<b>Clay mineralogy</b>	Clay minerals, which usually cause changes in soil volume, are montmorillonite, vermiculite and some mixed layer minerals. Illite and kaolinites which are rarely expansive, can be expansive if the particle sizes are highly fine	Grim (1968); Mitchell (1973, 1976) ; Snethen et al. (1977)
<b>Soil-water chemistry</b>	Increased cation concentration and increased cation valence prevents the swelling. To illustrate, Na <sup>+</sup> cations will cause higher swelling than the Mg <sup>2+</sup> cations.	Mitchell (1976)
<b>Soil suction</b>	Soil suction denoted as the negative pore pressure in unsaturated soils which is an variable of effective stress. It is associated with pore size and shape, saturation, gravity, surface tension, electrical and chemical characteristics of the soil particles and water.	Snethen (1980); Fredlund and Morgenstern (1977)
<b>Plasticity</b>	In generale, soils which display plastic behavior over broad range of water content and have high liquid limits have larger potential for swelling and shrinking. Swell potential can be stated by examination of plasticity.	
<b>Soil structure and fabric</b>	Dispersed clays expected to swell less than flocculated clays. Particles that exposed to cementitious reactions decrease the swelling potential. Compaction changes the Fabric and structure of soil.	Johnson and Snethen (1978); Seed et al. (1962)
<b>Dry density</b>	Higher repulsive forces between soil particles derive from the close orientation of the particles which is a result of the higher densities that causes large swelling potential.	Chen (1973); Komornik and David (1969); Uppal (1965)

Secondly, environmental factors have an impact on swelling behavior of soil. Initial and the variable moisture conditions, climate, drainage, water sources, permeability and temperature are the most important members of environmental factors. These factors are briefly explained in the Table 2.3. In general, the active zone which is defined as the upper part of the soil profile exposed to the shrinking and swelling movements. The upper part of the soil profile is not limited against movement at shallow depths. Therefore, the changes in the moisture content can be observed in active zones and it is susceptible to the climatic cycles.

**Table 2.3 :** Effects of the environmental conditions on the swelling potential (Nelson and Miller, 1992).

<b>Factor</b>	<b>Description</b>	<b>References</b>
<b>Initial moisture condition</b>	Higher imminence for water or higher suction is expected from a dried expansive soil, than the same soil at higher water content. On the contrary, a wet soil profile dries, it will lose water effortlessly and shrink more than the dry initial profile.	Nelson and Miller (1992)
<b>Moisture variations</b>	The active zone which is the upper part of the soil profile has importance to identify the thaw. The moisture changes can be observed in these regions broadly.	Johnson (1969)
<b>Climate</b>	The moisture and the depth of seasonal moisture variance rely on the precipitation and evapotranspiration. The maximum swell potential is observed in the subarid climatic zones which have short wet periods.	Holland and Lawrence (1980)
<b>Drainage and manmade water sources</b>	Surface drainage features provide sources of water at the surface. To illustrate, the leakage problems can result in soil to reach water at greater depth.	Krazynski (1980); Donaldson (1965)
<b>Permeability</b>	Migration of water and rates of swell are closely related to the soils which have high permeability.	Wise and Hudson (1971); De Bruijn (1965)
<b>Temperature</b>	Increasing temperature causes moisture to spread over pavements and cooler areas below buildings.	Johnson and Stroman (1976); Hamilton (1969)

As the last group indicated for this classification, stress conditions have great influence on the swelling potential of soil. Stress history, in situ conditions, loading and the soil profile affect the shrink and swell potential of soil (Nelson and Miller, 1992). Table 2.4 expresses these factors briefly.

**Table 2.4 :** Effects of the stress conditions on the swelling potential (Nelson and Miller, 1992).

<b>Factor</b>	<b>Description</b>	<b>References</b>
<b>Stress history</b>	A normally consolidated soil is less expansive than the same overconsolidated soil at the same void ratio. Cycles of wetting and drying procedure is decreasing the swelling pressure, but after some cycles the decreament of swelling will stop and tend to follow a stabilized behaviour. Swell pressure can increase on aging of compacted clays.	Mitchell (1976); Kassiff and Baker (1971)
<b>In situ conditions</b>	In order to presume the results of loading the soil mas or changing the moisture in the soil, the initial stress state is an essential element. It can be determined by the laboratory or in-situ tests.	Johnson (1969)
<b>Loading</b>	The alteration of volume can be represented by the magnitude of surcharge load that will occur for a given moisture content and density. The surcharge loads will reduce swell in order to balance the repulsive forces.	Holtz (1959)
<b>Soil profile</b>	The most drastic volumetric changes will occur if the soil is made from expansive clays. On the contrary, small movements expected if the soil is overlying on the bedrock at shallow depth. The thickness and location of expansive clay affects the potential movement.	Holland and Lawrence (1980)

## 2.4 Identification of Expansive Soils

The identification methods used to determine the swell potential of expansive soils can be sorted into three categories as written in below;

- Mineralogical and chemical methods
- Direct methods (oedometer tests)
- Indirect methods

The first category consists of measurement of mineralogical and chemical properties of soils, such as cation exchange capacity, total potassium content and specific surface area measurements. The second group of identification methods can be stated as geotechnical experimental method which includes oedometer laboratory tests. Lastly, physical properties of soils, such as Atterberg limits are indirect methods to investigate the swelling potential of soil. Common laboratory tests for the identification of expansive soils is given in the Table 2.5.

**Table 2.5 :** Laboratory tests used for the identification of expansive soils (Nelson and Miller, 1992).

Test	Reference	Properties Investigated	Parameters Determined
Atterberg Limits	ASTM Standards 1991 ASTM D-4038	Plasticity, consistency, upper limit water content of plasticity	Plasticity index
Plastic Limit (PL)	ASTM D-4318	Lower limit water content of plasticity	$LI = \frac{w-LL}{LL-PL} =$ Liquidity index
Shrinkage Limit	ASTM D-427	Lower limit water content of soil shrinkage	R= shrinkage ratio LS=linearshrinkage
Clay content	ASTM D-422	Distribution of fine-grained particle sizes	Percent finer than 2 $\mu$ m
Mineralogical tests	Whiting (1964)	Mineralogy of clay particles	
X-ray diffraction	ASTM STP (1970)	Characteristic crystal dimensions	Basal spacings
Differential thermal analysis	Barshad (1965)	Characteristic reactions to heat treatments	Area and amplitude of reaction peaks and thermograms
Electron microscopy	McCrone & Delly (1973)	Size and shape of clay particles	Visual record of particles
Cation-exchange capacity	Chapman (1965)	Charge deficiency and surface activity of clay particle	CEC (meq/100 g)
Free swell test	Holtz and Gibbs (1956)	Swell upon wetting of unconsolidated unconfined sample of air dried soil	Free swell = $(V_{sat} - V_{dry})/V_{dry} * 100\%$
Potential volume change meter	Lambe (1960)	One dimensional swell and pressure of compacted, remolded sample under semi-strain controlled conditions	Swell index (SI) Potential volume change (PVC)

**Table 2.5 (continued):** Laboratory tests used for the identification of expansive soils (Nelson and Miller, 1992).

Expansion index test	Uniform Building Code	One dimensional swell under 1 psi surcharge of sample compacted to 50% saturation initially	Expansion Index (EI)
California bearing ratio test	Yoder and Witczak (1975); Kassiff et al (1969)	One dimensional swell under surcharge pressure of compacted, remolded samples on partial wetting	Percent swell CBR (%)
Coefficient of linear extensibility (COLE) test	Brasher et al. (1966)	Linear strain of a natural soil when dried from 5 psi (33kPa) to oven dried suction	COLE and LE (%)

#### 2.4.1 Mineralogical and chemical identification methods

The mineralogy of a clay can be explained on the basis of crystal structure or by means of chemical analysis. The negative electric charges on the surface of the clay minerals, the cation exchange capacity and the strength of the interlayer bondings associate with the swelling potential of the clay layers. Nevertheless, these methods are that not sufficient to evaluate natural soil but it is beneficial for the evaluation of the material itself. The five common mineralogical methods can be stated as below;

- X-ray diffraction (XRD),
- Differential thermal analysis (DTA),
- Dye adsorption (MBT), and
- Electron microscope resolution (SEM).

The most common chemical methods that are used to identify clay minerals be listed as below;

- Cation exchange capacity (CEC),
- Specific surface area (SSA), and
- Total potassium (TP).

These methods are described in the following sections.

### 2.4.1.1 X-ray diffraction (XRD)

The most commonly preferred method for identification of clay minerals is X-ray diffraction (XRD). X-rays have wavelengths in the range of 0.01 to 100 Å (Mitchell and Soga, 2005). Two phenomena take place when electrons affect on a material;

- The target materials inner shell electron dislocates from its initial condition as the electron strikes. Afterwards, an electron from the outer shells falls into the vacancy to lower the energy state of the atom. An X-ray photon of wavelength and the particular position is emitted. Every shell has its own characteristic frequency, therefore, relationship between the intensity of radiation and wavelengths are shown in the Figure 2.16.
- The high-speed electron slows down in the electric fields near of the atomic core. This loss of energy generated to to heat and to X-ray photons.

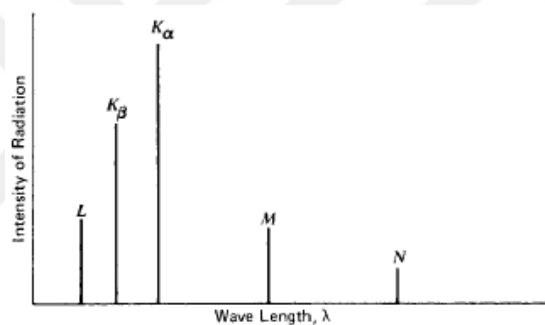


**Figure 2.16 :** X-ray generation by electron displacement (Mitchell and Soga, 2005).

X-ray diffraction is adequate for determination of clay minerals because each clay mineral group has the unique spacings. Therefore, the results can be interpreted easily. X-ray diffraction data for the clay minerals are provided by Grim (1968), Brindley and Brown (1980), Whittig and Allardice (1986), and Moore and Reynolds (1989). Geometrical display of an X-ray diffraction stated in the Figure 2.17.

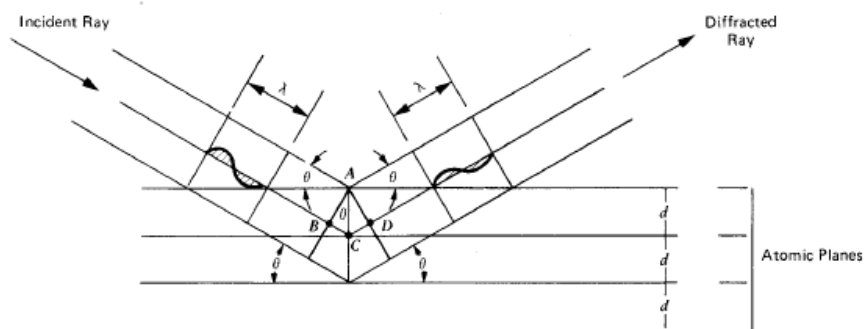


**Figure 2.17 :** Geometrical display of X-ray diffraction (Mitchell and Soga, 2005).



#### **2.4.1.2 Differential thermal analysis (DTA)**

Differential thermal analysis (DTA) can be done by simultaneously heating a test sample and a thermally neutral material at constant rate (commonly  $10^{\circ}\text{C}/\text{min}$ ) to over  $1000^{\circ}\text{C}$  and continuously scaling the differences in temperature between the sample and the neutral material. Differences in temperature between the sample and the neutral material reflect reactions in the sample because of the heating. Every mineral reflects unique endothermic and exothermic reactions (Mitchell and Soga, 2005). Differential thermal analysis can be useful when a material that can not be identified properly with one mineralogical method. For instance, DTA can be conducted in conjunction with XRD in order to identify the relatively difficult materials.

#### **2.4.1.3 Dye adsorption**

Numerous dyes have been used to trace water and identification of soils. The color contrast of the dye with soil is essential for this analysis. Bouma et al. (1977) used methylene blue to interpret macropores. Methylene blue is well-known to be rapidly and strongly adsorbed in the soil particles due to its cationic nature. Specific surface area and cation exchange capacity of clay changes according to the clay type and the amount of clay minerals, which can be traced by using blue methylene solution. Methylene blue test can be stated as another technique for identification of the cation exchange capacity of a clay soil (Cokca and Birand, 1993). This method does not involve expensive test apparatus and procedures. Correlations between soil index properties and methylene blue value (MBV) is very advantageous for investigation of expansive behavior of soil. Methylene blue test provides information about determination of specific surface area (Chiappone et al., 2004; Yukselen and Kaya, 2008), cation exchange capacity (Cokca and Birand, 1993), swell potential (Cokca, 2002; Cokca and Birand, 1993).

Other researchers have used dyes such as Lissamine Yellow FF (Trudgill, 1987) Pyranine (Omoti and Wild, 1979), Rhodamine WT (Smart and Laidlaw, 1977) and Brilliant Blue FCF (Flury et al., 1994), to analyse flow paths in the soil.

#### **2.4.1.4 Scanning electron microscope (SEM)**

Electron microscopes can focus on distances less than  $100 \text{ \AA}$ , which leads to researchers be able to work on clay particles. The main purpose of the microscopic examination is to determine mineralogic composition, texture and internal structure. Electron diffraction can be also useful which is similar to X-ray diffraction. The only

difference is an electron beam used instead of an X-ray beam. (Mitchell and Soga, 2005). Secondary electrons emitted from a sample surface form to be three-dimensional images in the SEM. The SEM has a x20 to x150,000 magnification range and a depth of field 300 times greater than that of the light microscope. SEM is widely used due to direct investigation of the clay particles and fractures of these elements can be observed through it. The example SEM images of kaolinite in order of increasing magnification is given in the Figures 2.18.

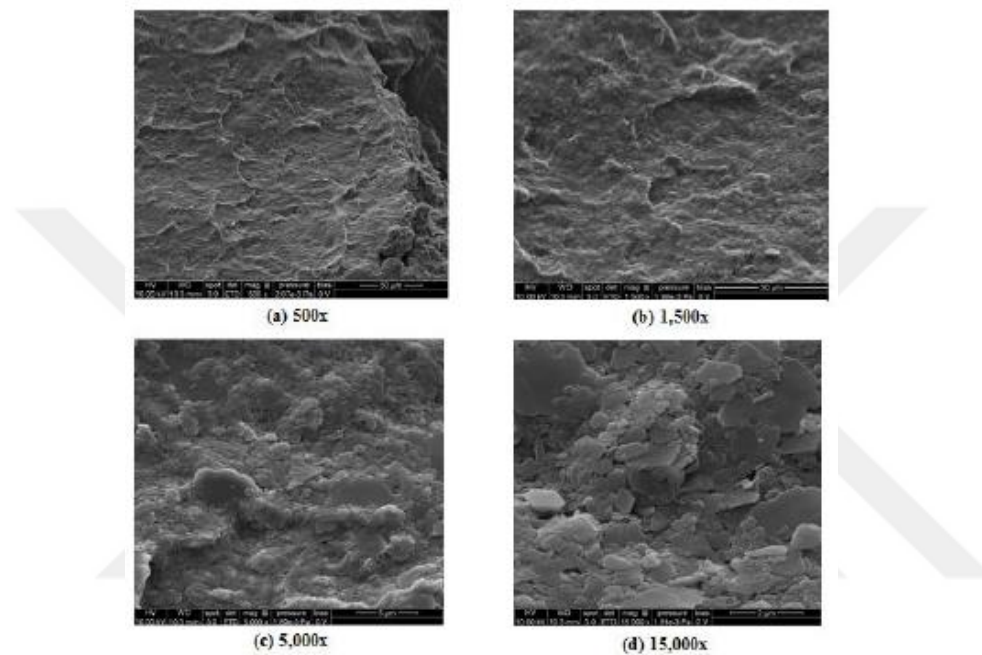


**Figure 2.18** : SEM images of kaolinite in order of increasing magnification (Velasco, 2013).

Ravina I. (1973), worked on the mineralogical composition of expansive clays by the use of the scanning electron microscope. Studies showed that the nonswelling clays appear as flat, thick plates while montmorillonite have a crinkly, ridged, honeycomb-like textures. Observing the degree of crinkling and interparticle bonding from scanning electron microscope can be used for the interpretation of expansive clays (Chen, 1988).

#### **2.4.1.5 Cation exchange capacity (CEC)**

The Cation exchange capacity (CEC) identified as the total number of exchangeable cations required to balance the negative charge on the surface of the clay particles. Milliequivalents per 100 grams of dry clay is the unit of CEC. One milliequivalent is defined as one milligram of hydrogen or any ion that will combine with one milligram

of hydrogen (Oweis et al. 1998). In the test procedure, redundant salts are removed from the soil and a known cation is replaced with the adsorbed cations by saturating the soil exchange areas (Nelson et al., 2015).

If a clay mineral is more active than other such like montmorillonite, a higher CEC value expected after the test results. Generally, swelling potential increases with the increasing CEC values. For the three common clay minerals, values of CEC are given in the Table 2.6 (Mitchell and Soga 2005).

**Table 2.6 :** Typical Values of CEC, SSA, and TP for Clay Minerals (Mitchell and Soga 2005).

Clay Mineral	Cation Exchange Capacity (CEC) (meq/100 g)	Specific Surface Area (SSA) (m <sup>2</sup> /g)	Total Potassium (TP) (%)
Kaolinite	1–6	5–55	0
Illite	15–50	80–120	6
Montmorillonite	80–150	600–800	0

McKeen and Hamberg (1981) developed a system that is based on engineering properties of soils and CEC. As a result of the studies which were conducted to define mineralogical groups, the chart was developed by assigning COLE values to different areas on a graph that consists of activity versus cation exchange activity to point out potentially expansive soils, stated in the Figure 2.19 (Nelson et al., 2015).

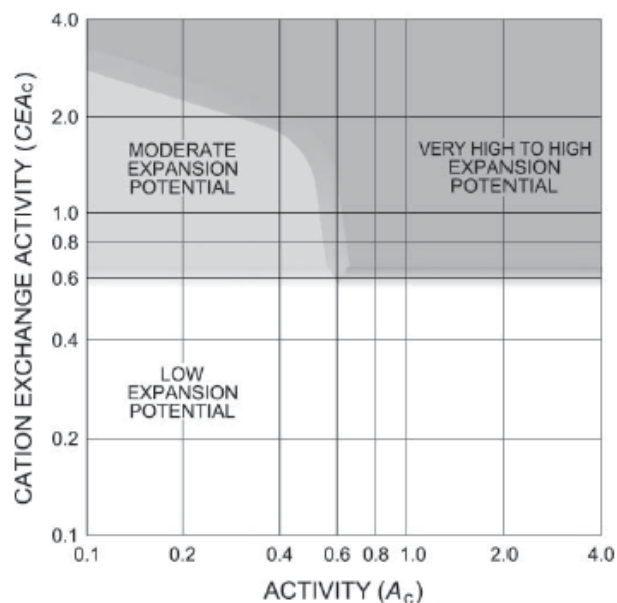


**Figure 2.19 :** Expansion potential as indicated by clay activity and  $CEA_c$  (Nelson et al., 2015).

The main problems that can be encountered during the measurement of CEC can be stated as follows,

- The presence of soluble salts and carbonates,
- The effect of cation and anion type,
- The pH effect and the use of buffered solutions and

Grim (1968) determined the order of replaceability of the common cations in clays from most to least easy cations as;

$\text{Li}^+ > \text{Na}^+ > \text{K}^+ > \text{Rb}^+ > \text{Cs}^+ > \text{Ca}^{++} > \text{Sr}^{++} > \text{Ba}^{++} > \text{H}^+$

Na-montmorillonite swells more than Ca-montmorillonite because the calcium cation is strongly adsorbed compared to the sodium cations.

#### **2.4.1.6 Specific surface area (SSA)**

The total surface area of soil particles in a unit mass of soil stated as the specific surface area (SSA). High SSA causes high water retention capacity that is one of the major factors of potential expansive movements of soil (Chittoori and Puppala 2011). Nevertheless, if a soil has a high organic part, that may have a highly reactive surface can cause a high SSA. Therefore, SSA must be used in conjunction with other laboratory tests to identify the potential swell accurately. The montmorillonite minerals have an SSA about 10 times higher than the kaolinite group (Nelson et al., 2015).

#### **2.4.1.7 Total potassium (TP)**

The Total Potassium method just used to identify the illite minerals. Because the only clay mineral that includes potassium is illite. Therefore, this method provides the amount of potassium ions and gives information about the presence of illite (Chittoori and Puppala 2011). In addition to this, high potassium content represents low expansion potential.

#### **2.4.2 Direct methods (oedometer tests)**

The swelling potential and swelling pressure of an expansive clay can be investigated most accurately by using direct measurements which involves the use of the one-dimensional consolidometer. Throughout the experimental researches, numerous

loadings and surcharge loads have been used to represent the site conditions. Various test procedures explained in the Table 2.7. The swell test consists of unsaturated soil's initial loading phase. After the loading, sample allowed to swell when water is added under the specified load. Overburden load can be stated with this initial loading. Further loads can be applied depending on requirements of the experimental studies. Conventionally, the swelling pressure is expressed as the pressure that need to reverse the condition of sample to initial state (Nelson et al. 1995).

**Table 2.7 : Swell prediction tests using oedometers (Nelson et al. 1995).**

<b>Test Name</b>	<b>Description</b>	<b>Reference</b>
Double oedometer method	Two tests performed on adjacent samples; a consolidation-swell test under a small surcharge pressure and a consolidation test, performed in the conventional manner but at natural moisture content.	Jennings and Knight (1957)
Volumenometer method	In specialized apparatus, air-dried samples were filled with water under overburden pressure slowly	DeBruijn (1961)
Sullivan and McClelland method	Constant volume test, samples initially at overburden pressure on inundation	Sullivan and McClelland (1969)
USBR method	Double sample test, a consolidation-swell under light load, and a constant volume test	Gibbs (1973)
Simple oedometer	Improved from double oedometer test. Single sample loaded to overburden, then unloaded to constant seating load and allowed to swell, followed by consolidation procedure	Jennings et al. (1973)
Controlled strain test	Constant volume swell pressure obtained by incremental, strain-controlled pressure reduction	Porter and Nelson (1980)
University of Saskatchewan	Constant volume test. Analysis corrects for sample disturbance and apparatus deflection characteristic reactions to heat treatments	Fredlund et al. (1980)

Essential factors that affect the swelling tests indicated as below;

1. Sample Condition

Undisturbed sample reflects the in-situ conditions of soil and the stress history but disturbed samples do not represent these conditions.

2. Water Content

The duration of sample's waiting period inside the ring before wetting, the developing of evaporation and the temperature and humidity conditions of laboratory affect the the initial water content of sample.

### 3. Surcharge load

The swelling pressure will decrease as the increasing load applied.

### 4. Duration of Test

The duration for the completion of swell tests is one of the most essential factor that affects the results of the tests. It depends on the permeability of the clay, the water content, the dry density and thickness of the sample (Chen, 1988).

Jenning and Knight (1957), used the oedometer for determination of expansive soil's swelling pressure. The swelling pressure expressed as during the wetting process, applied pressure that prohibit the specimen from additional swelling movements. In another procedure that the soil specimen is permitted to swell under a force, thereafter increasing the loads until the soil specimen is in its initial state. This test referred as consolidation swell test. The swelling pressure determined as the final applied force on the specimen during the process (Chen, 1988). Knight (1957) recommended a method which consists of two normally consolidated and similar samples and focused on the void ratio versus applied effective pressure on the specimens. This application is referred as the double oedometer test.

Undisturbed samples tend to have higher swelling potential than the disturbed samples. It was displayed that the increasing dry unit weight of the soil and clay content of the soil increases the swelling pressure. Though the surcharge load and initial water content have opposite effects to swelling pressure (El-Sohby and El-Sayed, 1981; Basma et al, 1995). Basma et al (1995), conducted a restrained swelling test that consists of a compacted sample under incremental forces until it reaches equilibrium state of deformation, after the specimen is exposed to water and waited for fully swelling behavior occurs. The ratio of the maximum expansion to its initial height termed as the swelling potential of the soil.

The most commonly used methods are specified by ASTM standards. ASTM D-4546 provides three alternative test methods for determination of the swell pressure. The sample should be confined and loaded axially through the experiment for all three test

methods. These methods are Method A, Method B and Method C mentioned and explained in below, respectively.

#### 2.4.2.1 Method A

Method A widely used to determine the one-dimensional wetting-induced swell of compacted or natural soils for different vertical stresses. The sample is submerged in the water and left to swell with a 1 kPa load until the primary swelling is completed. After end of the primary swelling is completed, loads applied up to reaching the initial void ratio and initial height is acquired. Four or more samples can be used by applying different loads to different specimens until the primary swell is completed under the constant vertical stress. The final deformations and water contents and dry densities are recorded. Figure 2.20 shows the deformation versus vertical stress curve due to vertical loading by using the method A.

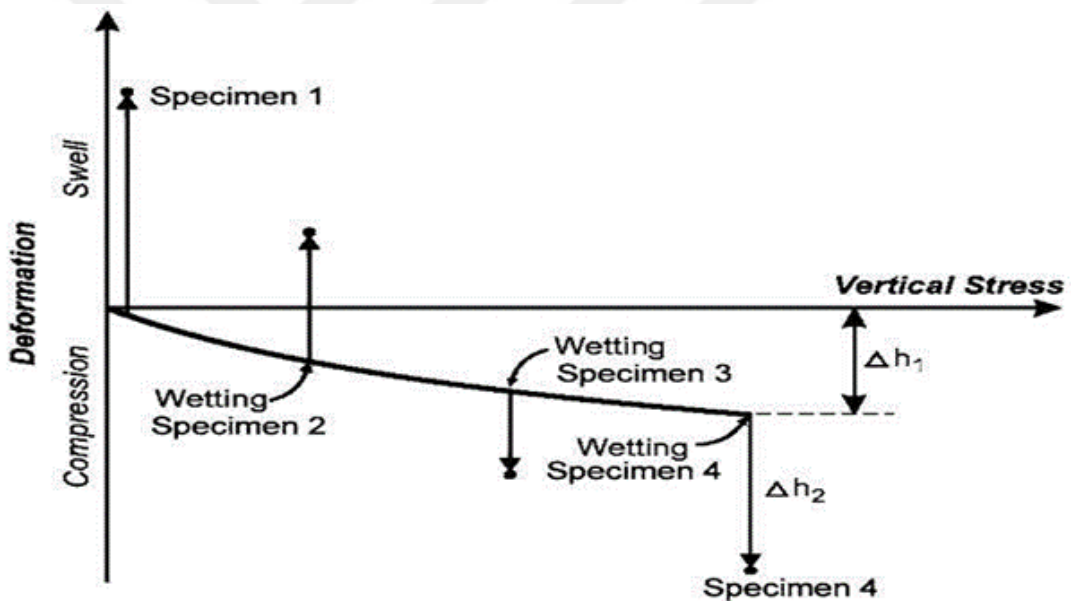


**Figure 2.20 :** Deformation versus vertical stress, method A (ASTM, 2014).

#### 2.4.2.2 Method B

Method B consists of a vertical pressure which is equivalent to the in-situ vertical overburden pressure. Afterwards, the sample is permitted to get in contact with water and allowed to be submerged. After achieving the stable condition which can be stated that movements become insignificant for measuring the expansion or settlements at the applied forces. The swelling pressure is determined by applying the final load which will originate the initial height of the sample. Figure 2.21 shows the deformation versus vertical stress curve due to vertical loading by using the method B.

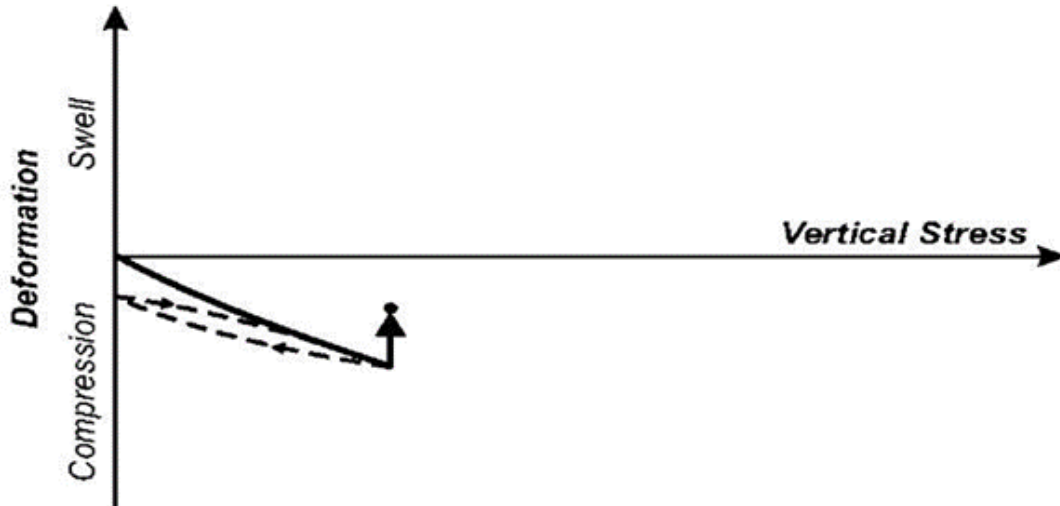


**Figure 2.21** : Deformation versus vertical stress, method B (ASTM, 2014).

### 2.4.2.3 Method C

This method is the most commonly used method for determining the swelling pressure. This method can be stated as loading-after-wetting test. The procedure of method C includes the samples height remained constant by applying vertical loads after the sample get in contact with the water and submerged into it. Therefore, volume of the sample will not change during the test. The pressure that do not perform any volumetric change on the soil sample and maintain the initial height can be stated as the swelling pressure. Figure 2.22 shows the deformation versus vertical stress curve due to vertical loading by using the method C.

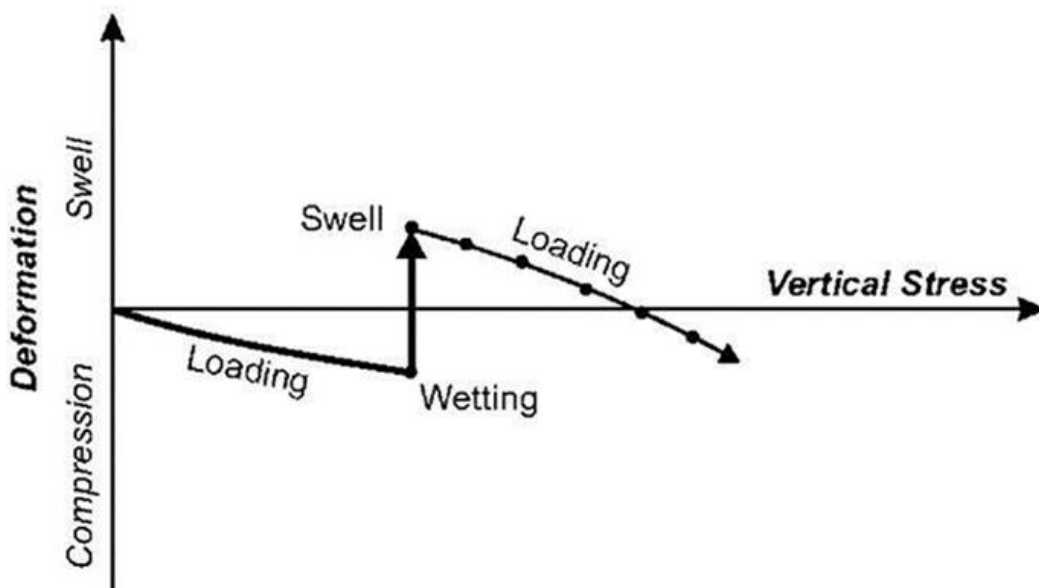


**Figure 2.22** : Deformation versus vertical stress, method C (ASTM, 2014).



### **2.4.3 Indirect methods**

Index properties, pvc method and activity method can be given as members of indirect methods for evaluating the swelling properties of soil. None of the indirect methods should be used independently. Direct methods offer the most useful data for a practicing engineer. The tests are simple to perform and do not require any costly laboratory equipment. Still, a large number of test samples need to be prepared to minimize the error rate of tests.

#### **2.4.3.1 Classification based on index properties tests**

Soil property tests can be used for the evaluation of the swelling potential of expansive soils. Such tests may include:

- Atterberg limits tests and
- Colloid content tests

A qualitative evaluation of the degree of possible expansion of soils is given in numerous classification systems to ensure the rating of expansive movements. In the literature, expansion ratings commonly stated as "high," "medium," and "low" for alternative conditions.

#### **Atterberg Limit Tests**

Atterberg limit tests are very common and frequently exhibited test so as to estimate the swell potential of soils. Numerous researches have used the index properties of soil in order to identify the swell potential. Holtz and Gibbs (1956), showed that liquid limit and plasticity index are advantageous parameters for determining the swelling behavior of clay. Table 2.8 shows the observations that combines the data from index tests and degree of soil expansions which prepared by Holtz and Gibbs (1956). Altmeyer (1955) suggested the relationship between the shrinkage limit or linear shrinkage to probable swell by percentage which is indicated in the Table 2.9. A correlation was generated by Chen (1965), that consists of the liquid limit, standard penetration blow count numbers and the sample passed from the sieve no.200 to estimate the potential expansion (Table 2.10). In 1988, Chen also created a method for identifying the potentially swelling soils by just using the plasticity index. The approaches of many researchers to investigate the relationship between swelling potential and the plasticity index of soils are shown in the Table 2.10.

**Table 2.8 :** Expansive soil classification based on colloid content, plasticity index and shrinkage limit (Holtz and Gibbs, 1956).

<b>Colloid Content (% minus 0.0001 mm)*</b>	<b>Plasticity Index (%)*</b>	<b>Shrinkage Limit (%)*</b>	<b>Probable Expansion (Total Volume Change %)</b>	<b>Degree of Expansion</b>
>28	> 35	< 11	> 30	Very High
20-31	25 – 41	7 – 12	20 – 30	High
13 – 23	15 – 28	10 – 16	10 – 20	Medium
< 15	< 18	> 15	< 10	Low

\*Based on Vertical Loading of 1.0 psi

**Table 2.9 :** Expansive soil classification based on shrinkage limit or linear shrinkage (Altmeyer, 1955).

<b>Linear Shrinkage</b>	<b>Shrinkage Limit (%)</b>	<b>Probable Swell (%)</b>	<b>Degree of Expansion</b>
< 5	> 12	< 0.5	Noncritical
5 – 8	10 – 12	0.5 – 1.5	Marginal
> 8	< 10	> 1.5	Critical

Snethen et al. ( 1977) stated that liquid limit and plasticity index are the most convenient parameters to identify the swelling potential of soil. In-situ soil suction indicates the environmental conditions of soil sample which is an important factor for evaluating the swell potential of soils. Results of the research is shown in the Table 2.11. Common plasticity characteristics of clay minerals are given in the Figure 2.23.

**Table 2.10 :** Relationship between plasticity index and degree of expansion (Chen, 1988).

<b>Degree of Expansion</b>	<b>Plasticity Index (%)</b>			
	<b>Holts and Gibbs (1956)</b>	<b>Seed et al. (1962)</b>	<b>Raman (1967)</b>	<b>Chen (1975)</b>
<b>Low</b>	< 20	< 10	< 12	0 – 15
<b>Medium</b>	12 – 34	10 – 20	12 – 23	10 – 35
<b>High</b>	23 – 45	20 – 35	23 – 32	20 – 55
<b>Very High</b>	> 32	> 35	> 40	> 35

**Table 2.11 :** Expansive soil classification based on liquid limit, plasticity index and in-situ suction (Snethen et al. 1977).

LL (%)	PI (%)	$\mu_{nat}$ (soil suction at natural moisture content)	Potential Swell (%)	Potential Swell Classification
> 60	> 35	> 4	> 1.5	High
50 – 60	25 – 35	1.5 – 4	0.5 – 1.5	Marginal
> 50	< 25	< 1.5	< 0.5	Low

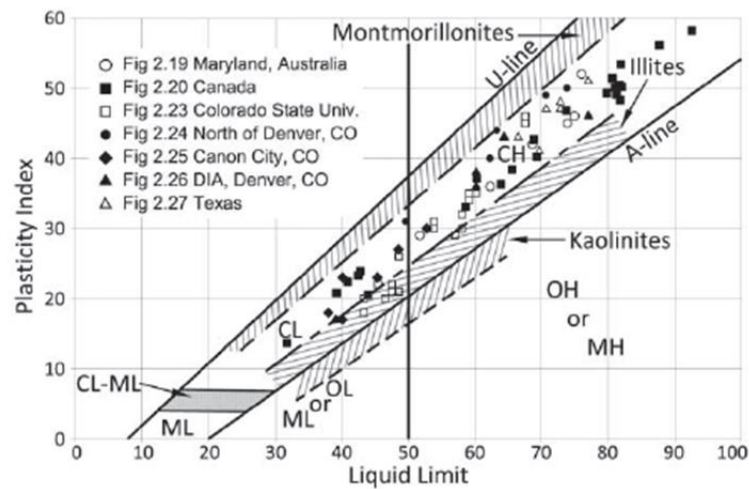


**Figure 2.23 :** Plasticity characteristics of clay minerals (Holtz et al., 2011).

Skempton (1953), defined the activity by using the Atterberg limits and clay contents which is stated in the Equation 2.1, as follows;

$$A = \frac{PI}{\% \text{ by weight finer than } 2 \mu m} \quad (2.1)$$

Where;

A : Activity

PI : Plasticity Index

Skempton proposed three different classes based on the activity results. If a soil's activity resulted in between 0.75 and 1.25, stated as normal. If it is smaller than 0.75, described as inactive. Lastly, if the activity is greater than 1.25, the class is designated as active. The most expansive clays belong to active group. In the Table 2.12, different activity values are given for different clay mineral types. Based on the percentage of clay and activity, a correlation is given in the Figure 2.24 (Seed et al., 1962).

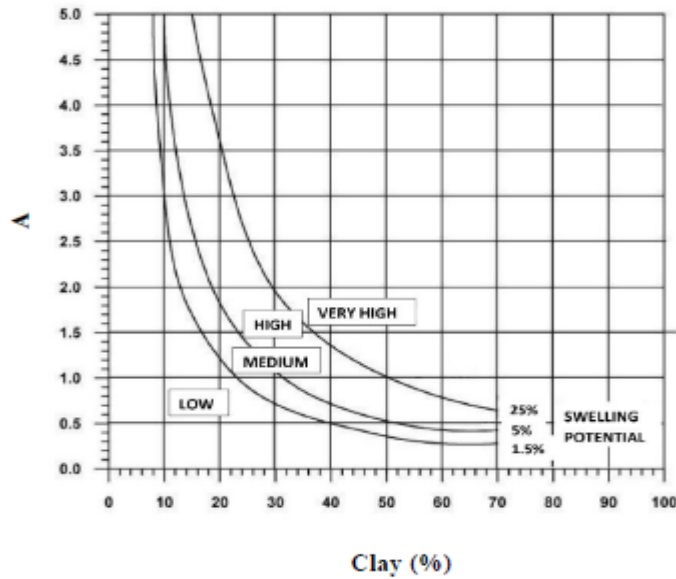


**Figure 2.24 :** Classification chart based on activity and percentage of clay (Seed et al., 1962).

**Table 2.12 :** Typical values of activities for various clay minerals zone (Nelson and Miller, 1992).

Mineral	Activity
Kaolinite	0.33 to 0.46
Illite	0.9
Montmorillonite (Ca)	1.5
Montmorillonite (Na)	7.2

### Colloid content tests

The equation 2.2 expresses the relationship between the percentage of clay size and swelling potential of any given clay.

$$S = KC^X \quad (2.2)$$

Where,

C = Percentage of clay particles size, determined by a hydrometer test

X = An exponent depending on the type of clay, and

K= Expansion coefficient depending on the type of clay.

S = Swelling potential, stated as percentage of swell under 1 psi surcharge for a sample which compacted according to the AASHTO.

Numerous researchers had done experimental studies to make correlations between the swelling potentials and engineering parameters of various soils. To the extent that, Skempton (1953), also contributed by proposing a chart regarding the plasticity index and the clay content of soil (Figure 2.25). Van der Merwe (1964), made a chart that expresses the relationship between plasticity index and the clay content of expansive soils (Figure 2.26). In addition to that, Dakshanamurthy and Raman (1973), constituted a classification chart that based on the index properties (Figure 2.27).

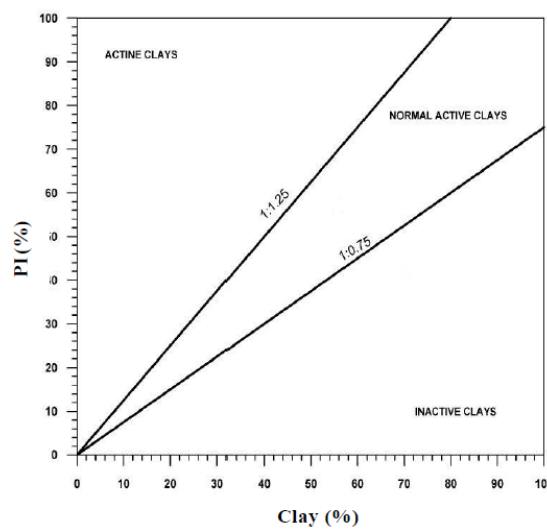


**Figure 2.25 :** Classification chart based on plasticity index and clay content (Skempton, 1953).

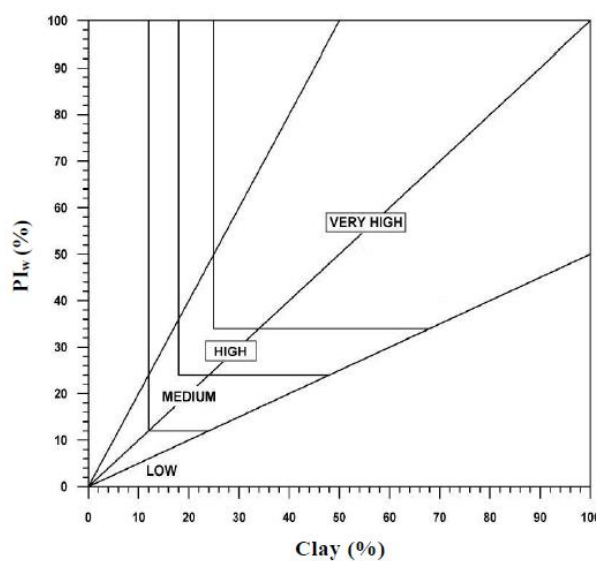


**Figure 2.26 :** Classification chart based on weighted plasticity index and clay content (Van der Merwe, 1964).

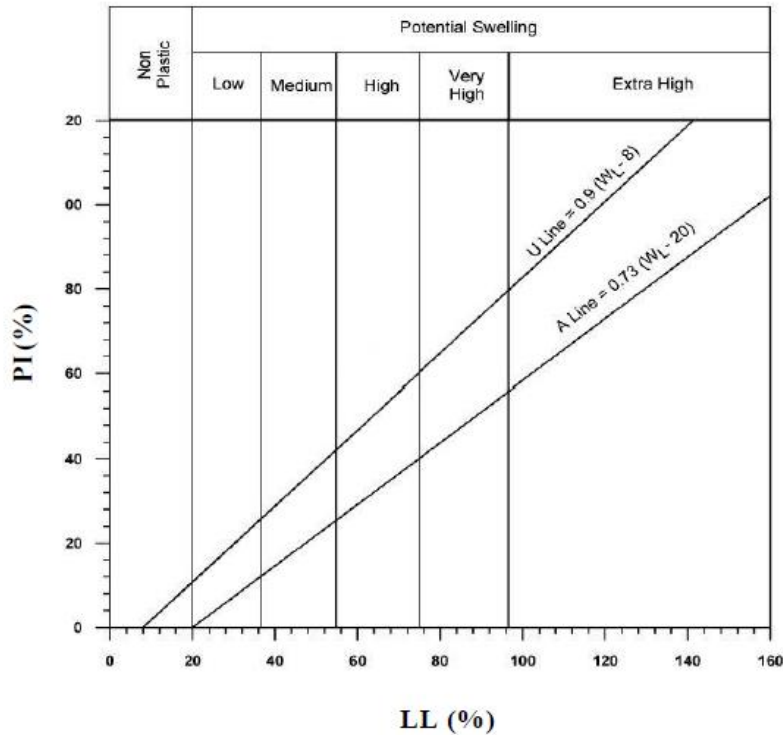


**Figure 2.27 :** Classification chart based on plasticity index and liquid limit (Dakshanamurthy and Raman, 1973).

#### 2.4.3.2 Free swell tests

Free swell test can be described as which consists of one dimensional consolidometer used as an instrument so as to identify the swelling behavior of soil (Chen, 1975).

To summarize the procedure of the test, 10 cm<sup>3</sup> oven dried sample which passed through the sieve no.40 placed into 100 cm<sup>3</sup> graduated cylinder and let the sample absorb the water. The free swell value is defined as the percentage of initial soil volume which is estimated by the subtraction of final state and initial state of soil (Nelson and Miller, 1992). The free swell test parameters expressed in the Equation 2.3.

$$FS = [(V - V_0) / V_0] \times 100 \quad (2.3)$$

Where,

V: Sediment volume of 10 g of oven dried soil passed through sieve No. 40 placed into graduated cylinder which contains distilled water

V<sub>0</sub>: Volume of dry soil

One of the very first implementations of this test was conducted by Holtz and Gibbs (1956), asserted that high swelling commercial bentonite has a free swell value of from

1200 to 2000 percent. Afterwards, they indicated that soils can show expansive movements under light loadings when they exposed to water especially which acquires free swell value as low as 100 percent. In spite of that, volumetric changes does not expected if soils having free swell value below 50 percent under light loadings. In contrast with this information, Dawson (1953), made several free swell tests with Texas clays and mentioned that harsh climatic factors in conjunction with the expansion characteristics of the soil can drastically affect the swelling behavior of the clay. Researcher stated that Texas clays have free swell values are in between the range of 50 percent.

The free swell index (FSI) method determines the swell potential of expansive soils indirectly. This process consists of two 10 g of oven dried soil specimens. One of the sample get in contact with the distilled water while other with kerosene in the graduated jars with distilled water. After at least 24 hours the final volume of the samples recorded and free swell index can be determined by using the following Equation 2.4, stated in below.

$$FSI = [(V - V_k) / V_k] \times 100 \quad (2.4)$$

Where,

V: Sediment volume of 10 g of oven dried soil passed through sieve No. 40 placed into graduated cylinder which contains distilled water

V<sub>k</sub>: Sediment volume of 10 g of oven dried soil passed through sieve No. 40 placed into graduated cylinder which contains kerosene.

From the Table 2.13, swelling potentials of soils based on the free swell index can be viewed. In the Table 2.14, typical free swell values for common clay minerals exhibited.

Sridharan et al. (1986) suggested a rapid method to identify clay type in soils by the free-swell technique called modified free swell index (MFSI). This method arise from the ratio between the equilibrium soil volume to the dry weight of the soil. The MFSI explained in the Equation 2.5 and Table 2.15 gives information about the soil expansivity classification based on MFSI.

$$MFSI = V/10 \quad (2.5)$$

**Table 2.13 :** Expansion potential based on free swell index (Nelson et al., 2015).

Free Swell Index (FSI)	Expansion Potential
< 20	< 20 Low
20–35	Medium
35–50	High
> 50	Very high

**Table 2.14 :** Typical values of free swell for clay minerals (Grim, 1968; Shamburger et al., 1975).

Clay Mineral	Free Swell (%)	
	Grim (1968)	Shamburger et al. (1975)
Na-montmorillonite	1400–2000	1400–1600
Ca-montmorillonite	45–145	65–145
Illite	60–120	60–120
Kaolinite	5–60	5–60

**Table 2.15 :** The soil expansivity classification based on MFSI (Sridharan et al., 1986).

MFSI (cm <sup>3</sup> /g)	Sediment volume in carbon tetrachloride (cm <sup>3</sup> /g)	Clay type	Soil expansivity
<1.5	1.10-3.00	Non-swelling	Negligible
1.5-2.0	>1.1 and <MFSI	Mixture of swelling and non-swelling	Low
1.5-2	<1.1	Swelling	Moderate
2.0-4.0	<1.1	Swelling	High
>4.0	<1.1	Swelling	Very High

#### 2.4.3.3 Potential volume change (PVC)

T. W. Lambe (1960), proposed a method called the potential volume change (PVC). Swelling pressure of a compacted sample can be measured by using the soil PVC meter



and can be adapted for the field or laboratory conditions. The procedure of the test includes placing a remolded soil sample into a consolidometer ring. The sample is permitted to swell against a proving ring after the wetting. The swell index is stated as the pressure on the ring and is correlated to potential volume change using the chart shown in the Figure 2.28 and Table 2.16 (Nelson and Miller, 1992).

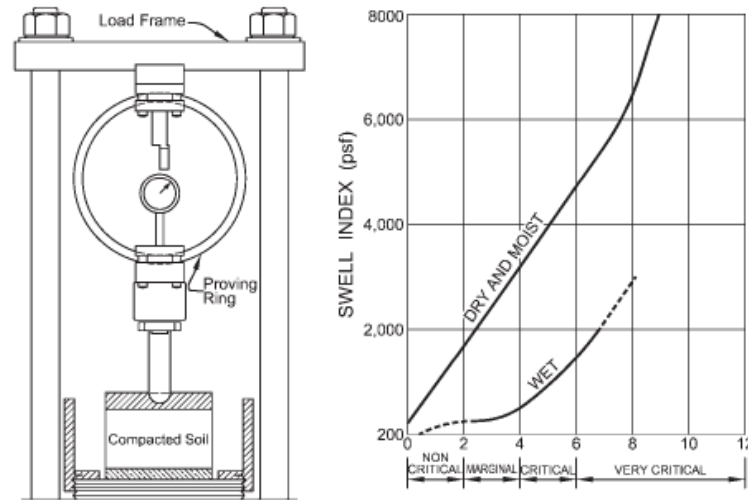


**Figure 2.28** : PVC apparatus and swell index versus PVC (Lambe, 1960).

**Table 2.16** : Swelling potential according to PVC values (Nelson and Miller, 1992).

PVC	Category
< 2	Not Critical
2 - 4	Marginal
4 - 6	Critical
> 6	Very Critical

#### 2.4.3.4 Expansion index (EI) test

The expansion index test was developed which is similar to the potential volume change (PVC) test, but in EI Test under constant surcharge load the swelling is allowed (Nelson et al., 2015). Soil passed through the sieve no.4 and brought to approximately the optimum water content. Then soil sample must be cured for 6 to 30 hours and compacted. After this process, the sample must be saturated to %50. A vertical stress of 6.9 kPa is applied on the sample and wetted. For 24 hours, volume changes need to be recorded. Finally The EI can be determined from the Equation 2.6.

$$EI = 100 \times \Delta h \times F \quad (2.6)$$

Where;

$\Delta h$ : Percentage of swell

F: Fraction passing No.4 Sieve

The Uniform Building Code (1997) indicates that if an expansion index greater than 20, specific design must be considered so that ensure the stability of structures constructed on these soils. Classification and determination of the expansive soils regarding the expansion index is shown in the Table 2.17. Sridharan and Prakash (2000), proposed an expansive soil classification based on oedometer percent expansion that is given in the Table 2.18

**Table 2.17 :** Classification of the expansive soils regarding the expansion index (ASTM, 2011).

<b>Expansion Index</b>	<b>EI Potential Expansion</b>
0-20	Very Low
21-50	Low
51-90	Medium
91-130	High
>130	Very High

**Table 2.18 :** Proposed expansive soil classification based on oedometer percent expansion (Sridharan and Prakash, 2000).

<b>Oedometer expansion (%)</b>	<b>Free swell ratio</b>	<b>Clay type</b>	<b>Soil expansivity</b>
<1	<1.0	Non-swelling	Negligible
1-5	1.0-1.5	Mixture of swelling and non-swelling	Low
5-15	1.5-2.0	Swelling	Moderate

**Table 2.18 (continued) :** Proposed expansive soil classification based on oedometer percent expansion (Sridharan and Prakash, 2000).

Oedometer expansion (%)	Free swell ratio	Clay type	Soil expansivity
15-25	2.0-4.0	Swelling	High
>25	>4.0	Swelling	Very high

#### 2.4.3.5 Standard absorption moisture content (SAMC)

Yao et al. (2004), proposed a method that was published in China's Specifications for Design of Highway Subgrades. Standard absorption moisture content (SAMC) is the equilibrium water content of a soil under standard conditions. Undisturbed soil sample placed on a porous plate within a constant humidity container over a saturated solution of sodium bromide. Two measurements of the weight of the soil sample must be done when the equilibrium state occurs and after the test which is oven dried (Nelson et al., 2015). The SAMC is determined by the Equation 2.7 stated as below;

$$SAMC (\%) = (W_e - W_s) / W_s \quad (2.7)$$

Where;

$W_e$  = weight of sample at equilibrium (77°F and 60 % relative humidity) and

$W_s$  = weight of oven dry sample.

The method for classifying expansive soils based on the standard absorption moisture content, plasticity index, and free swell values shown in Table 2.19.

**Table 2.19 :** Classification standard for expansive soils (Yao et al., 2004).

Standard Absorption Moisture Content (%)	Plasticity Index (%)	Free-Swell Value (%)	Swell Potential Class
< 2.5	< 15	< 40	Nonexpansive
2.5–4.8	15–28	40–60	Low
4.8–6.8	28–40	60–90	Medium
> 6.8	> 40	> 90	High

### 2.4.3.6 Coefficient of linear extensibility (COLE)

U.S. Soil Conservation Service, National Soil Survey Laboratory uses the coefficient of linear extensibility test (COLE) to identify expansive soils (Brasher et al., 1966). The COLE test done for undisturbed and unconfined sample on drying from 33 kPa suction to oven dry suction (1000 MPa) which specify the change in sample dimensions in terms of the linear strain of sample (Nelson et al. 1995).

The COLE is stated in the Equation 2.8 below;

$$COLE = \Delta L / \Delta L_D = (\gamma_{dD} / \gamma_{dM})^{0.33} - 1 \quad (2.8)$$

Where;

$\Delta L / \Delta L_D$  = linear strain relative to dry dimensions

$\gamma_{dD}$  = dry density of oven dry sample

$\gamma_{dM}$  = dry density of sample at 33 kPa suction

The COLE has been associated to swell index from the potential volume change test by various researchers. (Parker et al., 1977; Schafer and Singer, 1976). A relationship between the ratio of LE to clay content is given in the Table 2.20.

**Table 2.20 :** Common LE/Clay values of clay minerals (Nelson et al. 1995).

LE / Percent Clay	Mineralogy
>0.15	Smectites (montmorillonite)
0.05-0.15	Illites
<0.05	Kaolinites

## 2.5 Empirical Swell Prediction Methods

Empirical procedures are usually based on the test data which are developed from the particular geographic region. In order to decrease time and cost of laboratory testing methods, many studies have done to evolve empirical relationships for prediction of heave, but the major disadvantage of them is that they are based on a limited data and only can be applied in the regions they were developed (Nelson and Miller, 1992). The most successful empirical methods in the literature that focused on the determination of swelling potential are stated in the Table 2.21.

**Table 2.21** : Empirical methods to identify behavior of swelling mechanism (Nelson et al., 2015).

Reference	Equation
Seed et al. (1962)	$S \% = 0.00216 I_p^{2.44}$ for undisturbed $S \% = 0.0036 I_p^{2.44}$ for disturbed soils $S \% = 3.6 \times 10^{-5} A^{2.44} c^{3.44}$ $I_p$ = plasticity index $c$ = clay content $A$ = activity ( $I_p / c$ )
van der Merwe (1964)	$\Delta H = Fe^{-0.377D}(e^{-0.377H} - 1)$ $H$ = volume change, $\Delta H$ = total swell $F$ = correction factor for degree of expansiveness $D$ = the thickness of non-expansive layer
Ranganathan and Satyanarayana (1965)	$S \% = 0.000413 IS^{2.67}$ $IS$ = shrinkage index, $(LL - SL)$ $LL$ = liquid limit $SL$ = shrinkage limit
Nayak and Christensen (1971)	$S \% = 0.00229 I_p^{2.67} (1.45c) / w_i + 6.38$ $p_s$ (psi) = $[(3.58 \cdot 10^{-2}) PI^{1.12} c^2 / w_i^2] + 3.79$ $w_i$ = initial water content $p_s$ = swelling pressure
Vijayvergiva and Ghazzaly (1973)	$S \% = (0.44 LL - w_i + 5.5) / 12$ $\text{Log}(S \%) = 0.0526 \gamma_d + 0.033 LL - 6.8$ $\gamma_d$ = dry unit weight
Schneider and Poor (1974)	$\text{Log } S\% = 0.90(PI/w) - 1.19$ for $S = 0$ ft $\text{Log } S\% = 0.65(PI/w) - 0.93$ for $S = 3$ ft $\text{Log } S\% = 0.51(PI/w) - 0.76$ for $S = 5$ ft $\text{Log } S\% = 0.41(PI/w) - 0.69$ for $S = 10$ ft $\text{Log } S\% = 0.33(PI/w) - 0.62$ for $S = 20$ ft
McCormack & Wilding (1975)	$S \% = 7.5 - 0.8w_i + 0.203c$
Brackley (1975b)	$S \% = (5.3 - (147e/I_p) - \text{Log}P) \times (0.525I_p + 4.1 - 0.85w_i)$ $P$ = surcharge load
O'Neil & Ghazzally (1977)	$S \% = 2.77 + 0.131LL - 0.27w_n$ $w_n$ = natural water content
Chen (1975)	$S \% = 0.2558 e^{0.00838 I_p}$
Weston (1980)	$S \% = 0.00411 w_{LL}^{4.17} \sigma_v^{-3.86} w_i^{-2.33}$ $w_{LL}$ = weighted liquid limit
Bandyopadhyay (1981)	$\% = 0.00114 A^{2.559} c^{3.44}$
Picornell & Lytton (1984)	$\Delta H = \Sigma[f_i (\Delta v / v)_i] H$ $H$ = the stratum thickness $(\Delta v/v)_i$ = volumetric strain $f_i$ = the effects of the lateral confinements factor

**Table 2.21 (continued) :** Empirical methods to identify behavior of swelling mechanism (Nelson et al. 2015).

Basma (1993)	$S \% = 0.00064I_p^{1.37}c^{1.37}$
Cokca (2002)	$S \% = -121.807 + 12.1696 MBV + 27.6579 \text{Log}\psi_i$ MBV = methylene blue value
Erguler & Ulusay (2003)	$p_s = -227.27 + 2.14w_i + 1.54LL + 72.49\gamma_d$
Erzin & Erol (2004)	$\text{Log } p_s = -4.812 + 0.01405I_p + 2.394\gamma_d - 0.0163w_i$
Sabtan (2005)	$S \% = 1.0 + 0.06(c + I_p - w_i)$ $p_s = 135.0 + 2.0(c + I_p - w_i)$
Azam (2007)	$S \% = 0.6 I_p^{1.188}$
Yilmaz (2009)	$S \% = 2.0981e^{-1.7169 IL}$ IL = liquidity index = $[(LL - w_n) / I_p]$
Turkoz and Tosun (2011)	$S \% = -57.865 + 37.076 \rho_d + 0.524MBV + \varepsilon$ $\varepsilon$ = mean-zero Gaussian random error term
Cimen et al. (2012)	$(S \% )_1 = (0.3139\gamma_d^{0.3552} - 0.1177 w_i^{0.4470})I_p^{0.9626}$
	$(\text{Log } p_s)_1 = 0.0276I_p - 365.2118\gamma_d^{-2.4616} - 0.0320w_i + 2.2292$
	$(S \% )_2 = (0.4768\gamma_d^{0.3888} - 0.0033 w_i^{1.6045})I_p^{0.7224}$
	$(\text{Log } p_s)_2 = 0.0239I_p - 1285.3723\gamma_d^{-3.2768} - 0.0396w_i + 2.3238$
	$(S \% ) = \text{mean } (SP_1, SP_2)$ $\text{Log } p_s = \text{mean } [(\text{Log } p_s)_1, (\text{Log } p_s)_2]$
Zumrawi (2013)	$S \% = 24.5 (q^{-0.26}) (I_p c)^{1.26} [F_i - 7.1(q^{0.22})(I_p c)^{1.26}]$ q = surcharge $F_i$ = initial state factor

### **3. THE EFFECTS OF FREEZE-THAW CYCLES ON SOIL**

Over the past several years, frozen ground engineering has developed to meet the requirements of people. This demandings lead to star the researches related to frozen ground engineering topics. Considering the cold climate conditions in our country and in the world, freeze effects gained importance in terms of engineering applications and negatively affects almost all structures from infrastructure to superstructure. The determination of the behavior during the freezing of soils and the prevention of negative consequences are among the subjects of geotechnical engineering. Geotechnical engineering considerations must obtain an understanding of the freezing process, the effects of thawing in the frozen ground, swelling and settlement behavior of frozen grounds.

#### **3.1 Frozen Soils**

Frozen ground is soil or rock with a temperature below 0°C which is not related to water and ice content that is contained in the soil layers. It is observed that frozen soil is relatively impermeable and shows high strength characteristics. In the frozen soils, the ice acts as a binding element which increases the strength and prevents the water seepage. Frozen grounds can be separated into two different groups. These groups can be stated as follows;

- Permanently frozen ground (permafrost) can be described as the grounds which are located at a temperature below 0°C throughout the year.
- Seasonally frozen ground is defined as the soil located in the regions where temperatures below 0°C only during the winter season (Andersland and Ladanyi, 2004).

##### **3.1.1 Seasonally frozen soils**

The active layer, subsurface temperature and permanently frozen soil layers are important engineering design criterias of frozen soils. Temperature and frost

penetration are the most essential factors of frozen ground engineering (Andersland and Ladanyi, 2004).

The cold regions commonly divided into three different categories which are based on the freezing conditions. In cold regions, ground may be frozen seasonally, permafrost layer can be seen in the whole region or observed in some areas beneath the examined land surface. In polar regions, permafrost layer can be observed up to more than 1 km below ground and annual ground surface temperature must be smaller than  $-3^{\circ}\text{C}$  to occur (Andersland and Ladanyi, 2004).

Ground temperatures are determined by ground surface temperatures, heat flow and soil thermal properties. Andersland and Ladanyi (2004), expressed the surface temperature behavior with respect to time as a periodic function which is stated in the Figure 3.1. In the Figure 3.2, temperature attenuation with depth is shown. Figure 3.2 is an important figure for the disclosure of the active zone which will be discussed in the following section.

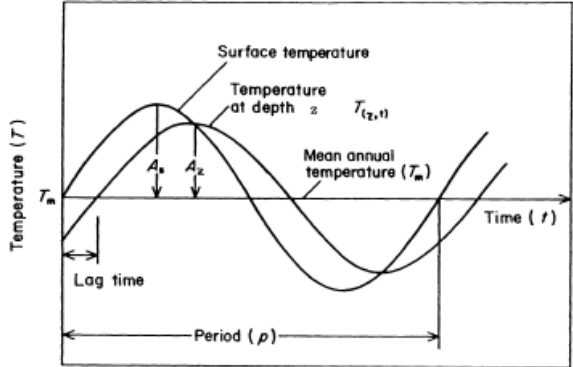


**Figure 3.1 :** Sinusoidal fluctuations of surface and ground temperatures (Andersland and Ladanyi, 2004).

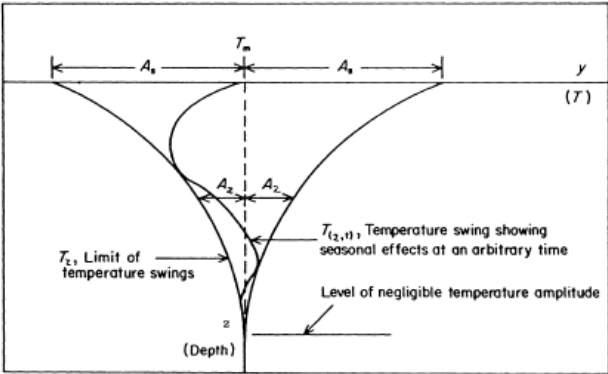


**Figure 3.2 :** Conceptual temperature attenuation with depth (Andersland and Ladanyi, 2004).



### 3.1.2 Active zone

The active zone can be defined as the top layer of ground in which temperature changes around 0°C during the year. In consequence of an increase of the water content in the upper part of the soil profiles, swelling problem occurs. The climatic conditions affect the water content where the regions close to the surface. This affected zone is denoted as the active zone (Chen, 1988). Water content profiles in the active zone given in the Figure 3.3 below.

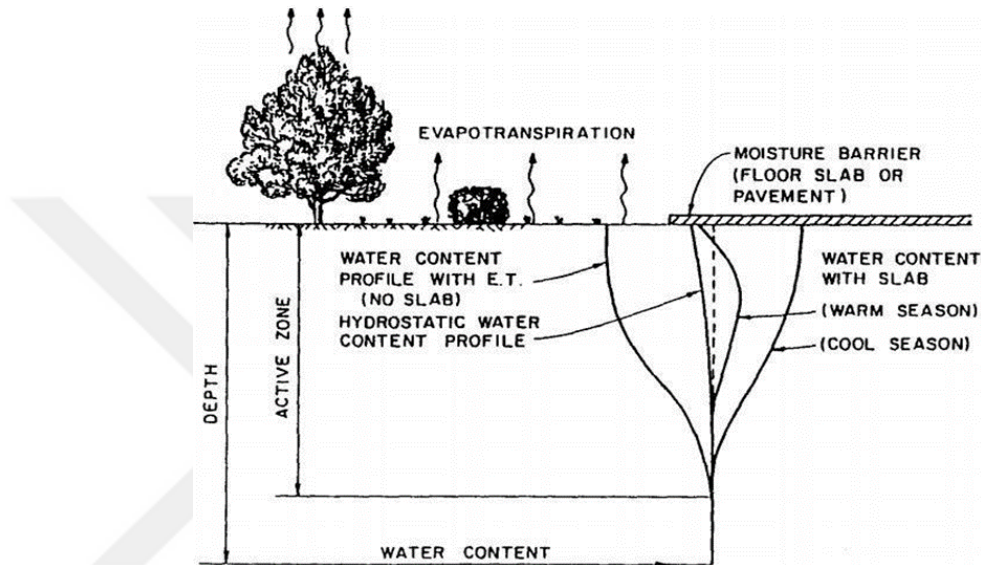


**Figure 3.3 :** Water content profile in the active zone (Nelson and Miller, 1992).

In-situ recordings of the water content profile can be used to identify the depth of active zone. Several research studies have been done in order to identify the active zone depth by using in-situ instruments for several seasons. The in-situ data of soil suction and water content have been illustrated by Hamberg (1985), made observations and taken moisture readings from 1981 to 1984 in Colorado and stated that the seasonal fluctuations tend to be stabilized at a depth of 5.5m. Figure 3.4 indicates the water content profile of the site in Colorado. By using the same approach to any different site, the average active zone depth can be estimated.

After taking the mutiple seasonal recordings of a region, the active zone depth of a field can be calculated by plotting the liquidity index against the depth of the soil profile. Active zone depth can be expressed when the LI does not change with the increasing depth of the soil (Das, 2015). Liquidity index of the soil can be determined by using the Equation 3.1. The procedure is illustrated in the Figure 3.5.

$$LI = (W_n - PL) / PI \quad (3.1)$$

Where;

LI: Liquidity index of the soil

$W_n$ : Moisture content of the soil

PL: Plastic limit of the soil

PI: Plasticity index of the soil

Due to the freezing of the active layer, expansive movements can be observed in frost-susceptible soils. Water expands about 9% in volume with the effect of freezing which causes the heave. The volumetric change in a frozen soil is caused by the ice lenses formed on the upper part of the ground and the water propagates from the bottom of the ground to the frozen zone by the effect of capillarity. The region between the frozen layer and the non-frozen layer can be defined as a transition region. This region continues until the ice lenses begin to form.

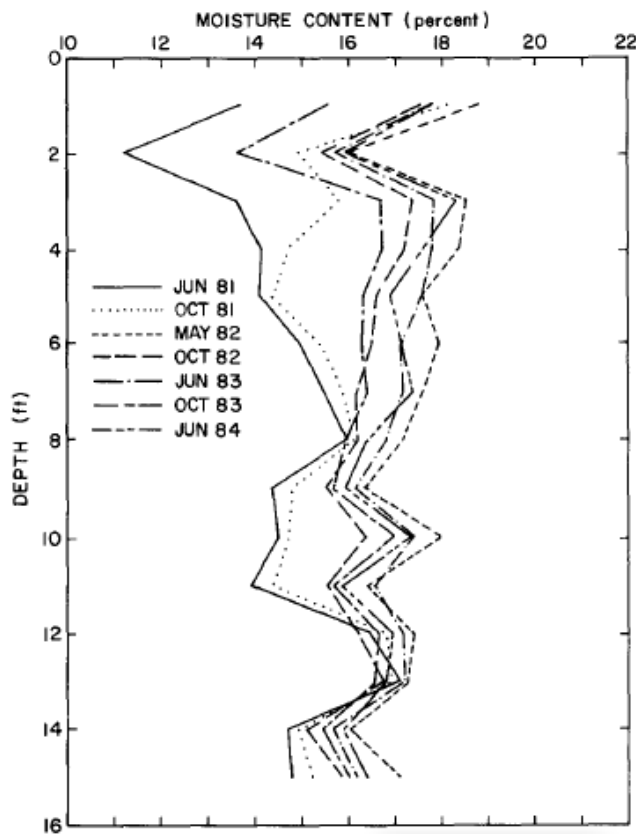


**Figure 3.4 :** Seasonal water content profiles in Colorado (Hamberg, 1985).

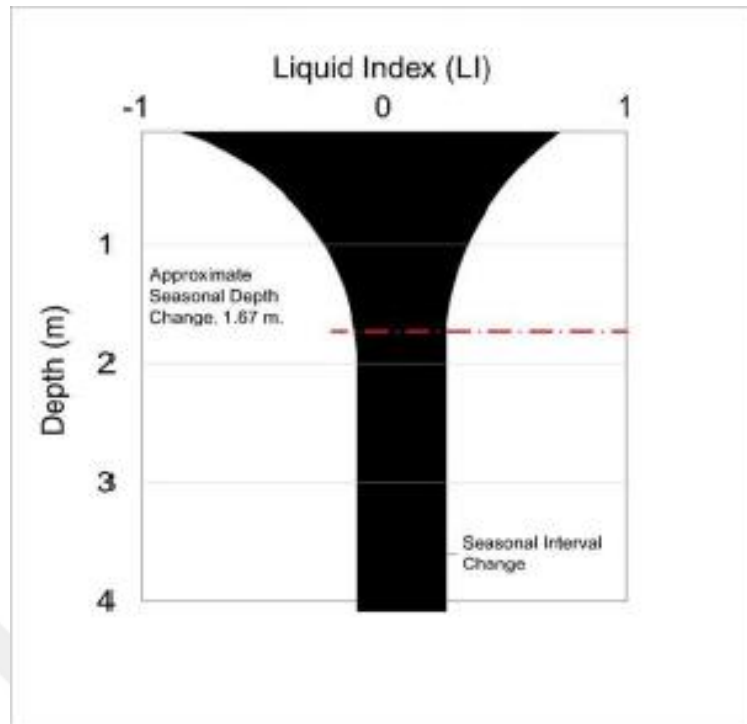


**Figure 3.5 :** Determination of active zone depth (Das, 2015).

For designing especially the highway structures, Frost heave must be considered in the cold regions. This expansive movements commonly occur during the freezing process. After the winter, with the increasing temperature values thawing occurs which will cause the disappearance of ice lenses formed in the ground.

Prevention of frost action in the active layer is common problem for engineers. A typical problem is shown in Figure 3.6. The most damage will be observed on the pavement structure is stated when water can not drain downward through frozen soil.

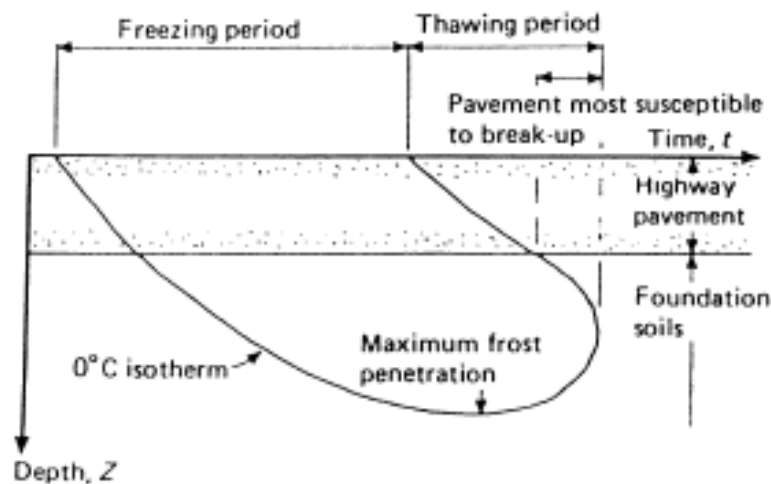


**Figure 3.6 :** Seasonal ground freezing beneath a pavement structure (Andersland and Ladanyi, 2004).

### 3.1.3 Permanently frozen soils (permafrost)

Permanently frozen soils (permafrost) is defined as soil or rock which exists below 0°C over at least two consecutive years (Brown and Kupsch, 1974). The climate conditions and soil properties are the two important factors to shape the formation and existence of this frozen soil structures. Permafrost can be observed in continuous and discontinuous zones. Brown et al. (1981), illustrated a common permafrost profile in cold regions in the Figure 3.7.

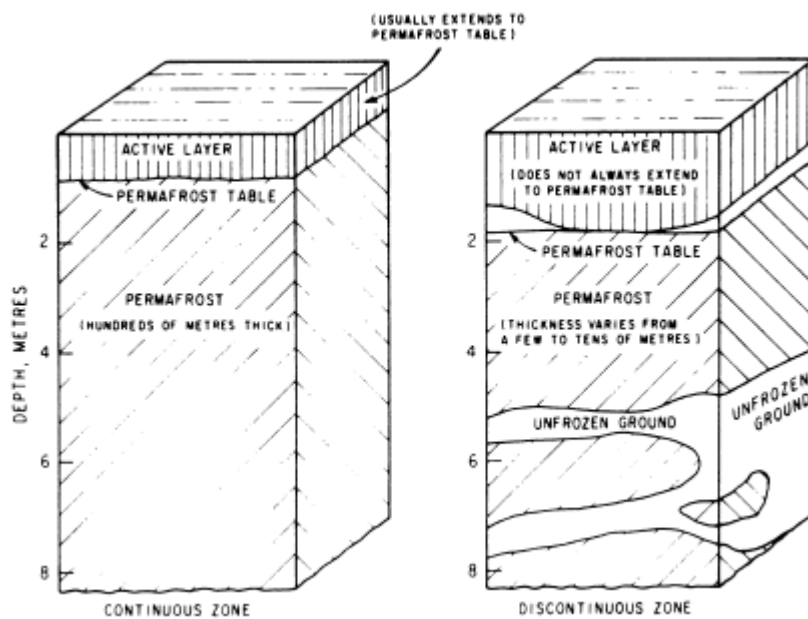


**Figure 3.7 :** Typical profile of permafrost in cold regions (Brown et al., 1981).

#### 3.1.3.1 Ice wedges

Ice wedges are vertically configured ice masses that located near to the permafrost surface. Lachenbruch (1963), illustrated a schematic of ice wedge evolution in the Figure 3.8. Ice wedges are wider at the top (1 cm to 3 m) than at the bottom and range in height from 1 to 10 m (Andersland and Ladanyi, 2004). When the tensile stress exceeds the tensile strength of the frozen soil, cracks are observed. These cracks can be very narrow on the surface of the soil but with the increasing depth cracks can be wider up to several meters. These cracks are filled with water in the spring season and freezes in the winter which will be called ice wedges. The ice wedge forms below the active layer and can not be seen at the surface level. Repetative seasonal changes develop more critical and greater cracks which can be observed at the ground surface.

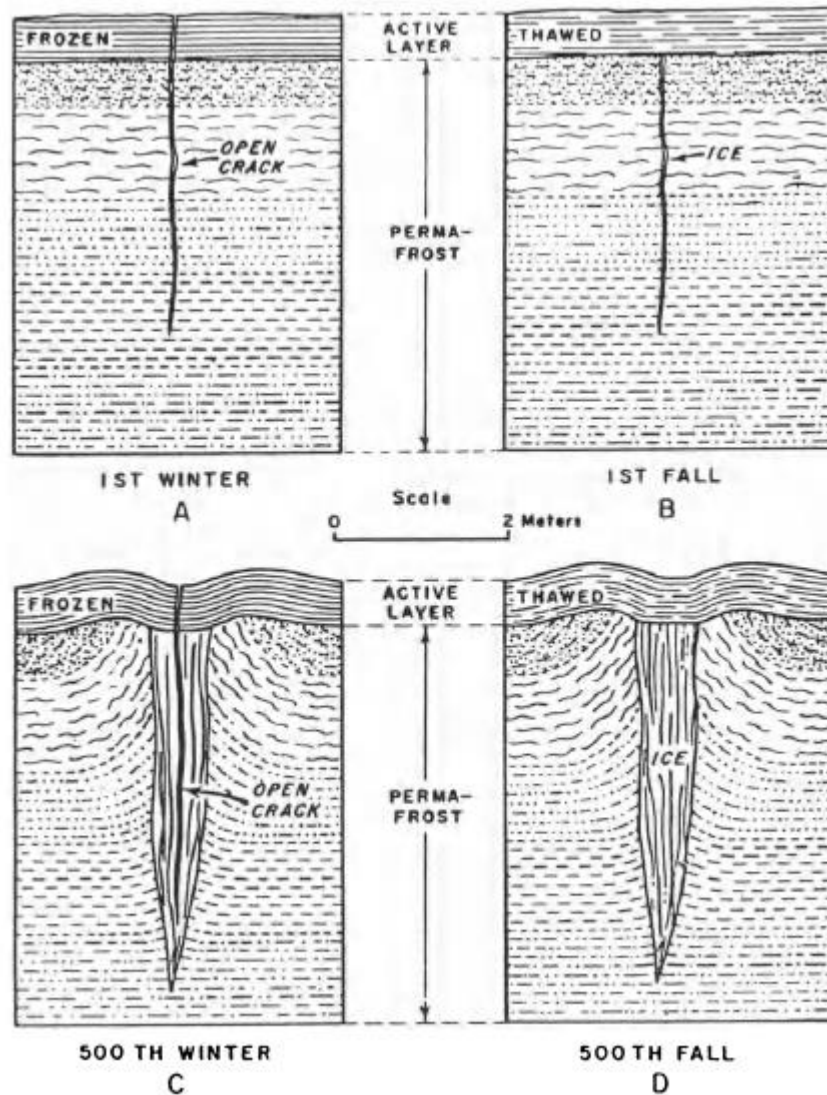


**Figure 3.8 :** Schematic of ice-wedge evolution (Lachenbruch, 1963).

### 3.1.3.2 Pingos

Pingos can be defined as a conical hill with a circular base occurred in the continuous and discontinuous permafrost zones (Brown and Kupsch, 1974). There are two pingo types which are called closed and open systems. Price (1972) addressed the closed-system pingos and stated that these structures occur in poorly drained shallow lake basins. If the lake is defined as deep that means the maximum winter ice thickness is smaller than the depth of these lakes. A typical pingo development includes a decrease in the water table which will affect the heat balance system is shown in the Figure 3.10. In open systems, water is provided by near resources such as springs located in the unfrozen permafrost zones. The hydraulic gradient helps water to flow to the ground. When water reaches to the surface it becomes frozen and through the years,

this water supply generates ice masses. An example of typical pingo is given in the Figure 3.9.



**Figure 3.9 :** A typical example of pingo which located in Canada (Mackay, 1973).

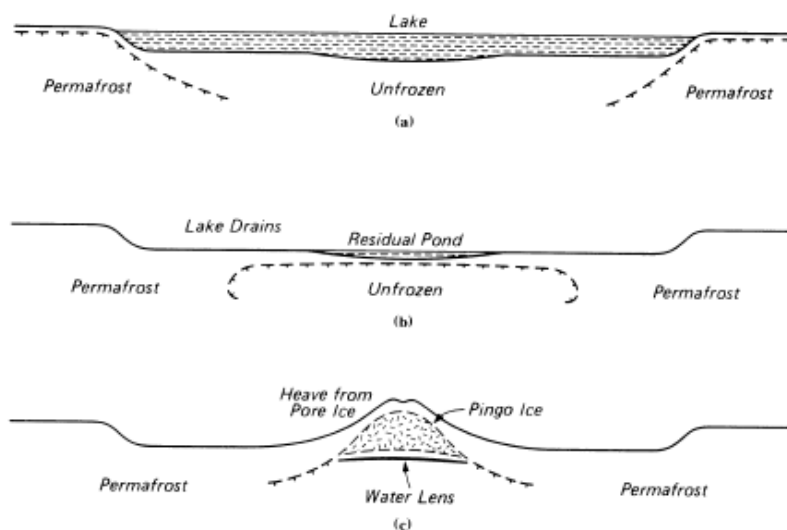


**Figure 3.10 :** Schematic drawings of pingo growth (Mackay, 1992).

### 3.2 Freezing Process

The freezing process can be defined as the water in the voids of saturated or partially saturated soils freezes with the temperature is below the 0°C. This freezing process causes increase in the volume by approximately 9%. This expansion does not mean that void volume will increase about 9% because some of the water may be thrown out during freezing. The rate of lowering the temperature is one of the most crucial factor which affects the behavior of soil during freezing. To illustrate, silty soils behavior depends on the rate of change in temperature. If the temperature lowered at a relatively

constant and slow rate, ice lenses will form horizontally in the surface of soil due to exposure to freezing. Therefore, these soils involve frozen soil layers which separated by ice lenses. These ice lenses can just occurred in the fine grained soils and be several meters height in the permanently frozen soils. This freezing behavior is given in the Figure 3.11. Figure 3.11 (a), indicates a closed freezing system of silt sample. It is defined as closed system as it is provided to form ice lenses by using water in the soil. The formation of ice lenses is limited to the movement of water from the bottom of the sample to the surface. The lower part of the sample is consolidated by the upward movement of water by capillarity. When the water content reaches to the shrinkage limit in the bottom part of sample, the ice layer formation ends (Andersland and Ladanyi, 2004). The other samples b) and c) indicates the open systems. These silt samples get in contact with the ground water table which provides water flow into the sample throughout the freezing process. In open systems, ice lenses can be up to several meters in thickness.

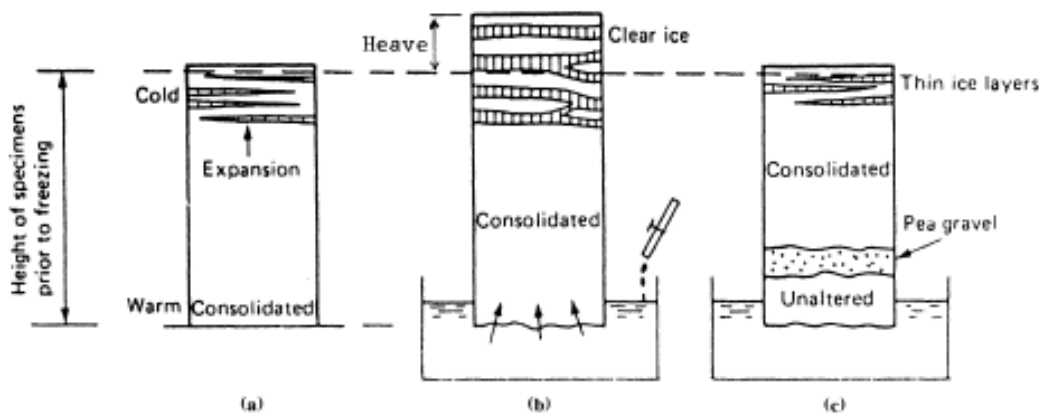


**Figure 3.11** : Ice formation in soils: a) closed system; b) open system; c) pea gravel layer changes upper part of specimen into a closed system (Terzaghi, 1952).

In the field, open systems can be observed when the vertical distance between the water table and freezing depth is smaller than the capillary height which can easily be calculated by using the following Equation 3.2;

$$h_c \text{ (m)} = \frac{0,03}{D_{10}} \text{ (mm)} \quad (3.2)$$

Where;

$h_c$  : maximum capillary rise

$D_{10}$  : the effective pore diameter

Due to the freezing and thawing process, loss in bearing capacity expected which leads to severe damages especially for the highway structures that located in the cold climatic regions.

### 3.3 Thawing Process

During thawing process the ice lenses begin to disappear and as a result, the soil accomodate itself to the final void ratio. The increase in water due to the melting of the ice lenses may exceed the absorption capacity of the soil. For fine grained soils with low permeability, excessive pore water pressure may be temporarily created until the end of drainage. Bearing capacity of soil decreases with the rapid thawing. The volume change due to thawing for a frozen fine grained soil sample is stated in the Figure 3.12.

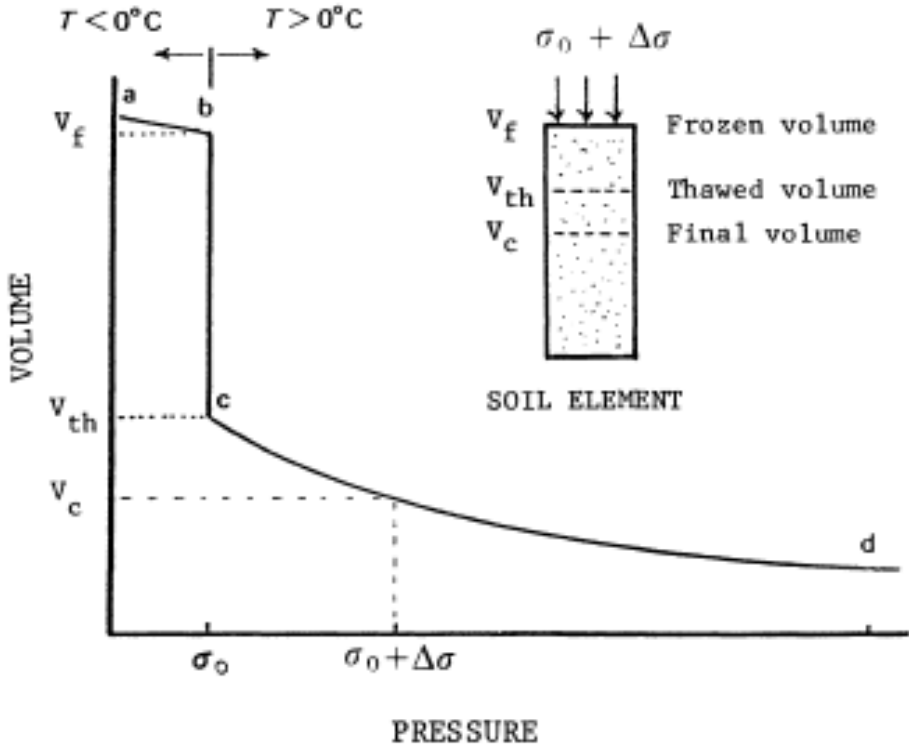


**Figure 3.12 :** Relation between volume and pressure for a frozen soil subjected to thawing (Andersland and Ladanyi, 1994).

In the Figure 3.12, between the point a and point b demonstrates the interval where the sample is frozen and void ratio is slightly decreased due to the increasing effective stress. When the volume of the ice decreases under applied force as indicated from point b to point c, a large decrease in the void ratio occurs. This represents the change in the volume of water under loading and the discharge water. After the completion of



the first drainage, curve restricted between from point c to point d states the consolidation phase of fine grained soil.

A new concept called thaw settlement is encountered which produced by the melting of ice lenses in the soil. Thawing generates excessive water content in the subgrades which is very fatal for road, highway structures and embankments under heavy loads.

Thaw settlement may be generated by three different principles stated as follows;

- phase change,
- settlement of the soils under their own weight and
- settlement of the soils under applied loads (Andersland and Ladanyi, 1994).

### **3.4 Frost Action**

Seasonally frozen soil thaws during the spring seasons which causes the melting of ice lenses that have formed located in the soil. This process causes thaw weakening or decrease in bearing capacity. This whole process is called frost action. There are some important requirements to fulfill the frost action. Soil must be susceptible to the frost, a water resource must be located and low temperatures must be acquired in order to observe ice lenses in the fine grained soil.

Frost action creates some critical conditions that need to be taken into consideration by engineers such as heave of the pavements and decrease in the bearing capacity for soils located under the foundations. The non-homogenous structure of soil evokes differential expansive movements which causes serious distortions for road pavement structures and foundations. Therefore, frost susceptibility of soils must be considered and determined before the design phases.

### **3.5 Frost Susceptibility of Soils**

The soil needs to be susceptible to freezing in order to form ice lenses which cause deformation on the ground. Frost susceptibility can be defined regarding soil's frost behavior. Great damages may occur on structures whether by freezing or thawing processes.

U.S. Army Corps of Engineering has proposed frost design and soil classification system that based on the USCS and percentage of soil particles which are smaller than

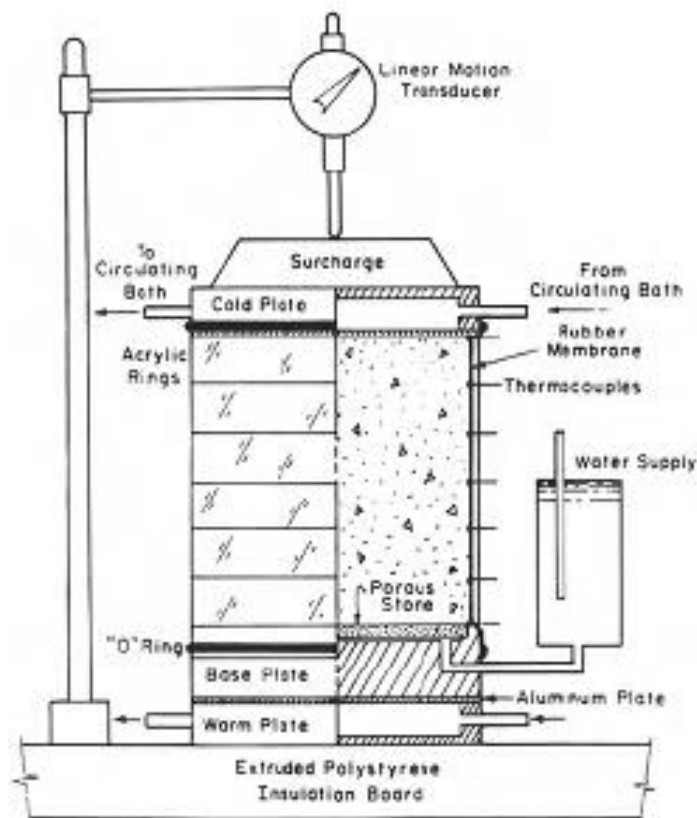
0.02 mm. This system allows to estimate the frost susceptibility of the ground with general laboratory tests. This system is shown in Table 3.1. The percentage of particles smaller than 0.02 mm, soil type based on the USCS and laboratory freezing test must be performed in order to evaluate frost sensitivity.

Table 3.1 represents the frost susceptibility classification according to various soil types. The susceptibility to frost is listed from low to high. These are respectively; NFS, PFS, S1, S2, F1, F2, F3 and F4. The group classified as NFS and PFS are Non-Frost-Susceptible. PFS requires laboratory frost-heave test to determine frost susceptibility.

**Table 3.1 :** U.S. Army Corps of Engineers frost design soil classification system (Johnson et al., 1986).

<b>Frost susceptibility</b>	<b>Frost Group</b>	<b>Soil Type</b>	<b>Amount finer than 0.02 mm (%)</b>	<b>Typical soil type under USCS<sup>b</sup></b>
Negligible to Low Possibility	NFS	a.Gravels	0-1.5	GW,GP
		b. Sands	0-3	SW,SP
	PFS	a.Gravels	1.5-3	GW,GP
		b. Sands	3-10	SW,SP
Low to Medium	S1	Gravels	3-6	GW,GP, GW-GM, GP-GM SW,SP,
Very Low to High	S2	Sands	3-6	SW-SM, SP-SM
Very Low to High	F1	Gravels	6-10	GM,GW-GM, GP-GM GM,GM-GC,
Medium to High Very low to very high	F2	a.Gravels b. Sands	10-20 6-15	GW-GM, SM, SW-SM, SP-SM GP-GM
Medium to high Low to high Very low to very high	F3	a.Gravels b.Sands c.Clays $I_p > 12$	$> 20$ $> 15$ -	GM,GC SM, SC CL,CH
Low to very high Very low to high Low to very high	F4	a.Silts b.Very fine silty sands c.Clays $I_p < 12$	- $> 15$ -	ML, MH SM CL, CL-ML

The laboratory test to determine the frost susceptibility consists of soil specimens compacted to 95% or better as referred in the standards. Frozen at a penetration rate of about 6.3 mm/day, continuously supplied with a free water at 3.3°C at the base of the specimen. Johnson et al. (1986), recommended some improvements for the laboratory tests. Improved test equipment includes a temperature stabilized top and bottom plates also to lower the effects of friction membrane used in the cells. The test automated in order to collect the data continuously and more precisely to reduce the margin of the error rate. Two freeze-thaw cycles conducted for four different 150 mm height and 150 mm diameter samples compacted to reflect the field conditions. Water is available through the porous plates. Test duration is five days. The At the end of the first 8 hours of each two day F-T cycle heave rates recorded and used to evaluate susceptibility. Afterwards, A CBR test performed to analyze the thaw-weakening susceptibility. Schematic of freezing test equipment is shown in the Figure 3.13.



**Figure 3.13** : Schematic of freezing test equipment (Johnson et al., 1986).

The amount of swelling of the sample in mm/day indicates the sensitivity of the soil to frost. Frost-susceptibility classification for the laboratory tests are given in the Table 3.2.

**Table 3.2 :** Frost-susceptibility classification for the lab. tests (Johnson et al., 1986).

<b>Frost Susceptibility</b>	<b>Heave rate (mm/day)</b>	<b>Thaw CBR (%)</b>
Negligible	< 1	> 20
Very low	1 - 2	20 - 15
Low	2 - 4	15 - 10
Medium	4 - 8	10 - 5
High	8 - 16	10 - 5
Very high	> 16	< 2

### **3.6 Effects of the Freeze-Thaw Cycles on Geotechnical Properties**

The volume changes of the soil and the increase in the void ratio, which take place from freeze and thaw process, will cause some changes in the geotechnical properties of the soil. Permeability, void ratio, water content, porosity, consistency limits, swelling pressure, consolidation coefficient and strength parameters can be stated as influenced geotechnical parameters due to freeze-thaw cycles.

#### **3.6.1 Freeze-thaw effects on permeability**

Freeze and thaw cycles increases the void ratios of clayey soils (Andersland and Ladanyi, 2014). Konrad (1989), stated that freeze-thaw causes to an increase in vertical permeability of the thawed soil. Benson and Othman (1993), Chamberlain and Ayorinde (1991), indicated similar experimental results on the vertical permeability. The first three F-T cycles are the most crucial cycles in terms of to observe the changes in permeability (Konrad, 1989; Chamberlain and Ayorinde, 1991).

After freezing and thawing, soils are expected to undergo changes in their permeability due to changes in their physical properties. During the freezing state, the ice lenses are formed in the soil which leads to create capillary cracks in the soil after thawing. This process increases the water flow compared to before freezing-thawing. Therefore, as the number of freeze-thaw cycles increases, an increase in the permeability of the soil is expected (Isik, 2014).

Chamberlain and Gow (1979), stated that the permeability of fine-grained soils were changed by freezing and thawing. Repeated freeze and thaw cycles causes increase in the vertical permeability. Chamberlain et al.(1990), stated that freeze–thaw cycles induce an increase in hydraulic conductivity in consolidated samples. It was determined that the increase in permeability of the samples was greater with increasing water content.

Othman and Benson (1993), performed a series of permeability experiments on clay samples. Some of the clay samples were subjected to three cycles of freeze-thaw test under various effective stresses while other were not subjected to freeze-thaw test. The results are shown in Figure 3.14. After three freeze-thaw cycles, the coefficient of permeability increased by 100 times compared to the non freeze-thawed samples.

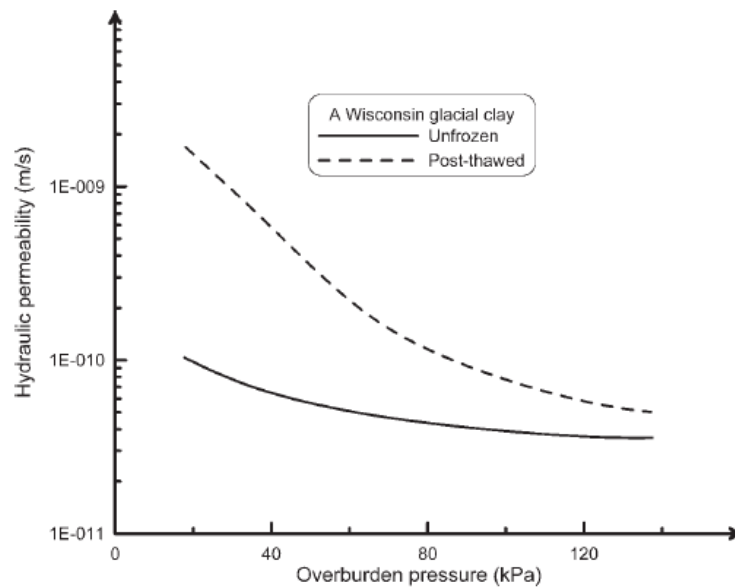


**Figure 3.14 :** Relationship of hydraulic permeability and overburden pressure for unfrozen samples and subjected to F-T cycles (Othman and Benson, 1993).

Konrad and Samson (2000), examined 25%, 35% and 50% kaolinite-silt mixtures that subjected to the one F-T cycle. As a result of the experiments, it was determined that the increasing amount of clay in the mixtures causes increase in the coefficient of permeability after the freeze-thaw effects.

Yıldız and Soğancı (2012), examined the effect of freezing and thawing on the permeability of two stabilized clayey soils. The permeability of the samples were determined with various F-T cycles before and after stabilization. Results of the study stated that for both clays, 6% lime additive material increased the hydraulic conductivity of the specimens 1000 times. After subjected to 3 freeze-thaw cycles, the

hydraulic conductivity of clay with 6% lime increased 10–20 times. For all samples, with the effect of freeze-thaw cycles, hydraulic conductivity increased. The reason for this is stated as various horizontal and vertical cracks formed during freeze-thaw which caused the increase of permeability.

**3.6.2 Freeze-thaw effects on void ratio**

Chamberlain (1981) and Eigenbrod (1996), stated that normally consolidated clay samples becomes denser with the effects of freeze-thaw cycles. Viklander (1998) stated that within the increasing number of F-T cycles, the void ratios do not change compared to the previous cycle and reaches to the residual value. Loose and dense soils may reach to the equal void ratio after numerous freeze-thaw cycles. In the Figure 3.15, the void ratio and F-T cycles relationship is expressed. It is observed that, with the increasing number of freeze-thaw cycles, the void ratio of the loose soil sample decreased and becomes denser. Conversely, dense soil tend to loosens with the increasing number of freeze-thaw cycles. Othman and Benson (1993), Eigenbrod (1996) and Viklander (1998), indicated that 1<sup>st</sup> F-T cycle has the greatest effect on the soil volume. Moreover, it does not change considerably after 3 to 5 F-T cycles which is stated in the Figure 3.16.

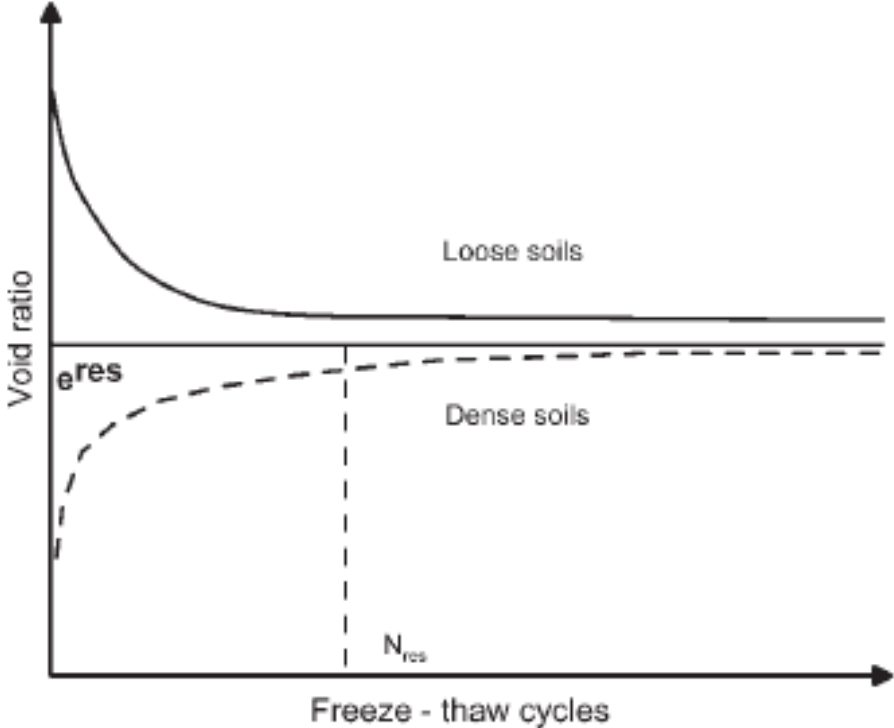


**Figure 3.15 :** Residual void ratio in terms of freeze-thaw (Viklander, 1998).

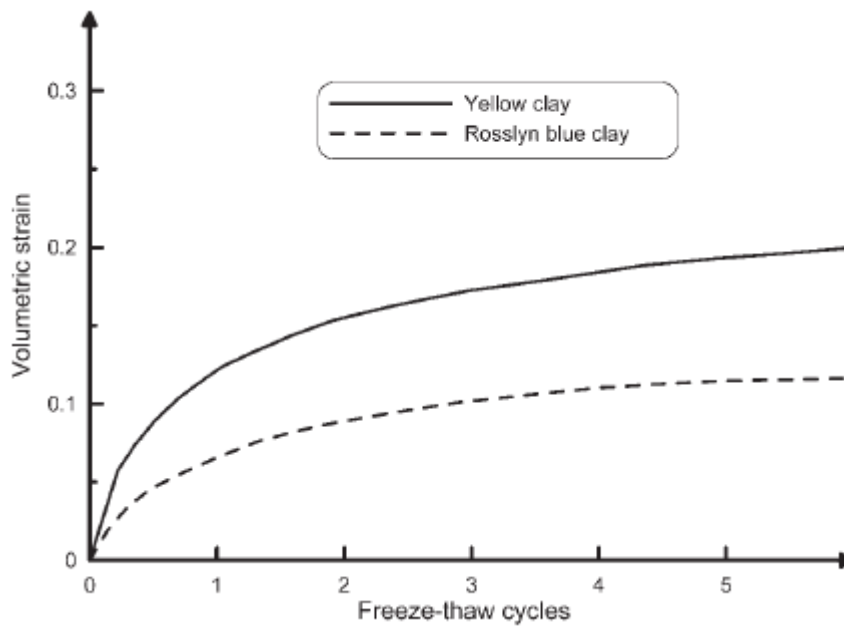


**Figure 3.16 :** Relationship between volumetric strain and number of freeze-thaw cycles (Eigenbrod, 1996).

### 3.6.3 Freeze-thaw effects on Atterberg limits

Soil parameters such as the liquid limit may be changed by freeze-thaw. Wang et al. (1995) and Viklander and Eigenbrod (2000), stated that F-T cycles may affect on the grain size distribution, which may alter the plastic limit. Throughout the experimental studies, decrease in the liquid limit after F-T cycles is observed. (Swan and Greene, 1998; Swan et al., 2013, Dagesse, 2015). Swan and Greene (1998) and Swan et al. (2013) reported a decrease in the plastic limit after 1 F-T cycle.

Dagesse (2015), studied on four samples with different clay contents. Researcher sorted the samples into two groups. First group indicates the samples which have maintained the initial structure. The second group was dispersed at a high water content. For 6 hours, at  $-15^{\circ}\text{C}$  freezing process conducted. After, for 6 hours at  $+15^{\circ}\text{C}$  thawing process was performed for 1, 5, 10, and 25 F-T cycles at 25% water content. Results of the tests show that, liquid limits and plastic limits increase with the increasing number of F-T cycles for the first group samples. On the other hand, liquid limits and plastic limits decrease with the increasing number of F-T cycles for the second group samples. In addition to that, regression analysis showed F-T cycles do not have significantly affect on soil plasticity which is expressed in the Figure 3.17, 3.18, respectively.

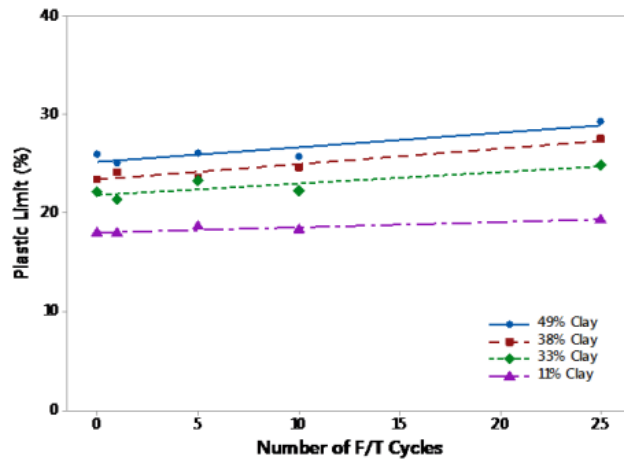


**Figure 3.17 :** Plastic limit vs. number of freeze-thaw cycles of naturally structured soils (Dagesse, 2015).

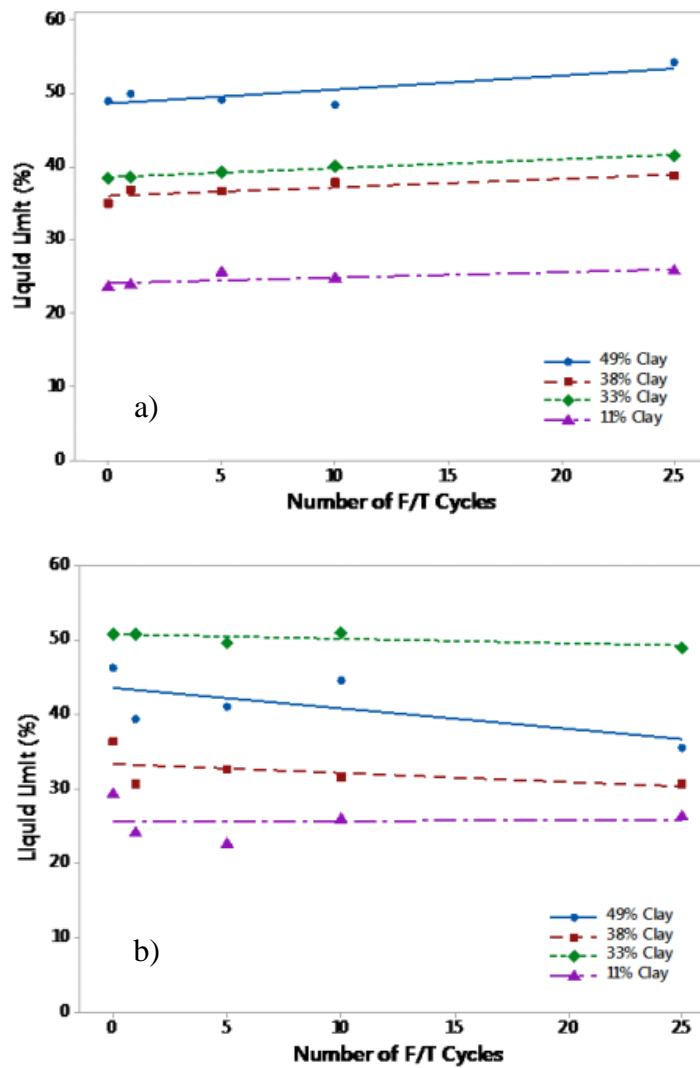


**Figure 3.18 :** a) Liquid limit vs. number of freeze-thaw cycles of naturally structured soils, b) Liquid limit vs. number of freeze-thaw cycles of unstructured soils (Dagesse, 2015).



### 3.6.4 Freeze-thaw effects on consolidation

Chamberlain and Blouin (1978), discussed that after freezing and thawing process, the coefficient of consolidation ( $C_v$ ) is increased and the consolidation is observed more quickly. The changes in permeability have been shown as the reasons for this.

Paudel and Wang (2010), presents laboratory test results of freeze-thaw effect on consolidation properties of fine grained soils from the Mackenzie valley, Canada. The samples were obtained from the bottom of the active layer at about 1 m depth below ground surface. A total of 32 remoulded samples were prepared with varying water contents to reflect the moisture conditions in the active layer. The samples were tested for coefficient of consolidation and hydraulic conductivity after 0, 3, 5 and 10 cycles of freezing and thawing. The consolidation coefficient continued to increase with the increasing number of freeze-thaw cycles, but the percentage of change was slowed. Figure 3.19 shows the correlation of the consolidation coefficient with the increasing freeze-thaw cycles.

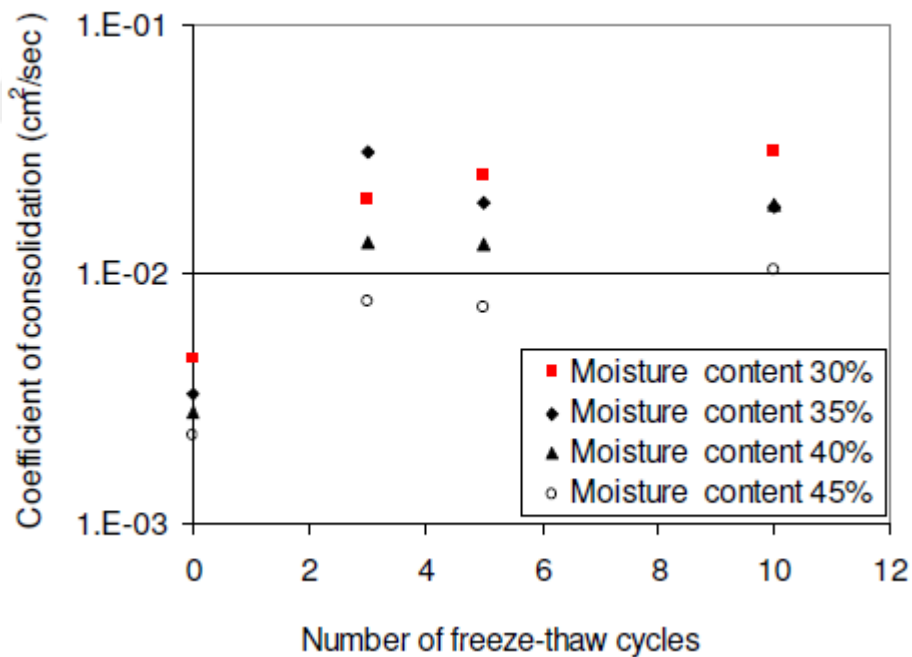


**Figure 3.19 :** Relationship of the consolidation coefficient and freeze-thaw cycles (Paudel and Wang, 2010).

Özgan et al. (2015), determined the change in the consolidation parameters and settlement results of clay soils exposed to repeated freeze-thaw cycles. After determining the index properties of the soil, sample was subjected to 30 freeze-thaw cycles and oedometer tests were performed. Consolidation settlements increased by

23.33% and 23.24% following freeze-thaw cycles. The results of the sieve analysis and hydrometer tests made after the cycles are interpreted as the reason for the increase in the settlements due to the separation of the soil particles after the freeze-thaw cycles.

### **3.6.5 Freeze-thaw effects on unconfined compressive strength**

Previous experimental studies have shown that the freeze-thaw cycles cause loss of strength. The failure planes generally observed by various researchers where the ice lenses formed inside the soil (Booth, 1981; Yong et al., 1982; Formanek et al., 1984; Ogata et al., 1985).

Ghazavi and Roustaie (2010), investigated the effect of freeze-thaw cycles on the compressive strength of fiber-reinforced clay. For this purpose, kaolinite clay reinforced by steel and polypropylene fibers is compacted in a laboratory and exposed to a maximum of 10 closed-system freezing and thawing cycles. The unconfined compressive strength of reinforced and unreinforced specimens is then determined. The results of the study show that for the soil investigated, the increase in the number of freeze-thaw cycles results in the decrease of unconfined compressive strength of clay samples by 20–25%.

Firoozi et al. (2015), investigated the influence of freeze-thaw cycles on the unconfined compression strength of lime stabilized kaolinite and illite. In this study, closed-system freezing was applied. Kaolinite and illite specimens were treated with various percentages of lime (1%, 3%, 5%, 7%). Then, the specimens subjected to the temperature of -15°C for 24 h. After, they are thawed at a temperature of 22°C for 24 h in a humidity room. After the 1, 2 and 3 F-T cycles, the unconfined compression tests were performed. All treatments present better unconfined compressive strength values than the ones of native soil under freeze-thaw cycles.

Hotineanu et al. (2015), examined the effect of the percentage of lime content and curing time used in improving on the strength parameters under various F-T cycles. In this study two types of clay (bentonite and kaolinite) were used. Samples were treated by using 5% and 3% by weight of lime. The samples were wrapped with paraffin so as not to lose their water content and were allowed to cure at different curing times (3, 28 and 300 days) at room temperature of 20° C. At the end of each curing time, the treated soil samples were subjected to 0, 1, 2, 5 and 10 freeze-thaw cycles in a closed system freeze-thaw chamber according to the standard. Unconfined compression tests

were conducted on the clay soil samples that were subjected to freeze-thaw cycles. As a result of the experimental studies, unconfined compressive strength values of the bentonite clay samples showed a tendency to decrease with the increasing cycles. The unconfined compressive strength of the lime-treated kaolinite clay increased, but the increase in strength was less than the treated bentonite, indicating that the kaolinite clay was less reactive. A decrease in unconfined compressive strength results with the increasing freeze-thaw cycles for the kaolinite clay was also observed.

Xie, Qu, Lai et. al. (2015), conducted several experiments to determine freeze-thaw effect of the samples which were collected from Qinghai-Tibet Plateau. The mechanical properties such as unconfined compression strength of the samples were examined after the soil subjected to various freeze-thaw cycles. Both freezing and thawing durations were determined as 12 hours. The freeze-thaw temperature difference was from  $-40^{\circ}\text{C}$  to  $20^{\circ}\text{C}$ , and freeze-thaw cycles were 0, 1, 3, 6, 9, 12, and 15. The soil samples after different freeze-thaw cycles were used in uniaxial and triaxial compression tests at room temperature of  $15^{\circ}\text{C}$ . After a fixed number of freeze-thaw cycles, all the samples were kept at a room temperature of  $15^{\circ}\text{C}$  for 24 h, and then used in two types of tests. Uniaxial compression tests were performed on the seven types of soil samples with a constant loading rate of 1.25 mm/min. The unconfined compression strength becomes stable after six freeze-thaw cycles. The initial freeze-thaw action, the variation of particle gaps, and the arrangement in the soil sample affect physical and mechanical behaviors directly.

Dayioglu (2015), investigated the expansive Belle Fourche clay from South Dakota. The experimental research focused on the class C fly ash, class F fly ash and lime treated samples with different curing times (0, 7 and 28 days). Unconfined compressive strength tests were conducted on the samples. Freeze and thaw effects on the strength properties of the clay and mixtures were investigated. It was observed that the lime treatment caused 1.82 times higher unconfined compressive strength than the untreated soil. Freeze thaw tests negatively effected the unconfined compressive strength of the soil samples. Freeze-thaw cycles reduced the unconfined compressive strength of the clay and the clay treated with class F fly ash. In the Figure 3.20, the unconfined compression strength of Belle Fourche clay samples which are exposed to F-T effect is given. 8 cycles of F-T caused an important reduction in unconfined compression strength of all mixtures.

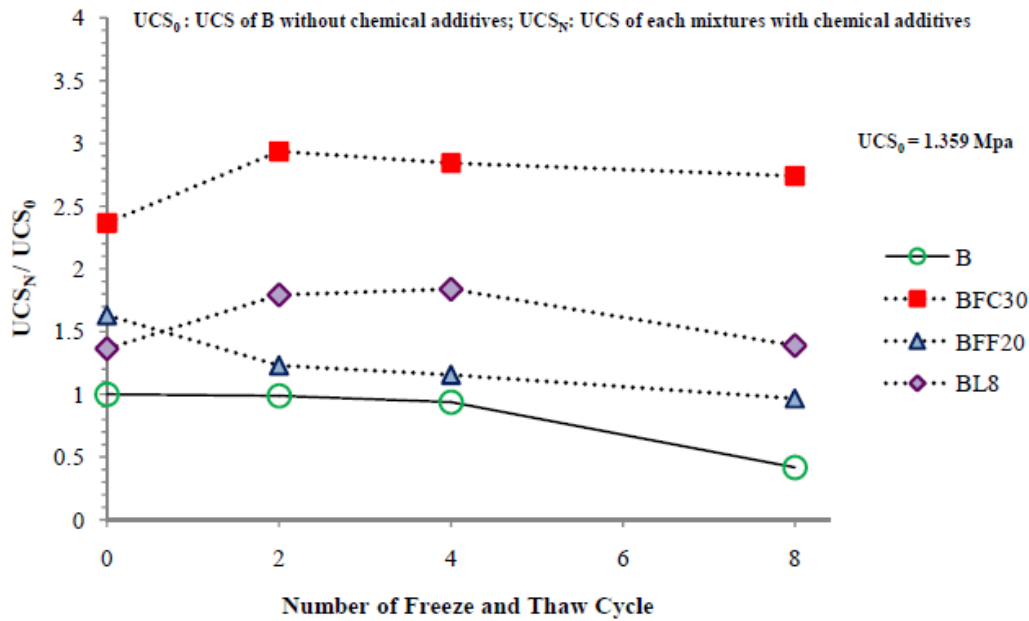


**Figure 3.20 :** Unconfined compression strength change with freeze and thaw effect (Dayioglu, 2015).

Sezer and Boz (2018), focused on the samples which contains 0, 0.5% and 1% by weight of 12 mm basalt and polypropylene fiber which were prepared by the standard Proctor compaction. Some fiber-clay mixtures were stabilized with 3% lime, while other samples were not treated with lime for comparison. All samples were cured in a humidity cabinet (relative humidity of  $95 \pm 2\%$ ) at an average temperature of  $20^\circ\text{C}$  for 28 days. After the curing, the samples were subjected to the freeze-thaw test after 0, 1, 3, 7 and 10 times following ASTM procedure. The results showed that with the increasing freeze-thaw cycles, the unconfined compressive strengths and ultrasonic pulse rates of the samples were reduced.

Ciftliklioglu (2018), investigated the strength behavior of high plasticity clays with no additive and stabilized by chemical additives. Samples containing 8%-12% fly ash and 3%-6% lime for the two clay types were prepared. 7 different freeze-thaw tests were carried out on these samples. After these experiments, the unconfined compression strengths of the samples were measured for each freeze-thaw cycle. It was aimed to observe the effect of the increasing freeze-thaw cycles on the natural and chemically stabilized soils and the effects of the physical properties of the soil. It was observed that the strength losses decreased after the first cycle, and became stable by the 10<sup>th</sup> cycle when the void ratio reached to its residual value. In general, unconfined compression strength of stabilized soils after freeze-thaw cycles showed higher values

than natural soil samples. The unconfined compression strength results of treated and untreated CH<sub>1</sub> samples for varying freeze-thaw cycles can be seen in the Figure 3.21.

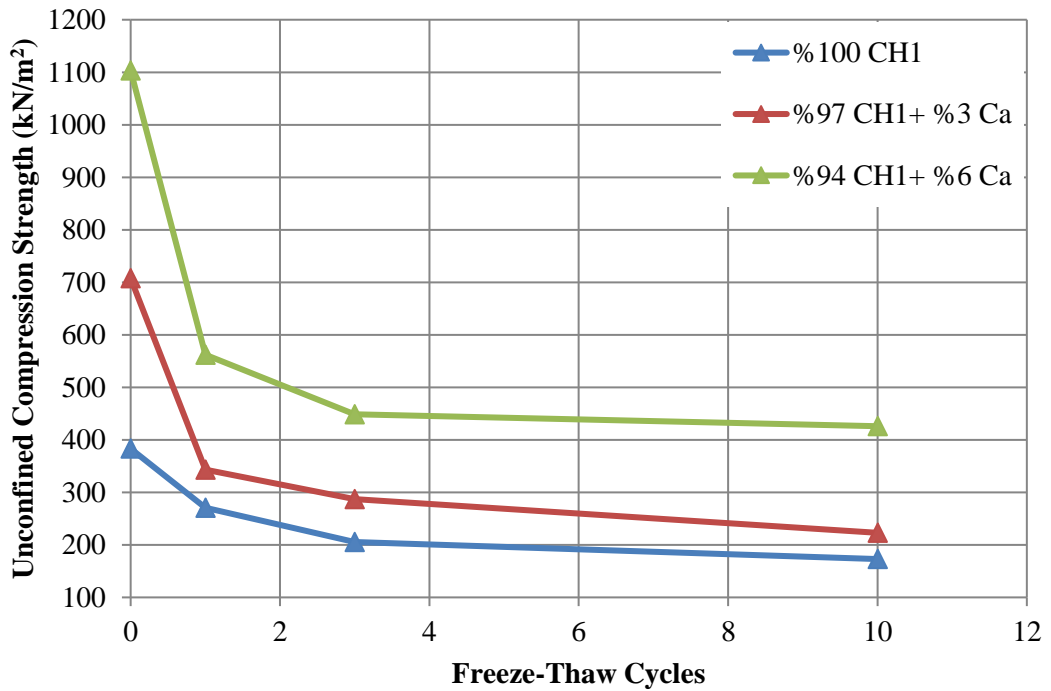


**Figure 3.21 :** Strength behavior of CH<sub>1</sub> clay and lime mixtures after different freeze-thaw cycles (Ciftliklioglu, 2018).

### 3.6.6 Freeze-thaw effects on swelling pressure

Schatz and Martikainen (2010) presents a set of results from laboratory studies on the effect of freezing and thawing on compacted bentonite. In order to evaluate the effect of freezing and thawing on compacted bentonite a series of experiments were conducted using closed, constant volume cells. Pre and post freezing swelling pressure measurements were performed on fully saturated bentonite samples, at dry density values of approximately 1.6 g/cm<sup>3</sup>, over five F-T cycles from room temperature to -18 °C with rapid temperature exposure. Measured swelling pressures of initial conditions at room temperature and after five F-T cycles are displayed in Figures 3.22. After the first F-T cycle, lower swelling pressure values acquired from the bentonite samples (90, 89, 88, 85, and 84 % of initial state).

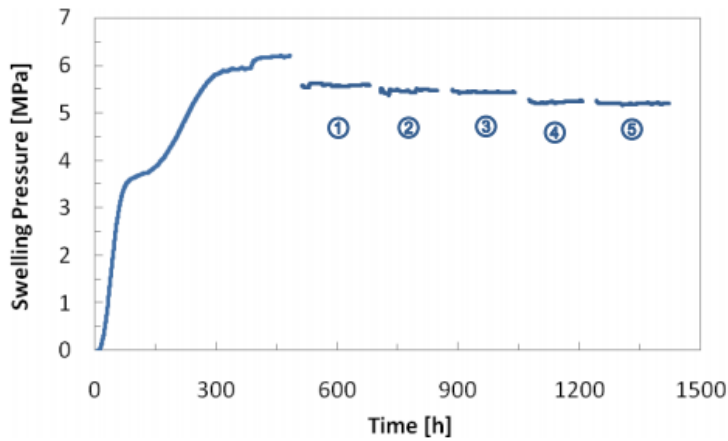


**Figure 3.22 :** Swelling pressure results of bentonite affected by five repetitive freeze- thaw cycles (Schatz and Martikainen, 2010).

Dayioglu (2015), investigated the effects of freeze and thaw on swelling potential. Belle Fourche clay without any chemical additive (B), Belle Fourche clay mixed with 30% class C fly ash (BFC30), Belle Fourche clay with 20% class F fly ash (BFF20), and Belle Fourche clay with 8% lime (BL8) were selected for the freeze and thaw effect investigation. Treated samples were cured in a moisture room for 7 days before experiencing freeze and thaw (F-T) cycles. These specimens were subjected to 2, 4, and 8 freeze and thaw cycles and then tested for swelling potential. The swelling pressure of Belle Fourche clay samples decreased with the increase of F-T cycles. The measured swelling pressures were normalized by dividing the swelling pressure of the mixtures of the clay and additives ( $SWP_N$ ) by that of Belle Fourche clay with no additive ( $SWP_0$ ). The relationship between the normalized swelling pressure values and numbers of F-T cycles are given in Figure 3.23.

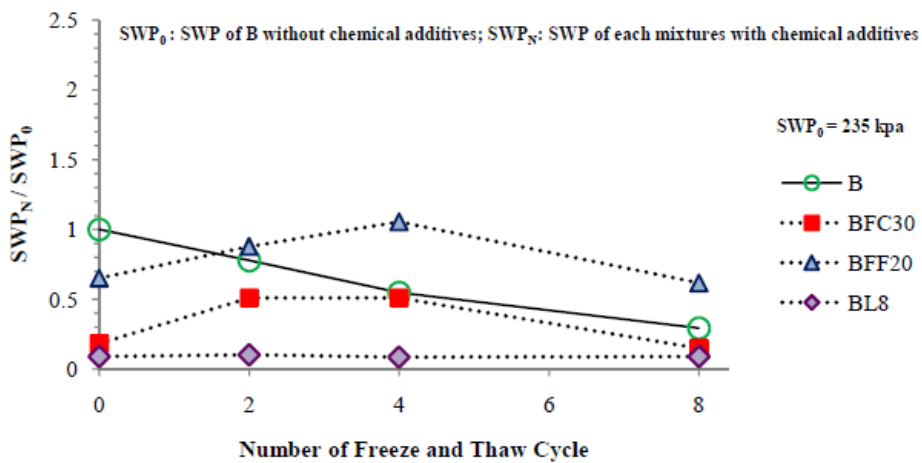


**Figure 3.23 :** Swelling pressure change with freeze and thaw effect (Dayioglu, 2015).

## **4. EXPERIMENTAL RESEARCH**

### **4.1 Purpose**

Within the scope of the study, the engineering properties tests of the soil samples will be performed according to ASTM Standards in the Soil Mechanics Laboratory of Istanbul Technical University. Materials which used in these experiments and the geotechnical properties of these materials are explained. The results obtained after the experiments were compiled in the last part. In accordance with the purpose and scope of the study, high plasticity and low plasticity clay samples will be used. Atterberg limit tests will be performed to determine the engineering properties. Soil classification will be done by determining the liquid limit, plastic limit and shrinkage limits of the samples. Sieve analysis and hydrometer analysis will determine the gradation curve of the samples.

The samples shall be prepared by Harvard miniature compaction test tool. Prepared samples will be subjected to freeze-thaw cycles in accordance with the ASTM Standards. At the end of cycles, swelling pressures will be measured with an oedometer to determine the swelling pressures. At the end of the experiment, water content will be calculated. Thus, the amount of water and void ratio in the sample will be determined. This procedure will be repeated for all different clay samples throughout the study.

The swelling pressures of the clay samples which are not exposed to freezing and thawing effect will be determined and the mineralogical properties of the samples will be obtained. It is expected that the swelling pressure may vary depending on the void ratio, compression energy, water content, dry unit volume weight, porosity and mineralogical structure. Decrease in the swelling pressure values of clay samples with the increasing number of freeze-thaw cycles is expected. Due to the freeze-thaw effect and the variation in water contents, voids and mineralogical structures of the samples, that lead to an expectation of decrease in swelling pressures. As a result of the tests, it is aimed to improve the engineering properties of the soils where if there is a possibility of swelling of the soil layers in different regions.

In this chapter, the selection of materials, the determination of soil index properties and soil preparation for experiments are explained. Thereafter, the testing procedures used through each experiment to assess soils swelling behavior and parameters that affect swelling mechanism are addressed in further subsections.

## 4.2 Laboratory Experiments

Experiments in this study performed at Istanbul Technical University, Faculty of Civil Engineering Geotechnical Engineering Laboratories. Experiments were conducted in guidance of the American Society of Testing Material (ASTM) standards.

### 4.2.1 Sieve analysis and hydrometer tests

Procedures for sieve analysis and hydrometer test are prescribed in ASTM C136/C136M. Sieve analysis and hydrometer test are experiments to determine the grain size distribution of soils. By performing the sieve analysis with the samples remaining on the sieve no.200 and performing the hydrometer test with the passing samples from the sieve no.200, the grain size distribution curve is obtained. Firstly, the test sample is dried at  $105 \pm 5$  ° C for 24 hours. Sieves placed in a scale to small to large sieve diameters, the dry sample is first sieved sequentially through the largest diameter sieve to the smallest. The quantities of the remaining soils are determined, and the values are recorded. Then, the grain size distribution curve is formed by calculating the diameters of the sieves and the ratio of these values to the initial total soil sample. The hydrometer test is applied for the sample passing through sieve no.200 with washing method which separates the soil particles smaller than grain size of 75 microns (Figure 4.1).



**Figure 4.1** : Hydrometer analysis tools.



The washed sample is dried, and 50 g dry sample is taken and kept in the container with the dispersing agent for 24 hours. Hydrometer analysis performed by using Stoke's law, which assists to calculate the precipitation rates of the particles according to their grain diameters in the 1000 ml suspension prepared with distilled water. The values obtained from the hydrometer test are combined with the sieve analysis to form the grain size distribution curve of the sample.

#### **4.2.2 Consistency (Atterberg) limit tests**

The consistency of fine-grained soils is majorly affected by the amount of moisture content present in these soils. Consistency limits or Atterberg limits defined as the moisture content when the soil changes from one state to another state (Murthy, 2002).

Fine-grained soil can exist in any of four states depending on water content, stated as;

- Solid state
- Semi solid state
- Plastic state
- Liquid state

Liquid Limit defined as the moisture content when the soil-water mixture passes from plastic state to liquid state. The soil sample behaves like a viscous fluid under its own weight at this state. Any change in water content either side of the liquid limit results in volume change of the soil. Casagrande liquid limit test can be conducted to define the liquid limit (LL) in laboratory. LL defined as the moisture content at which two sides of a groove come closer for 12.7 mm under the impact of 25 number of blows according to this method (Figure 4.2).



**Figure 4.2 :** Casagrande liquid limit apparatus.

The procedure is performed multiple times with a range of water contents, then the number of blows in the Casagrande liquid limit apparatus is determined and a graph of water content-number of blows is plotted on the semi logarithmic axis. The water content value corresponding to the 25 number of blows gives the liquid limit.

Plastic limit is defined as the moisture content when the soil-water mixture passes from semi-solid state to plastic state. The soil sample passes to semi-solid state by decreasing the water content. In the plastic state, the desired shape can easily be imparted to the soil without breaking or cracking the mixture. In the semi-solid state, the desired shape of the floor is hardly given, the mixture cracks. In the solid state, the mixture cannot be shaped, it is broken when it is tried to be shaped (Uzuner, 2014).

In ASTM D-4318, plastic limit (PL) is defined as the moisture content at which the soil begins to crumble when rolled up into a thread of 3.2mm in diameter. If cracks are formed on the cylinder mixture samples, the experiment is succeeded, and the water contents of the samples are determined.

Shrinkage Limit (SL) is defined as the maximum moisture content when the decrease in water content cause no change in total volume of soil but the increase in moisture content results in an increase in moisture content. Determination of volumetric shrinkage limit is performed according to ASTM D-427. The procedure involves the measurement of initial wet soil mass, dry soil mass and water content of the soil as a percentage of dry mass. Finally, shrinkage limit is calculated by using the Equation 4.1, stated as below;

$$SL = W - \{[(V - V_0) \times \rho_0 / M_0] \times 100\} \quad (4.1)$$

Where;

SL: Shrinkage limit

W: Initial water content of the soil

V: Volume of the mercury held in the shrinkage dish

V<sub>0</sub>: Volume of the mercury displaced into the evaporating dish

ρ<sub>0</sub>: Density of water equal to 1 g/cm<sup>3</sup> at 20°C

M<sub>0</sub>: Dry soil mass

Plasticity Index is expressed as the range of water content when a soil behaves plastically. It can be calculated by using the Equation 4.2.

$$PI = LL - PL \quad (4.2)$$

Where;

PI: Plasticity index

SL: Liquid limit

W: Plastic limit

#### 4.2.3 Specific gravity test

Specific gravity is defined as the ratio of the density of a substance to the density of a reference substance such as water. Determination of specific gravity explained in the ASTM D854. Samples are oven dried at 105 ° C for 24 hours. First, the pycnometers are filled with water, their surface is cleaned and their weights and pycnometer with 50 g oven dry soil are weighed and recorded. To avoid entrapped air in the suspension, air is drawn with vacuum pump. Finally, it is filled with distilled water and the sample is waited until soil sample is completely dissolved in the suspension. Then the weight is weighed and recorded. The Specific gravity of soil solids  $G_s$  is calculated using the following Equation 4.3.

$$G_s = (W_2 - W_1) / [(W_2 - W_1) - (W_3 - W_4)] \quad (4.3)$$

Where;

$W_1$  = Empty weight of pycnometer

$W_2$  = Weight of pycnometer + oven dry soil

$W_3$  = Weight of pycnometer + oven dry soil + filled water

$W_4$  = Weight of pycnometer + filled with water only

#### 4.2.4 Modified Harvard miniature compaction test

Compaction can be stated as rearrangement of soil particles by removing air voids using mechanical equipment. Optimum water content is defined as the moisture

content at maximum dry unit weight. The Harvard miniature compaction tool is used to determine the optimum water content and maximum dry unit weights of the soils and at the same time to easily obtain samples for various experiments. The soil sample required for the experiment is very small compared to the standard Proctor test. Thus, this tool provides a great advantage in large scale studies using different soil samples in various and proportions. In addition, the time and effort required for experiments with the modified Harvard miniature tool is also significantly reduced. The components of the modified Harvard miniature tool are as follows and shown in the Figure 4.3;

- Main body
- Hammer
- Mold
- Mold stabilizer
- Drop height stabilizer



**Figure 4.3 :** Modified Harvard miniature compaction test apparatus.

In order to calibrate the modified Harvard miniature tool, standard Proctor and modified Harvard miniature compaction tests were performed on the same samples each and several times. Different fall height and number of blows have been tried. In the first calibration tests, the parameters for the Harvard miniature compaction test

were taken as 18 blow numbers, 20 cm drop height and 3 layers. It was observed that the standart Proctor energy was not achieved due to friction that occurred while conducting the tests. Then 20 blow numbers, 20 cm drop height and 3 layers were tried in the modified harvard compaction test. After the calibration tests, the drop height decided as 20 cm and the number of blows per layer calculated as 20 in Modified Harvard Miniature compaction test. The Ca bentonite (CH<sub>4</sub>) compaction results are stated in the Figure 4.4. The same calibrations were repeated for each soil samples that will be used throughout the research.

Modified Harvard miniature compaction test performed within the scope of this thesis study, the soil sample passing through the sieve no. 40 was compacted in 3 layers and the 1110 g hammer blowed 20 times from 20 cm drop height for each layer. Table 4.1 shows the parameters of the standart Proctor, modified Proctor and Harvard miniature compaction tests.

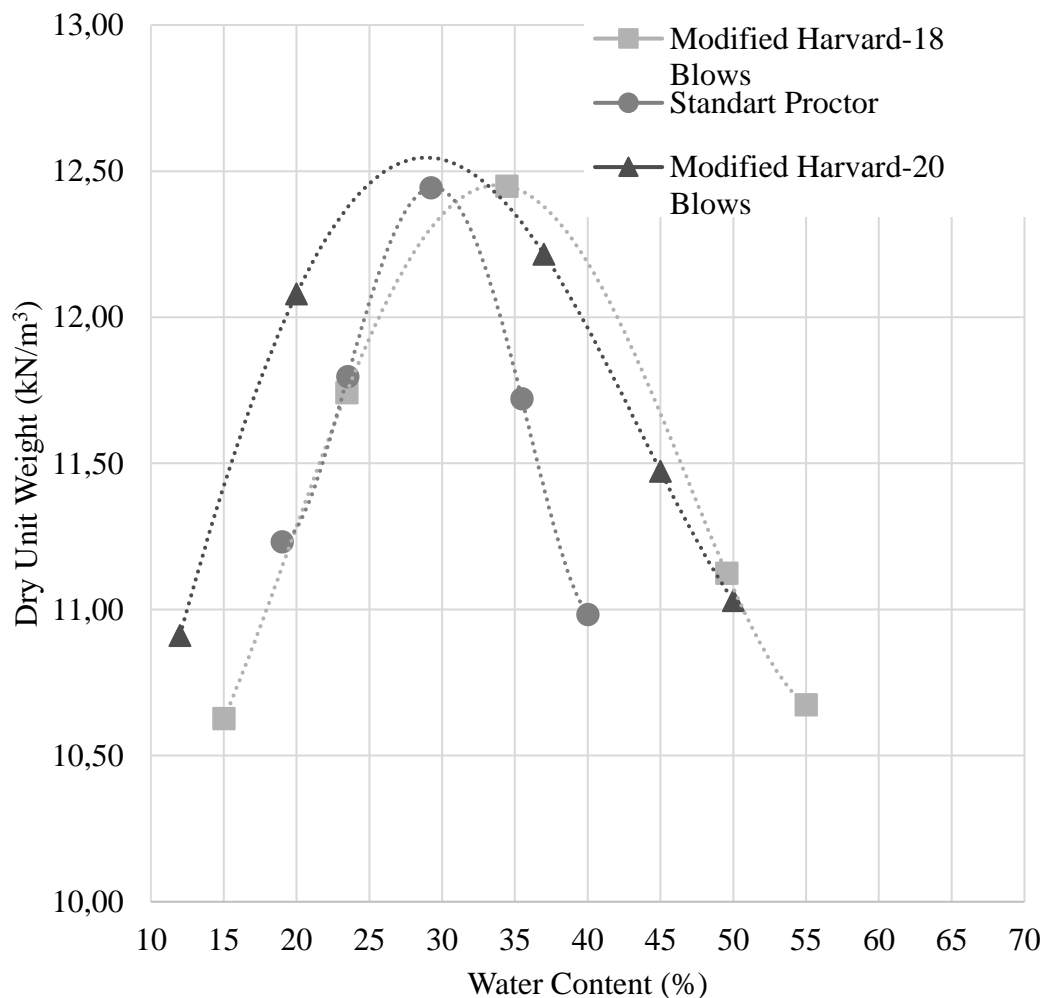


**Figure 4.4 :** Calibration results of modified harvard compaction test (CH<sub>4</sub>).

**Table 4.1** : Comparison of laboratory compaction tests.

	<b>Standard Proctor Test</b>	<b>Modified Proctor Test</b>	<b>Modified Harvard Miniature Compaction Test</b>
Number of Blows	25	56	20
Number of Layers	3	5	3
Hammer Weight (g)	2500	4500	1110
Drop Height (cm)	30,5	45,7	20
Volume (cm <sup>3</sup> )	944	2304	200
Energy (gr.cm/cm <sup>3</sup> )	6058	24992	6660

#### 4.2.5 Freeze–Thaw Cycle Experiments

The soil samples were subjected to freeze and thaw cycles in a closed system according to the method specified in Standard ASTM D560. The samples were cooled for 24 hours at the initial temperature ( $-23 \pm 2$  ° C). Then the samples removed from the refrigerant were allowed to dissolve in desiccators for 24 hours in laboratory conditions ( $23 \pm 2$  ° C). This 48 hour freeze-thaw process was determined as 1 freeze-thaw (F-T) cycle and experiments were continued using these F-T cycles throughout the research.

In order to examine the swelling pressure behavior of the samples according to different freeze-thaw cycles, swelling pressure tests corresponding to the cycles determined at the beginning of the research were carried out. Freeze-thaw cycles were selected considering the previous literature researches. All samples were subjected to 0, 1, 3, 5, 7, 10, 15, 20 and 25 freeze-thaw cycles. Thus, short- and long-term swelling characteristics of soil samples can be investigated.

#### 4.2.6 Swelling pressure tests

Swelling pressure tests were conducted in accordance with the ASTM standards. Method C followed throughout the research to determine the swelling pressures of samples. The procedure of method C includes the samples height remained constant by applying vertical loads after the sample get in contact with the water and submerged into it Therefore, volume of the sample will not change during the test. The pressure that do not perform any volumetric change on the soil sample and maintain the initial height can be stated as the swelling pressure. The swelling pressure samples were taken

from the top and bottom parts of the cylindrical samples of 10 cm height and 5 cm diameter which were formed in the Harvard miniature compaction apparatus. It is estimated that the void ratios at the top and bottom of the samples will vary and also show differences in swelling pressure behaviors after various freeze-thaw cycles. For this reason, at least 2 samples were prepared for each F-T cycle. A total of 3 samples were used for each freeze-thaw cycle, 2 in the bottom part and one in the top part. Samples were prepared with 3.5 cm diameter and 2 cm height rings. The time required for the materials to finish the swelling pressure tests showed differences. 3 different oedometer tests were established and conducted. To illustrate, the bentonites' swelling pressure test duration lasted longer than natural clays. The oedometers can be seen in the Figure 4.5.



**Figure 4.5 :** Oedometers in the I.T.U laboratories.

### **4.3 Material Selection**

Taking into consideration of the main purpose of this research, Istanbul Technical University Scientific Research Office supported this research with MYL-2017-40533 project code. A closed freezing system and materials were provided. The appropriate materials are selected based on their swelling potential to create test samples with different expansivity with a view to simulate the field conditions. The swell potential

of the investigated test samples are desired to be low to high in order to ensure that the test samples include necessary clay minerals to qualify for the research. Therefore, Na bentonite and Ca bentonite have been selected to achieve this study's purpose. In extend to that, three natural expansive soil samples undergo the same experiments. Bentonites were purchased from ÇANBENSAN Export CO. The other natural soil samples were obtained from Istanbul (Figure 4.6).



**Figure 4.6 :** Ca bentonite and natural soil samples.

The first sample, named CH<sub>3</sub>, is Na Bentonite. Sample CH<sub>4</sub> is Ca Bentonite. The other four natural soil samples named CH<sub>5</sub>, CH<sub>6</sub> and CL<sub>1</sub> respectively. The classification of these soil samples will be explained in the following section.

#### **4.3.1 CH<sub>3</sub> (Na Bentonite)**

The results of Atterberg (consistency) limits experiments on Na bentonite are shown in the Figure 4.7. The liquid limit, LL = 296%, plastic limit, PL = 41%, plasticity index, PI = 255% are determined as a result of the consistency limit tests. Gravel percentage was found as 0%, sand percentage was 1%, silt 37% and clay 62% as a result of sieve analysis and hydrometer tests. In Figure 4.7, the grain size distribution of sodium bentonite (CH<sub>3</sub>) is given. As a result of the consistency limits and grain size distribution, according to the Unified Soil Classification System (USCS), the sodium bentonite was determined as high plasticity clay (CH). Figure 4.8 shows the compaction results of CH<sub>3</sub> clay which obtained from the Harvard miniature compaction test. As a result of the Harvard compaction test for CH<sub>3</sub>, the optimum water content was determined 37% and the dry unit weight was 11.60 kN/m<sup>3</sup>.



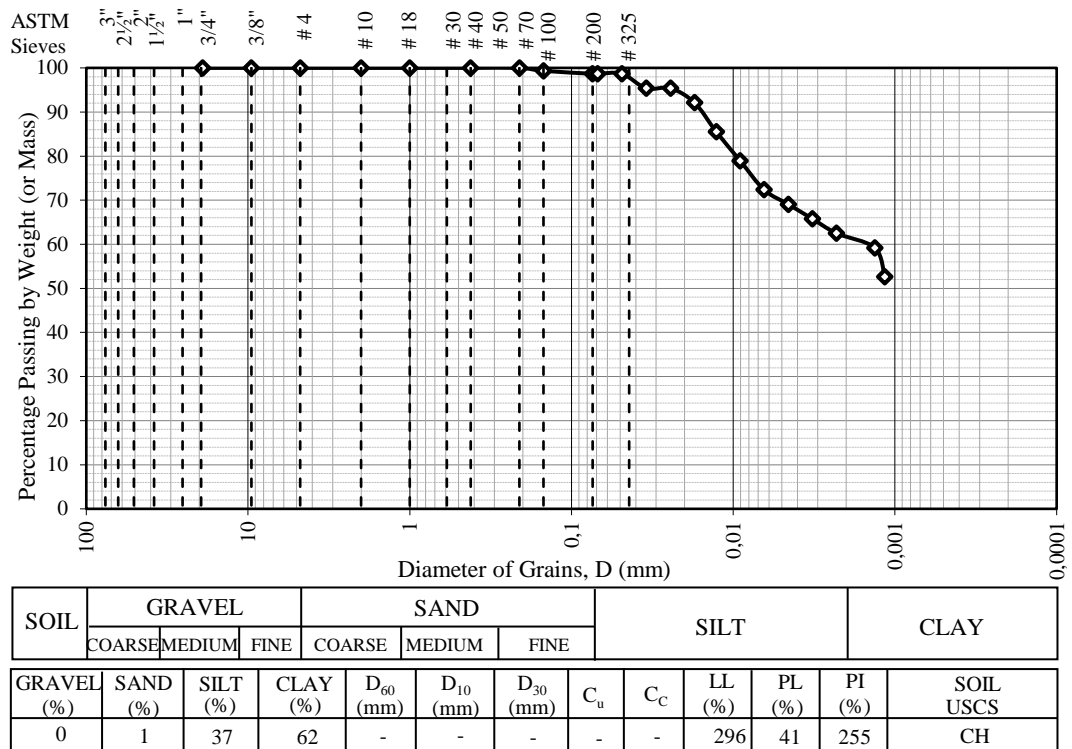


**Figure 4.7 :** Grain size distribution and classification of CH<sub>3</sub>.

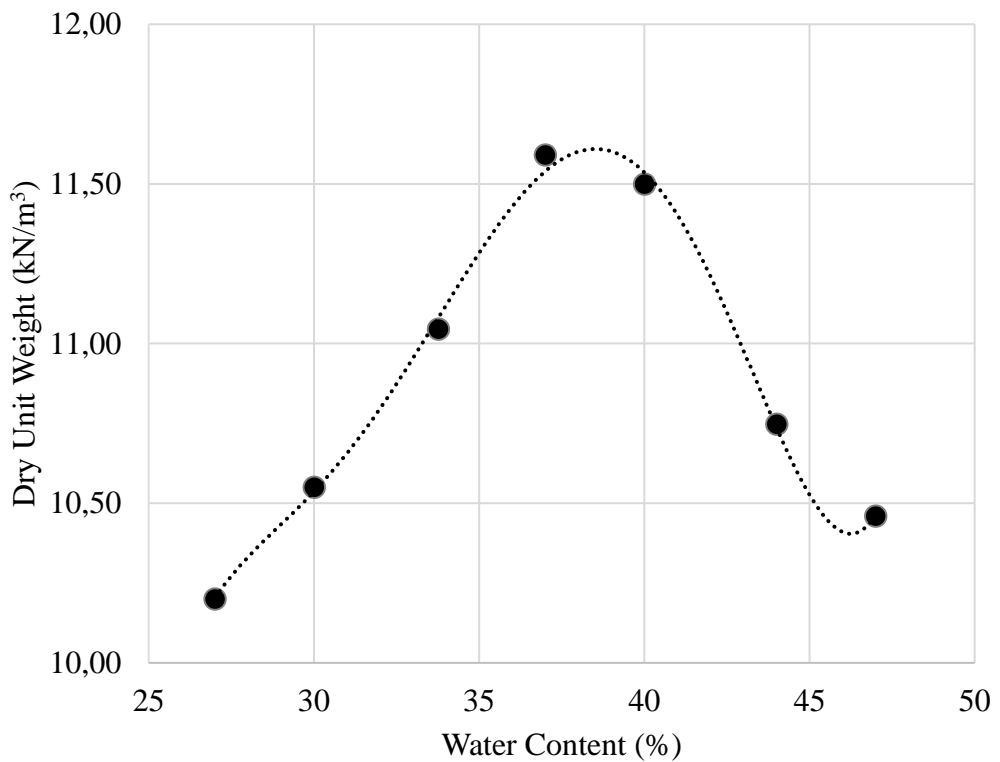
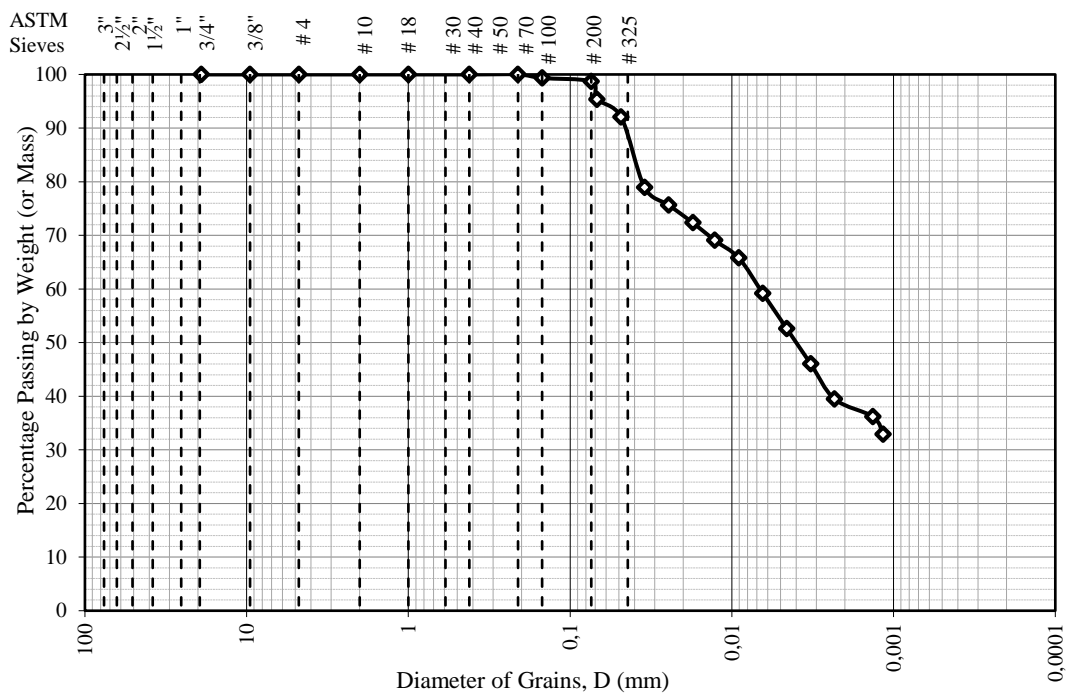


**Figure 4.8 :** Compaction test results of CH<sub>3</sub>.

### 4.3.2 CH<sub>4</sub> (Ca Bentonite)

The results of Atterberg (consistency) limits experiments on Ca bentonite are shown in the Figure 4.9. The liquid limit, LL = 288%, plastic limit, PL = 38%, plasticity index, PI = 240% are determined as a result of the consistency tests. Gravel percentage was found as 0%, sand percentage was 1%, silt 60% and clay 39% as a result of sieve analysis and hydrometer tests. In Figure 4.9, the grain size distribution of Ca bentonite (CH<sub>4</sub>) is given. As a result of the consistency limits and grain size distribution, according to the Unified Soil Classification System (USCS), it was determined as high plasticity clay (CH). Figure 4.10 shows the compaction results of CH<sub>4</sub> clay which obtained from the Harvard miniature compaction experiment. As a result of the Harvard compaction test for CH<sub>4</sub>, the optimum water content was determined 30% and the dry unit weight was 12.40 kN/m<sup>3</sup>.



SOIL	GRAVEL			SAND			SILT		CLAY			
	COARSE	MEDIUM	FINE	COARSE	MEDIUM	FINE						
GRAVEL (%)	SAND (%)	SILT (%)	CLAY (%)	D <sub>60</sub> (mm)	D <sub>10</sub> (mm)	D <sub>30</sub> (mm)	C <sub>u</sub>	C <sub>c</sub>	LL (%)	PL (%)	PI (%)	SOIL USCS
0	1	60	39	-	-	-	-	-	288	38	250	CH

**Figure 4.9 :** Grain size distribution and classification of CH<sub>4</sub>.

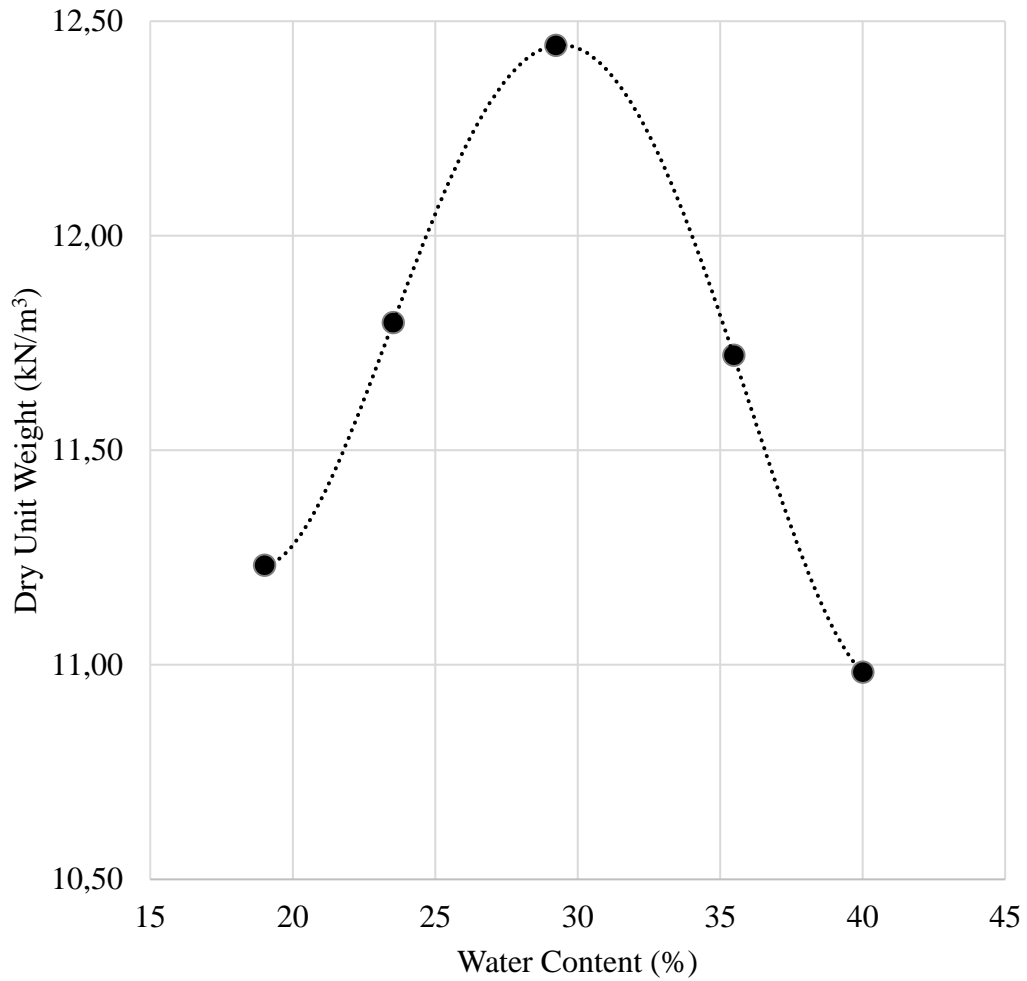
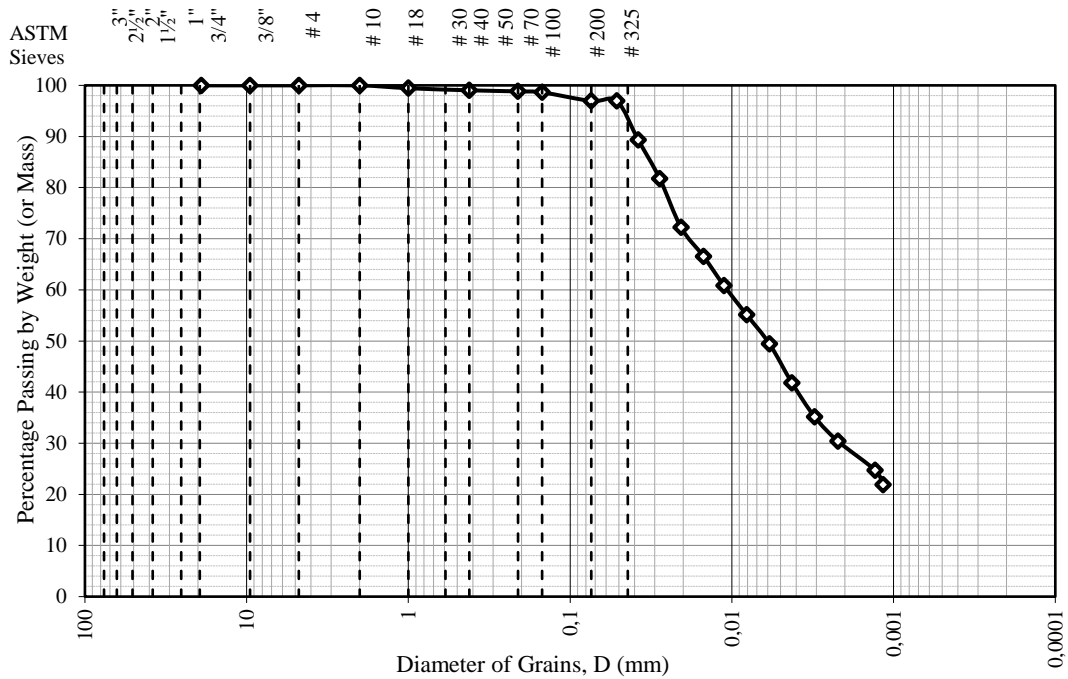


**Figure 4.10 :** Compaction test results of CH<sub>4</sub>.

### 4.3.3 CH<sub>5</sub>

The natural CH<sub>5</sub> clay used in this research was provided from a construction site located in the near district of Istanbul. The results of Atterberg (consistency) limits experiments on natural clay sample are shown in the Figure 4.11. The liquid limit, LL = 68%, plastic limit, PL = 20%, plasticity index, PI = 48% are determined as a result of the consistency tests. Gravel percentage was found as 0%, sand percentage was 3%, silt 68% and clay 29% as a result of sieve analysis and hydrometer tests. In Figure 4.11, the grain size distribution of CH<sub>5</sub> is given. As a result of the consistency limits and grain size distribution, according to the Unified Soil Classification System (USCS), the soil was determined as high plasticity clay (CH). Figure 4.12 shows the compaction results of CH<sub>5</sub> clay which obtained from the Harvard miniature compaction experiment. As a result of the Harvard compaction test for CH<sub>5</sub>, the optimum water content was determined 22% and the dry unit weight was 14.80 kN/m<sup>3</sup>.



SOIL	GRAVEL			SAND			SILT		CLAY			
	COARSE	MEDIUM	FINE	COARSE	MEDIUM	FINE						
GRAVEL (%)	SAND (%)	SILT (%)	CLAY (%)	D <sub>60</sub> (mm)	D <sub>10</sub> (mm)	D <sub>30</sub> (mm)	C <sub>u</sub>	C <sub>c</sub>	LL (%)	PL (%)	PI (%)	SOIL USCS
0	3	68	29	-	-	-	-	-	68	20	48	CH

**Figure 4.11 :** Grain size distribution and classification of CH<sub>5</sub>.

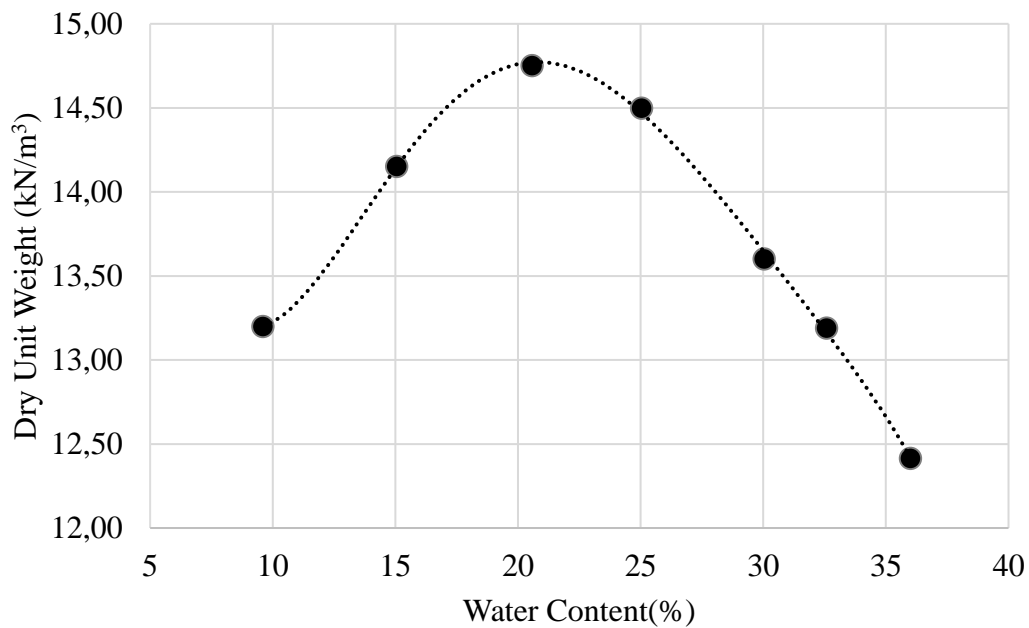


**Figure 4.12 :** Compaction test results of CH<sub>5</sub>.

### 4.3.4 CH<sub>6</sub>

The results of Atterberg (consistency) limits experiments on natural clay sample are shown in the Figure 4.13. The liquid limit, LL = 52%, plastic limit, PL = 28%, plasticity index, PI = 24% are determined as a result of the consistency tests. Gravel percentage was found as 0%, sand percentage was 44%, silt 45% and clay 11% as a result of sieve analysis and hydrometer tests. In Figure 4.13, the grain size distribution of CH<sub>6</sub> is given. As a result of the consistency limits and grain size distribution, according to the Unified Soil Classification System (USCS), the sodium bentonite was determined as high plasticity clay (CH). Figure 4.10 shows the compaction results of CH<sub>6</sub> clay which obtained from the Harvard miniature compaction experiment. As a result of the Harvard compaction test for CH<sub>5</sub>, the optimum water content was determined 23% and the dry unit weight was 14.70 kN/m<sup>3</sup>.

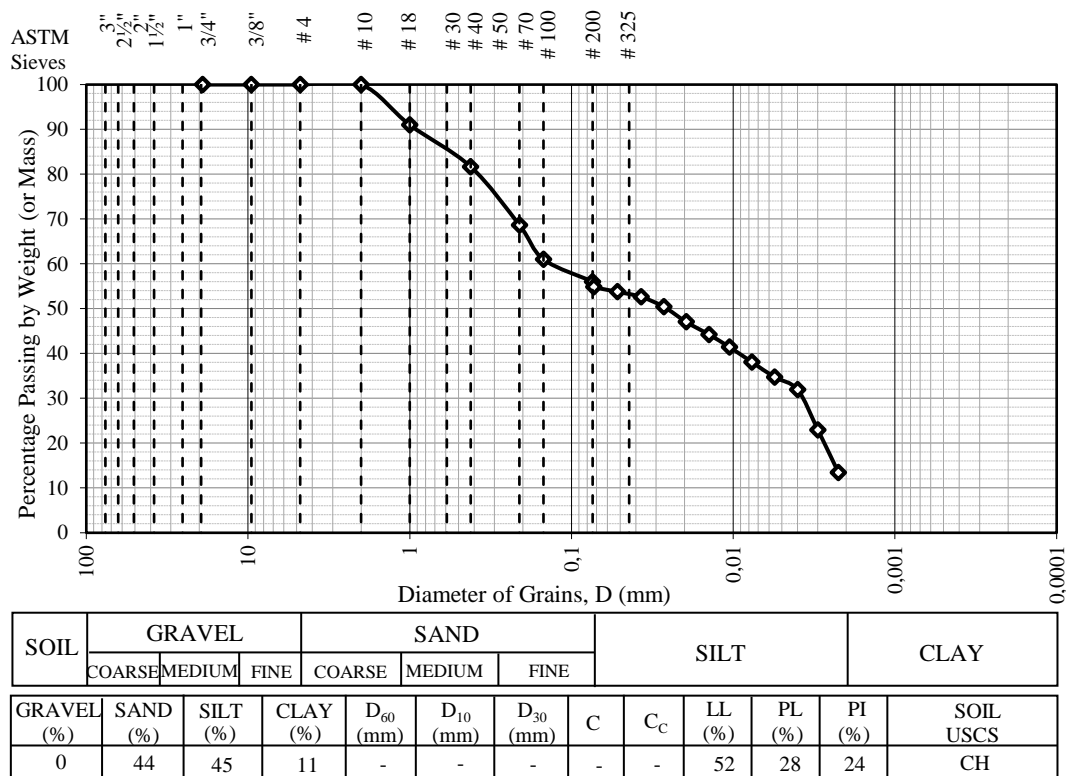


**Figure 4.13 :** Grain size distribution and classification of CH<sub>6</sub>.

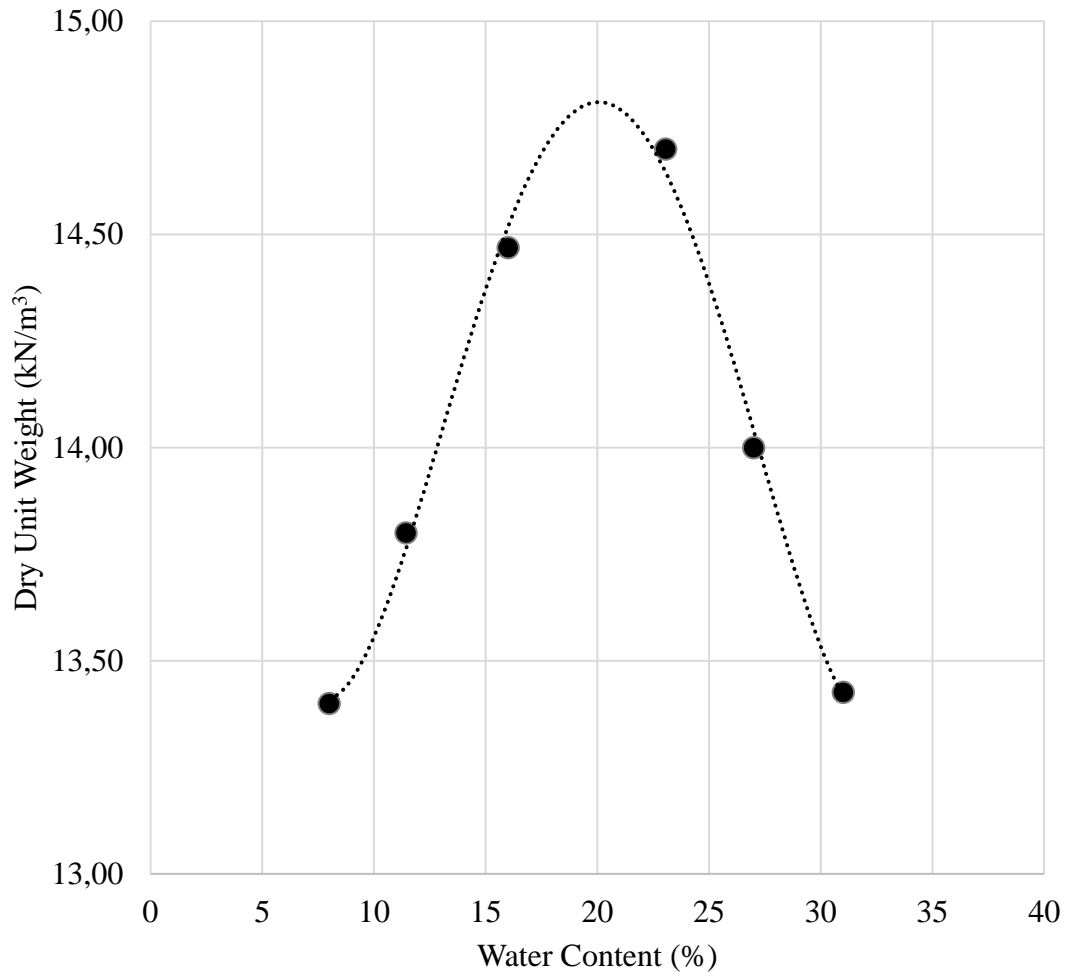
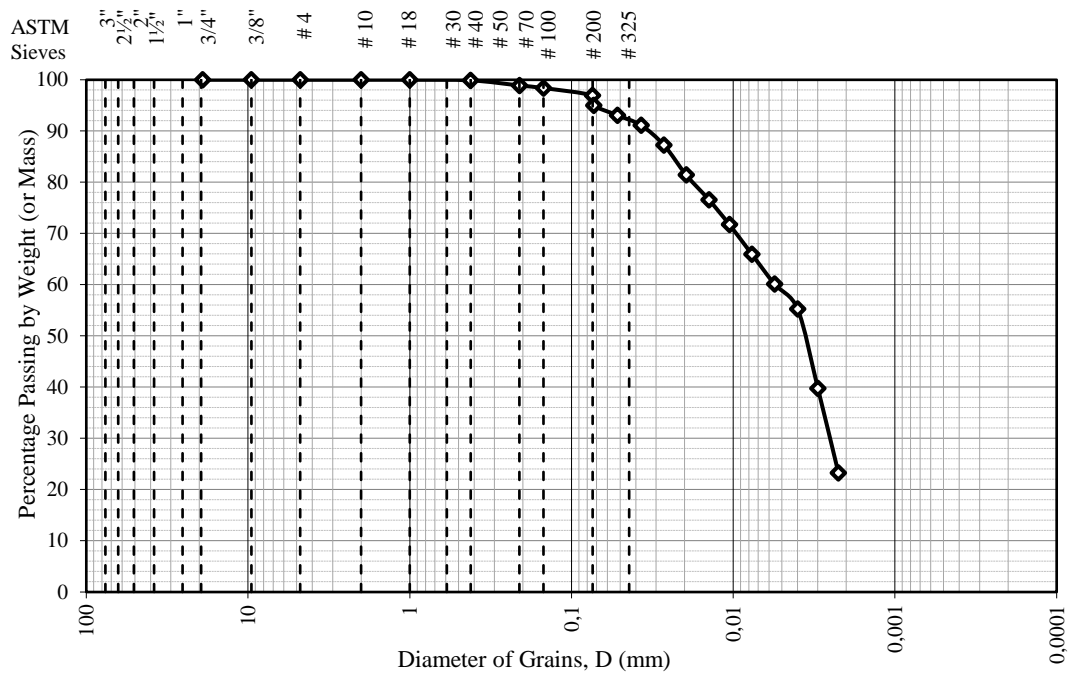


**Figure 4.14 :** Compaction test results of CH<sub>6</sub>.

#### 4.3.5 CL<sub>1</sub>

The results of Atterberg (consistency) limits experiments on natural clay sample are shown in the Figure 4.15. The liquid limit, LL = 36%, plastic limit, PL = 16%, plasticity index, PI = 20% are determined as a result of the consistency tests. Gravel percentage was found as 0%, sand percentage was %3, silt %78 and clay% 19 as a result of sieve analysis and hydrometer tests. In Figure 4.15, the grain size distribution of CL<sub>1</sub> is given. As a result of the consistency limits and grain size distribution, according to the Unified Soil Classification System (USCS), the natural clay was determined as low plasticity clay (CL). Figure 4.16 shows the compaction results of CL<sub>1</sub> clay which obtained from the Harvard miniature compaction experiment. As a result of the Harvard compaction test for CL<sub>1</sub>, the optimum water content was determined 15% and the dry unit weight 16 kN/m<sup>3</sup>.



SOIL	GRAVEL			SAND			SILT		CLAY			
	COARSE	MEDIUM	FINE	COARSE	MEDIUM	FINE						
GRAVEL (%)	SAND (%)	SILT (%)	CLAY (%)	D <sub>60</sub> (mm)	D <sub>10</sub> (mm)	D <sub>30</sub> (mm)	C <sub>u</sub>	C <sub>c</sub>	LL (%)	PL (%)	PI (%)	SOIL USCS
0	3	78	19	-	-	-	-	-	36	16	20	CL

Figure 4.15 : Grain size distribution and classification of CL<sub>1</sub>.

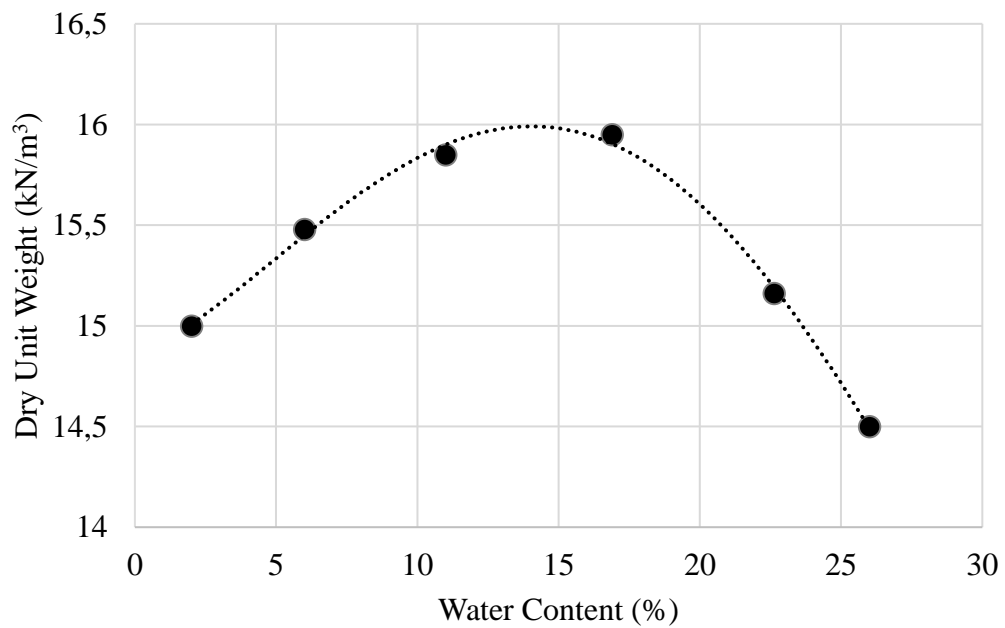


Figure 4.16 : Compaction test results of CL<sub>1</sub>.

Table 4.2 shows the index properties and compaction test results of the clay samples used during the experimental research.

**Table 4.2 :** The results of index tests for all samples.

Soil Samples	CH <sub>3</sub>	CH <sub>4</sub>	CH <sub>5</sub>	CH <sub>6</sub>	CL <sub>1</sub>
LL (%)	296	288	68	52	36
PL (%)	41	38	20	28	16
PI	255	250	48	24	20
$\gamma_s$ (kN/m <sup>3</sup> )	27	27	26,50	27	27
$\gamma_{dry}$ (kN/m <sup>3</sup> )	11,60	12,40	14,80	14,70	16,00
$\omega_{opt.}$ (%)	37	30	22	23	15
USCS	CH	CH	CH	CH	CL

#### 4.4 Evaluation of Laboratory Experiments

In this section, the effect of freeze-thaw cycles on the swelling pressure of high plasticity and low plasticity soils will be investigated. The swelling pressures of the clay samples that are not exposed to freezing and thawing cycles will be determined and the mineralogical properties of the samples will be obtained. It is expected that the swelling pressure may vary depending on the void ratio, compression energy, water content, dry unit volume weight, porosity and mineralogical structure. Therefore, the relationship with swelling pressure and engineering parameters of soils will be investigated in this section. Due to the freeze-thaw effect and the variation in water contents, voids and mineralogical structures of the samples, that lead to an expectation of decrease of swelling pressure values.

Firstly, the results of swelling pressure test before freeze-thaw experiments and relationships with engineering parameters were examined. Then, swelling pressure test results after freeze-thaw experiments were investigated.



#### 4.4.1 Swelling pressure tests before freeze-thaw cycles

The samples were prepared by using the Harvard miniature compaction apparatus at the maximum dry unit weight and optimum water content that obtained from compaction tests. Afterwards, for 24 hours samples were dried in the oven. Then, the optimum water content obtained from the compaction tests is gradually added to achieve a homogeneous mixture. The wetted samples in the optimum water content were compressed into three layers with 20 blow numbers from 20 cm fall height in the Harvard compaction apparatus and then samples removed from the mold and wrapped with stretch film to prevent the loss of water content. Figure 4.17 shows the samples that are extruded and wrapped with stretch film.



**Figure 4.17 :** Prepared soil samples.

The water content in the sample varies in different parts of the sample. For this reason, 2 swelling pressure samples were prepared from the upper and lower parts of the samples. It is expected that the bottom part of the sample will have more water content than the upper region due to the distribution of compaction energy. Therefore, the swelling pressure results will be different from each other. In order to inspect this phenomena, 2 bottom and 1 top sample prepared for each swelling pressure test. Only, for the CH<sub>5</sub> samples, 1 bottom and 1 top swelling pressure samples had to be prepared because of the limited amount of specimen.

Under the guidance of Method C of ASTM D-4546, one-dimensional swelling tests were performed. This method is the most commonly used method for determining the

swelling pressure. It can be stated as loading-after-wetting test. In this method, swelling pressure of the sample was determined by adding weight and do not perform any volumetric change in the sample which will keep the dial gauge reading in the zero. When the readings in the oedometer do not change and stabilized that means swelling pressure has reached the residual value. After observing dial gauge readings the test is completed. The pressure that do not perform any volumetric change on the soil sample and maintain the initial height can be stated as the swelling pressure. Samples were prepared with 3.5 cm diameter and 2 cm height rings. Figures 4.18 shows the samples prepared for the swell test and the swelling pressure test setup respectively.

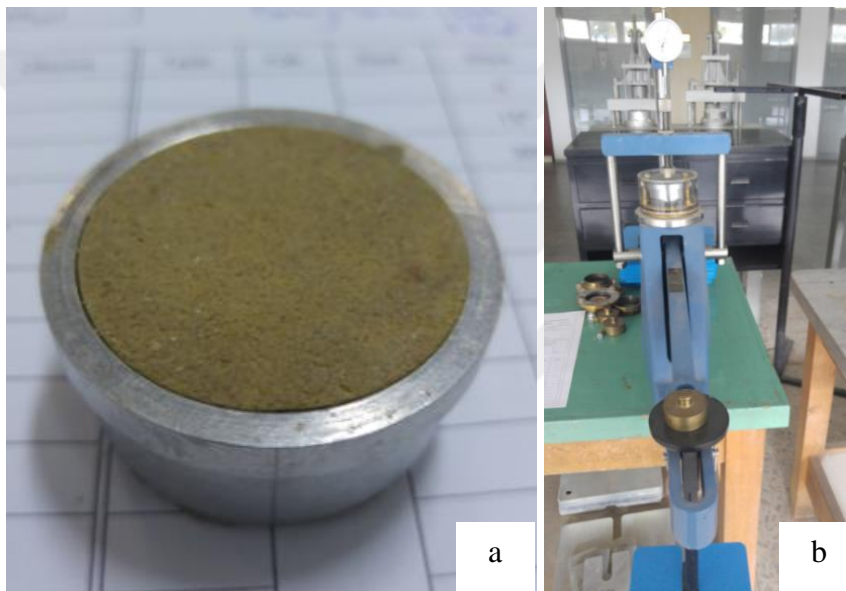


**Figure 4.18 :** a) Sample prepared for the swelling pressure test; b) one-dimensional oedometer swelling pressure test setup.

As a result of the tests, the general tendency was determined as the swelling pressures obtained from the bottom samples were evaluated greater than the results of the top samples for all clay samples. This condition may stems from the difference in void ratios. Therefore, the relationship between void ratio and swelling pressure results will be examined in the following sections.

The results of the CH<sub>3</sub> swelling pressures of the samples which are not subjected to the freeze-thaw shown in the Figure 4.19. As it is exhibited in Figure 4.19, the bottom sample swelling pressure was determined as 228 kPa. the top sample swelling pressure was calculated as 160 kPa.

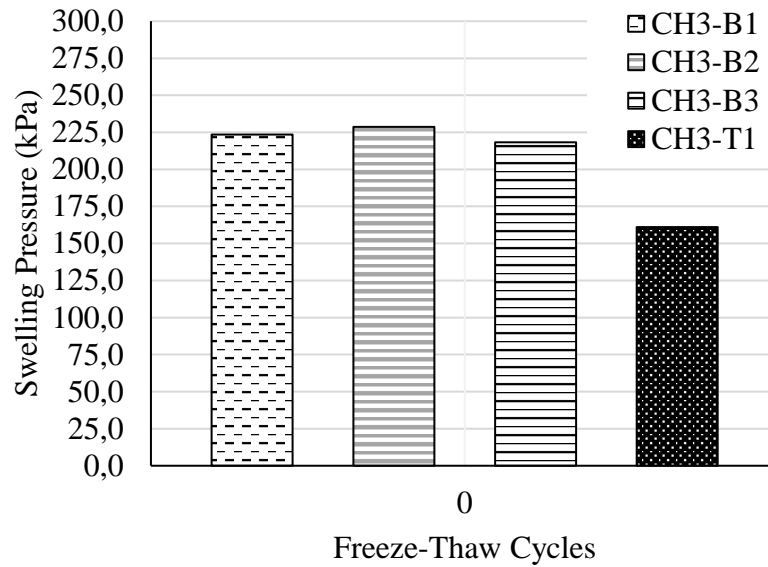


**Figure 4.19 :** Swelling pressure results of CH<sub>3</sub> samples which are not subjected to the freeze-thaw.

The results of the CH<sub>4</sub> swelling pressures of the samples which are not subjected to the freeze-thaw shown in the Figure 4.20. As it is exhibited in Figure 4.20, the bottom sample swelling pressure was determined as 130 kPa. the top sample swelling pressure was calculated as 104 kPa.

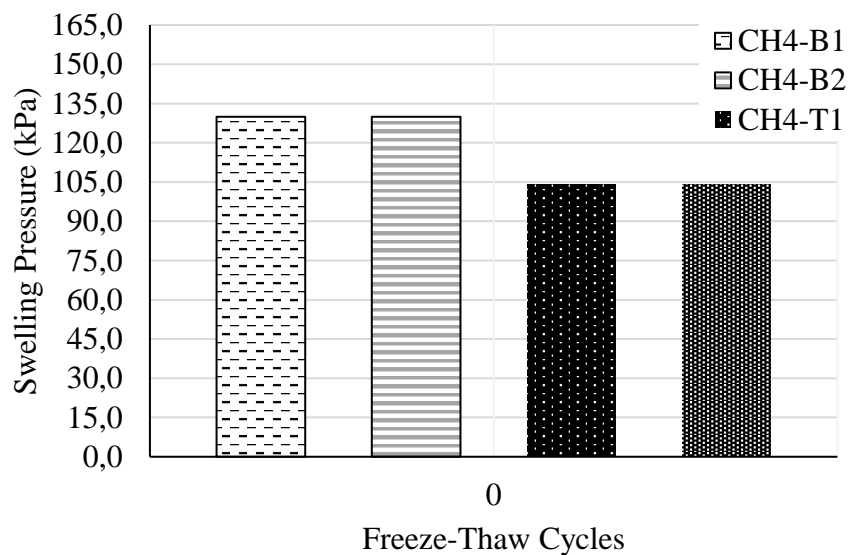


**Figure 4.20 :** Swelling pressure results of CH<sub>4</sub> samples which are not subjected to the freeze-thaw.

The results of the CH<sub>5</sub> swelling pressures of the samples which are not subjected to the freeze-thaw shown in the Figure 4.21. As it is shown in Figure 4.21, the bottom

sample swelling pressure was determined as 94 kPa. the top sample swelling pressure was calculated as 47 kPa.

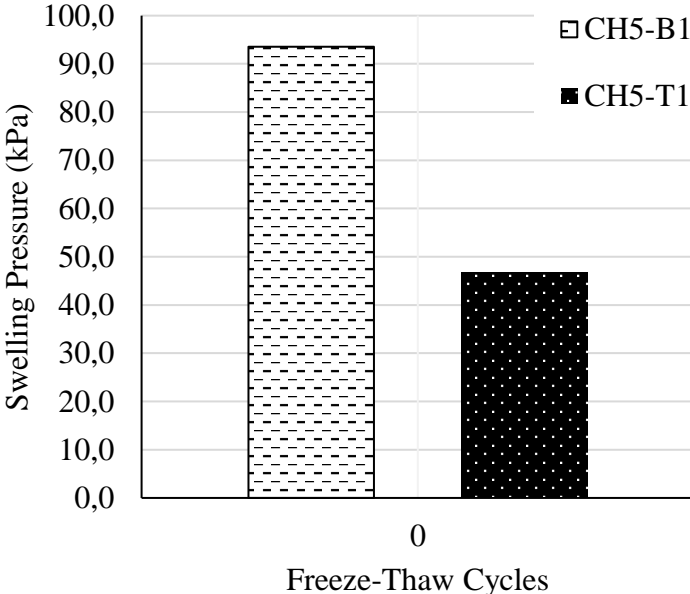


**Figure 4.21 :** Swelling pressure results of CH<sub>5</sub> samples which are not subjected to the freeze-thaw.

The results of the CH<sub>6</sub> swelling pressures of the samples which are not subjected to the freeze-thaw shown in the Figure 4.22. The bottom sample swelling pressure was determined as 60 kPa. the top sample swelling pressure was calculated as 5 kPa.

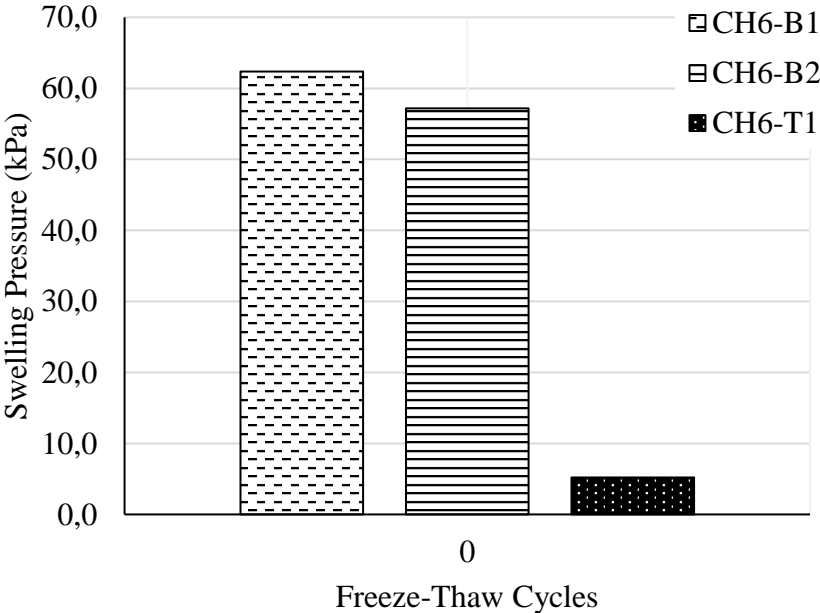


**Figure 4.22 :** Swelling pressure results of CH<sub>6</sub> samples which are not subjected to the freeze-thaw.

The results of the CL<sub>1</sub> swelling pressures of the samples which are not subjected to the freeze-thaw shown in the Figure 4.23. The bottom sample swelling pressure was determined as 57 kPa. the top sample swelling pressure was calculated as 21 kPa.

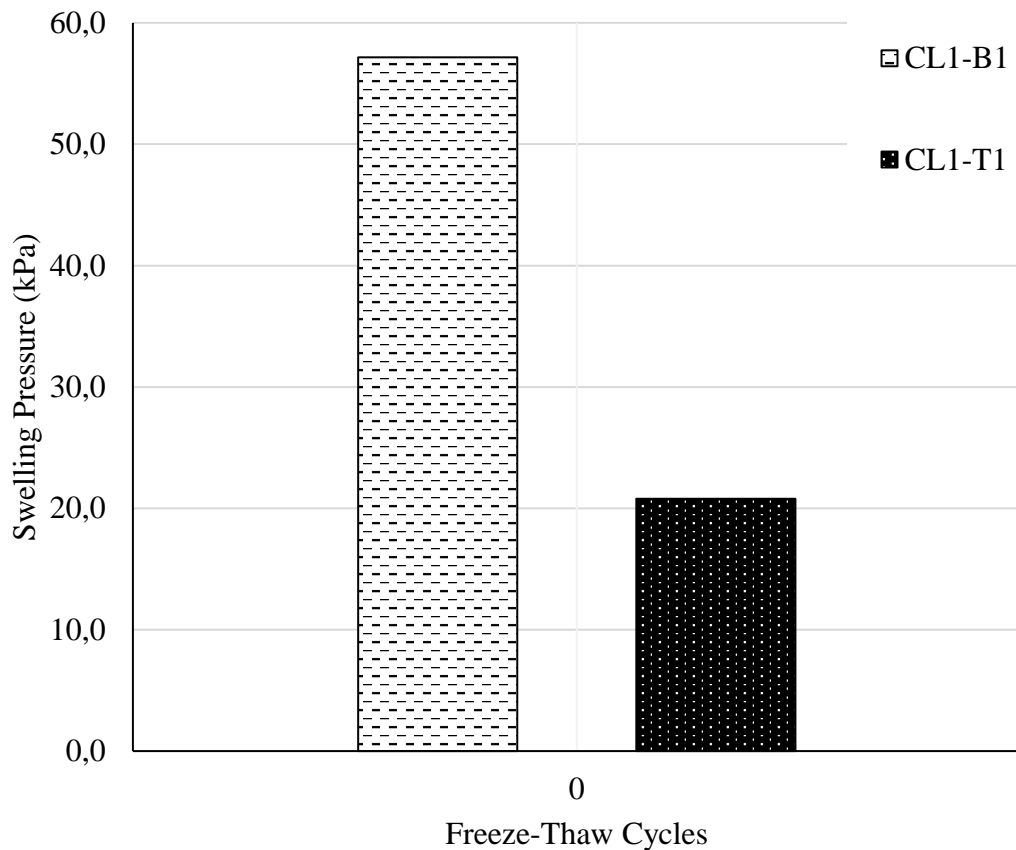


**Figure 4.23 :** Swelling pressure results of CL<sub>1</sub> samples which are not subjected to the freeze-thaw.

#### 4.4.2 Relationships between engineering properties and swelling pressure

The relationships between the engineering properties of the soils and swelling pressures ( $\sigma_s$ ) before the F-T cycles have been investigated. As the top and bottom part swelling pressures differed, the results were evaluated separately for more accurate correlations. The variation of swelling pressure of clay samples was investigated with respect to liquid limit, plastic limit, plasticity index, activity, maximum dry unit weight, optimum water content and void ratio.

In accordance with the previous experimental studies, It is observed significantly that with the increasing liquid limit values, the swelling pressure is increased for both bottom and top results. Figure 4.24 shows the correlation between the  $\sigma_s - LL$  (%) results.

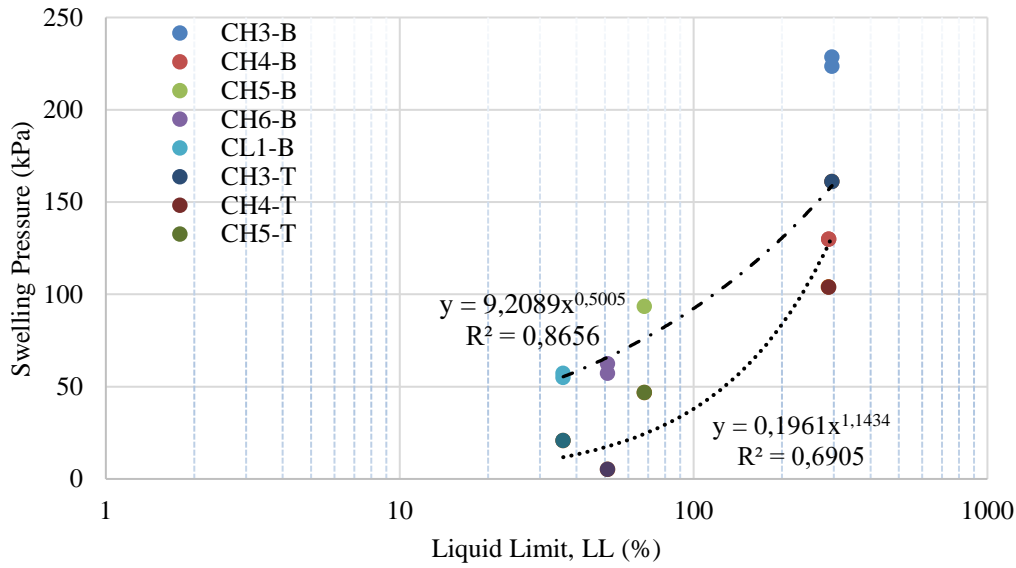


**Figure 4.24 :**  $\sigma_s - LL$  (%) relationship of samples which are not subjected to the F-T cycles.

Figure 4.25 shows the relationship between the plasticity index (PI) and the swelling pressures ( $\sigma_s$ ) without the F-T cycles. As plasticity index increased, swelling pressure increased for both top and bottom samples. As stated in the previous figures, the increasing trend of the swelling pressure was observed in the Figure 4.26 depending on the activity.

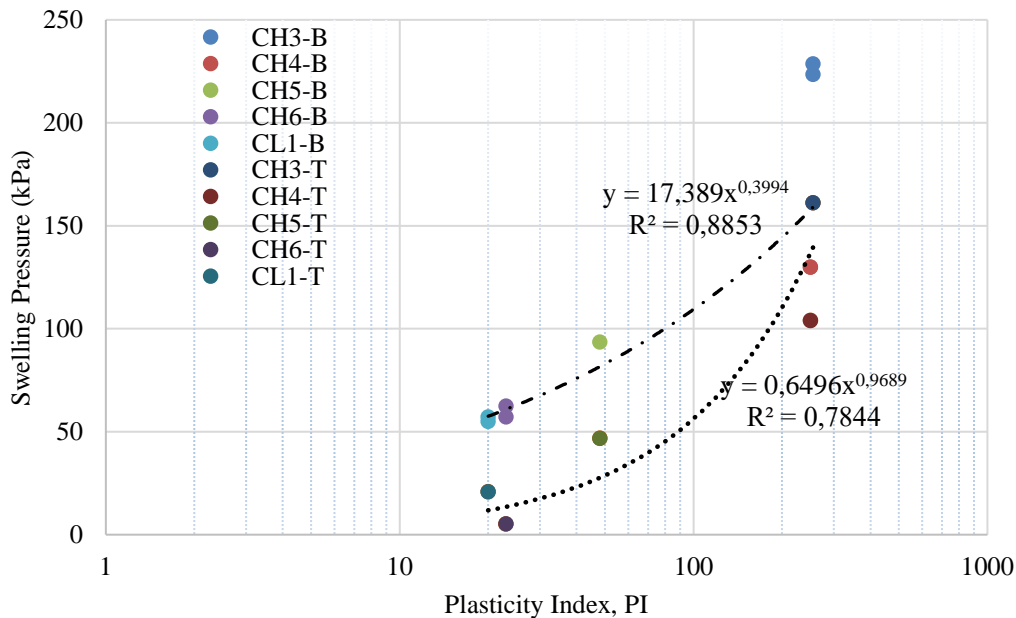


**Figure 4.25 :**  $\sigma_s - PI$  (%) relationship of samples which are not subjected to the F-T cycles.

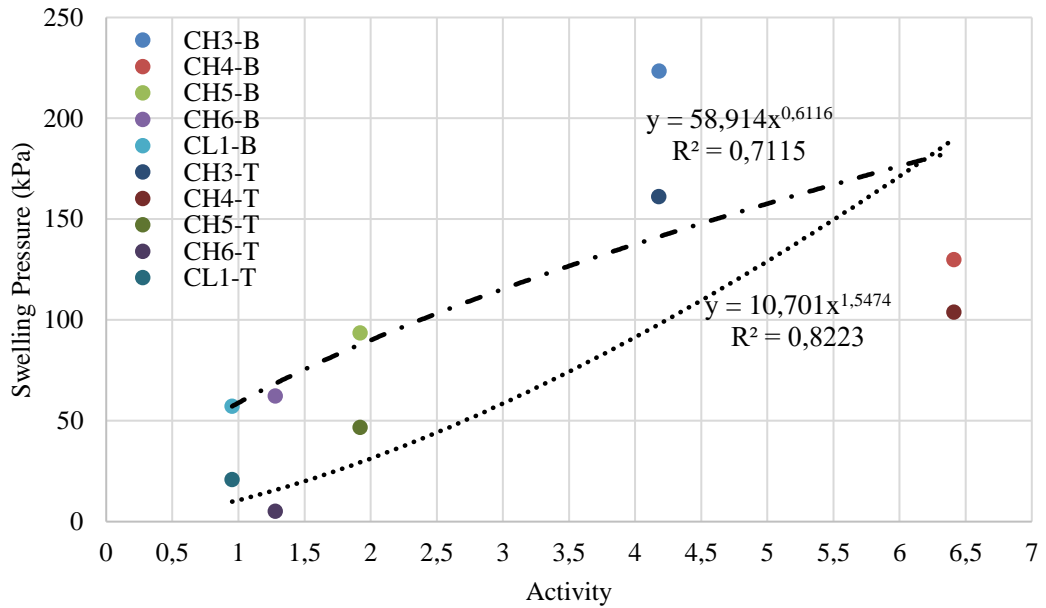


**Figure 4.26 :**  $\sigma_s$  – activity relationship of samples which are not subjected to the F-T cycles.

Figure 4.27 and 4.28 shows the relationship between the compaction parameters and the swelling pressures ( $\sigma_s$ ) without the effect of freeze-thaw. It is observed that, as optimum water content ( $W_{opt.}$ ) increased, swelling pressure increased for both top and bottom samples. However, as  $\gamma_{dmax}$  values increased,  $\sigma_s$  values were observed to decrease.

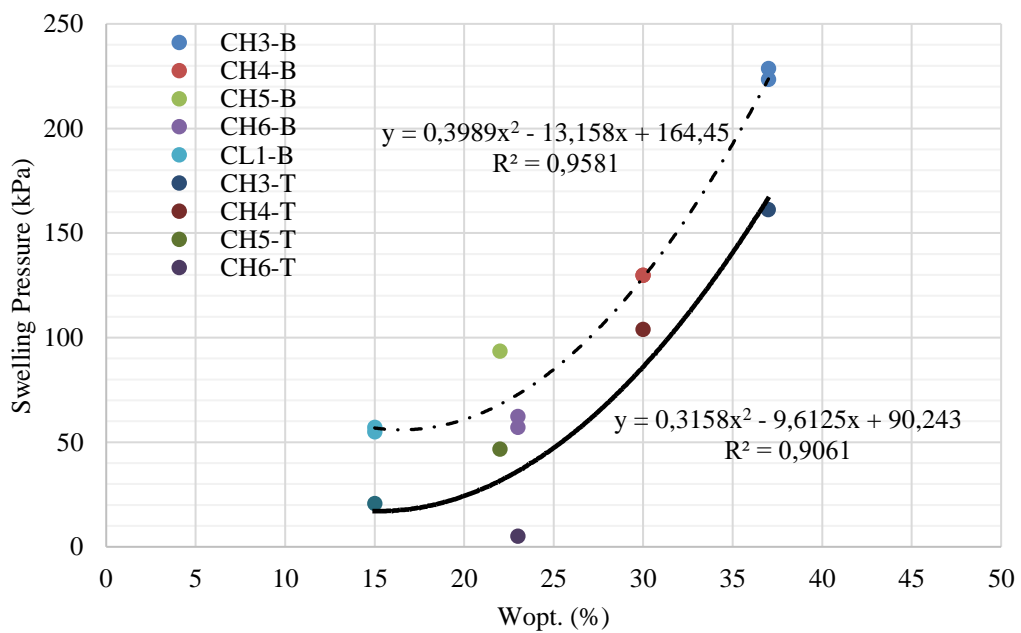


**Figure 4.27 :**  $\sigma_s$  –  $W_{opt.}$  (%) relationship of samples which are not subjected to the F-T cycles.

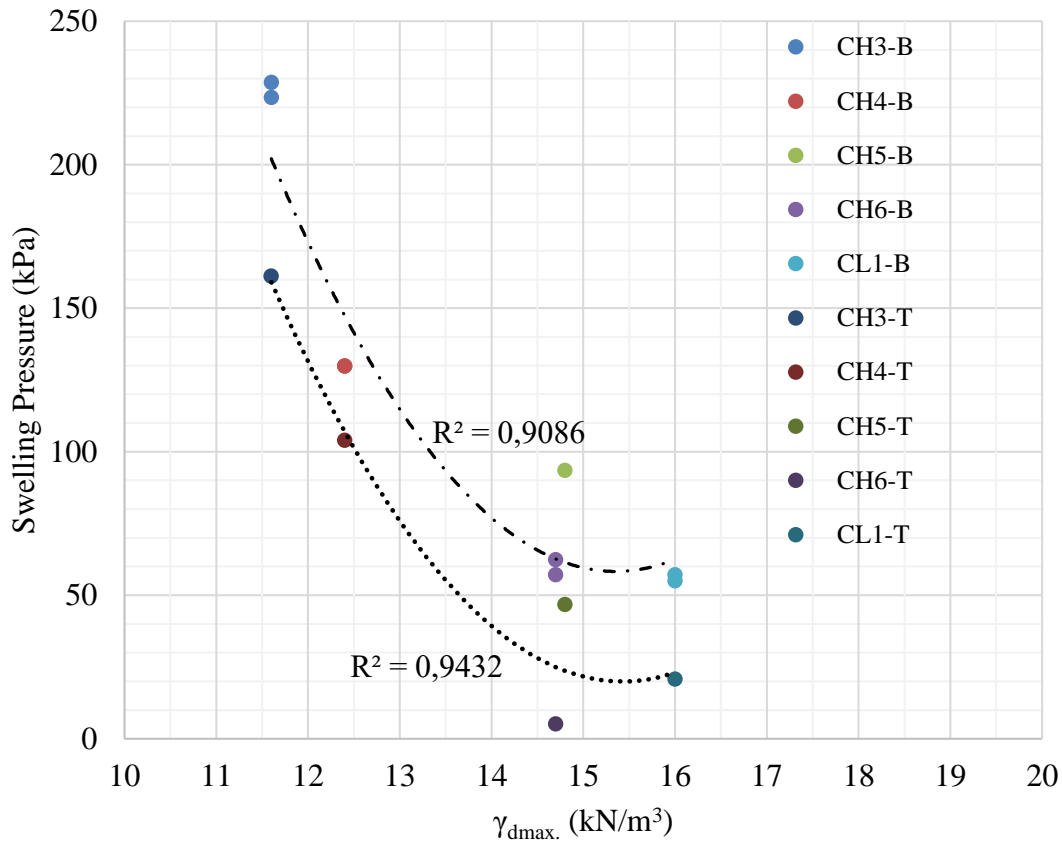


**Figure 4.28 :**  $\sigma_s - \gamma_{dmax}$  relationship of samples which are not subjected to the F-T cycles.

#### 4.4.3 Swelling pressure tests after freeze-thaw cycles

After the pre-freeze-thaw swelling pressure tests of the soil samples were performed, the freezing and thawing experiments were conducted in the closed system. A total of 8 F-T cycles were considered (1, 3, 5, 7, 10, 15, 20 and 25) for all clay samples. 2 bottom and 1 top swelling pressure samples were prepared for each freeze-thaw cycle which leads to a total of 24 samples for all clay samples. It is expected that the bottom sample which has relatively higher water content, cause faster decrease in the swelling pressure. The same procedure was followed throughout the research as determining the swelling pressure without F-T cycles. In accordance with the ASTM D560, the samples were frozen for 24 hours at the initial temperature ( $-23 \pm 2$  ° C). Then the samples removed from the refrigerant were allowed to dissolve in desiccators for 24 hours in laboratory conditions ( $23 \pm 2$  ° C) as seen in the Figure 4.29.



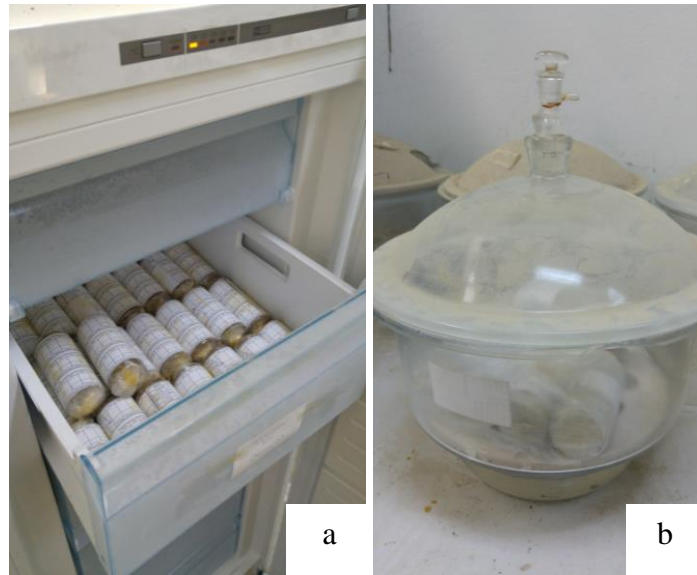


**Figure 4.29 :** a) samples exposed to freezing; b) thawing samples in desiccator.

#### 4.4.3.1 CH<sub>3</sub> results

Figure 4.30 shows the visual inspection of CH<sub>3</sub> that exposed to several F-T cycles. The results of the CH<sub>3</sub> swelling pressure tests which subjected to the various F-T cycles are shown in the Figure 4.31. As it is expressed in Figure 4.31, the bottom swelling pressures are higher than the top swelling pressure results. It was observed that the swelling pressure values of the top and bottom CH<sub>3</sub> sample are followed by a decrease trend after being exposed to F-T cycles and become stable after a numerous cycles. The results of the swelling pressure were stable after the 10<sup>th</sup> F-T cycle for the bottom CH<sub>3</sub> samples. For top CH<sub>3</sub> samples, the results of the swelling pressure were stabilized after the 7<sup>th</sup> F-T cycle. When the rate of swelling pressure was compared after 8 F-T cycles, the most rapid decrease in swelling pressure was observed at the end of the 1<sup>st</sup> F-T cycle. In the 1<sup>st</sup> F-T cycle, the volume of water in the sample expands due to freezing process. Ice lenses form through the horizontal lines. In the thawing process, these ice lenses melt and void ratio of the soil increases. The increasing void ratio and the segregation of the soil particles by irregular placement which causes the decomposition of flocculated soil structure can be shown.

At the end of the 1<sup>st</sup> F-T cycle, the swelling pressure decreased from 228 kPa to 145 kPa, decreased by 36% for bottom samples. In the top sample, it is also observed a decrease by 35 % from 161 kPa to 104 kPa. According to the results obtained after the 25<sup>th</sup> F-T cycle, an average 59% decrease in swelling pressure results was observed in both cases. The results of tests and normalized swelling pressure results of CH<sub>3</sub> after

F-T cycles is given in the Appendix A. In addition to that, the swelling pressure values of all soil samples according to the F-T cycles are given in the Appendix A.

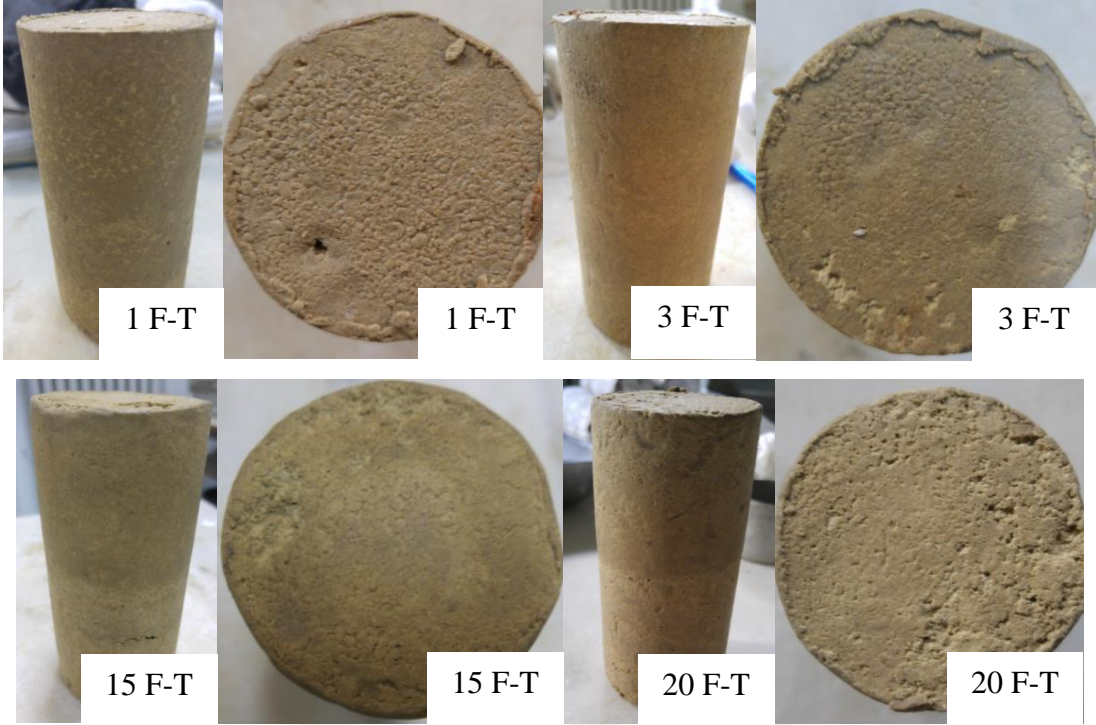


**Figure 4.30 :** Physical appearance of CH<sub>3</sub> clay after 1, 3, 15 and 20 F-T cycles.

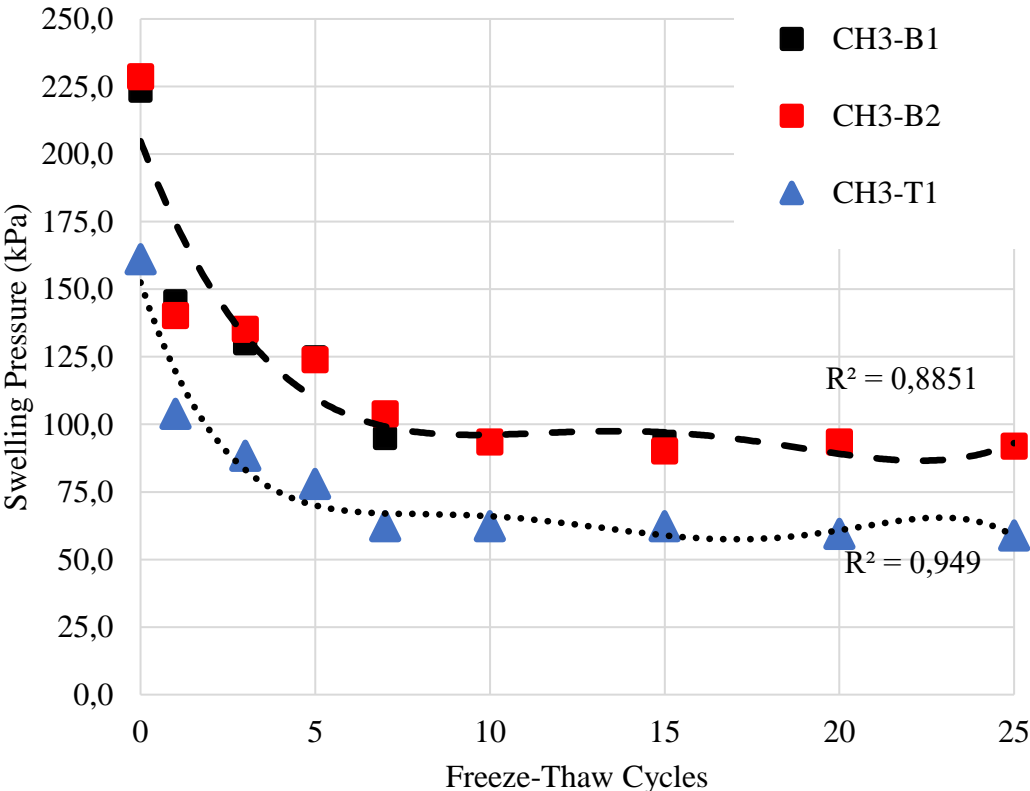


**Figure 4.31 :** Swelling pressure results of CH<sub>3</sub> samples after F-T cycles.

#### 4.4.3.2 CH<sub>4</sub> results

Figure 4.32 shows the visual inspection of CH<sub>4</sub> that exposed to 3, 5, 10 and 15 F-T cycles. The results of the CH<sub>4</sub> swelling pressure tests which subjected to the various freeze-thaw cycles are shown in the Figure 4.33. The swelling pressure values of the CH<sub>4</sub> are followed by a decrease trend after being exposed to freeze-thaw cycles and become stabilized. The results of the swelling pressure were stable after the 10<sup>th</sup> F-T cycle for both top and bottom parts. The most rapid decrease in swelling pressure was observed at the end of the 1<sup>st</sup> F-T cycle. At the end of the 1<sup>st</sup> F-T cycle, the swelling pressure decreased from 130 kPa to 100 kPa, decreased by 22% for bottom samples. In the top sample, it is also observed a decrease by 40 % from 104 kPa to 62 kPa. According to the results obtained after the 25<sup>th</sup> F-T cycle, an average 45% decrease in swelling pressure results was observed in both cases. Compared to the Ca and Na bentonite results, a greater swelling pressure decrease in Na bentonite was observed as a result of the freeze-thaw experiments. In addition, the decrease in swelling pressure observed at the end of the 1<sup>st</sup> F-T cycle was more than the Ca bentonite.

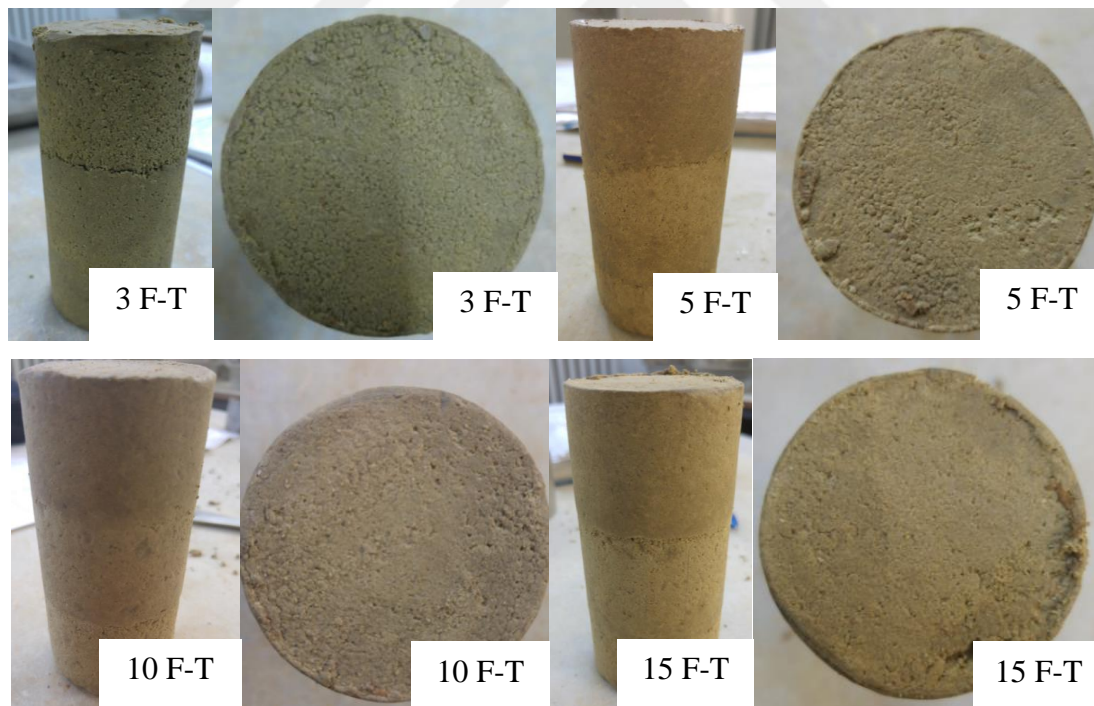


**Figure 4.32 :** Physical appearance of CH<sub>4</sub> clay after 3, 5, 10 and 15 F-T cycles.

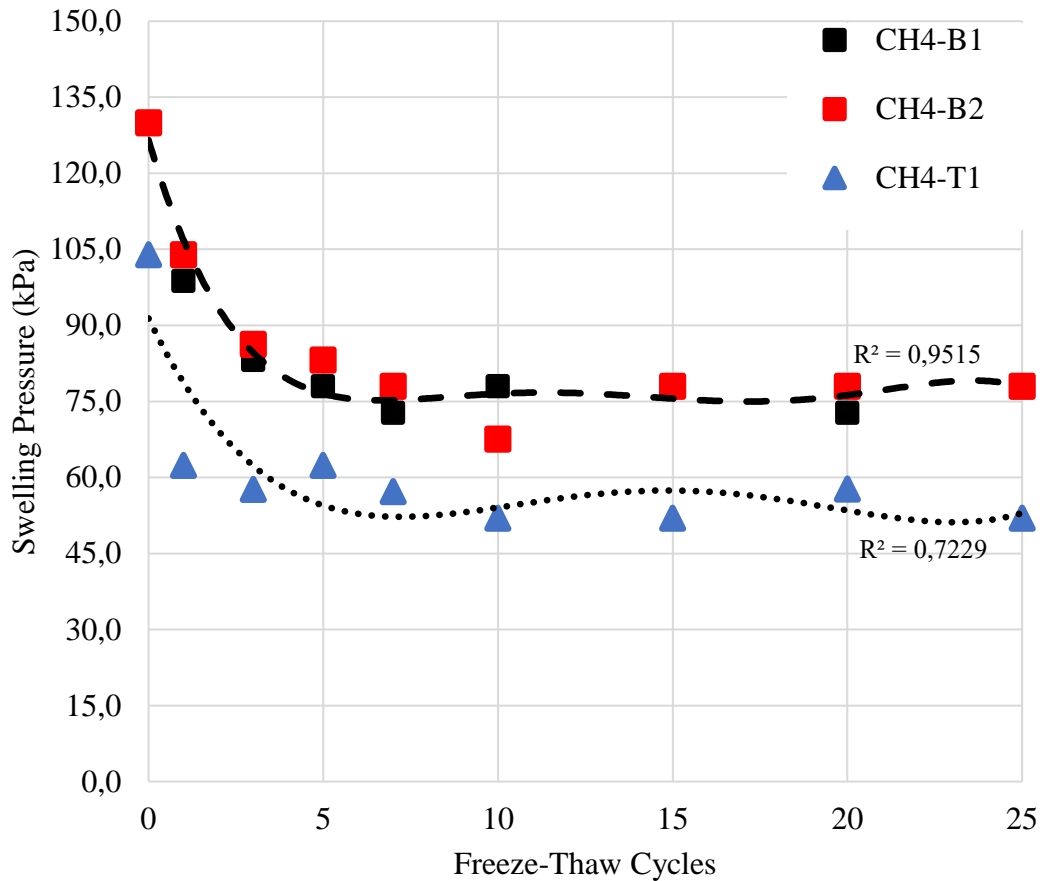


**Figure 4.33 :** Swelling pressure results of CH<sub>4</sub> samples after F-T cycles.

#### 4.4.3.3 CH<sub>5</sub> results

Figure 4.34 shows the visual inspection of CH<sub>5</sub> after 3, 5, 10 and 15 F-T cycles. The results of the CH<sub>5</sub> swelling pressure tests which subjected to the 8 different F-T cycles are shown in the Figure 4.35. In accordance with previous clay soils, test results show that the bottom swelling pressures are higher than the top swelling pressure results and after F-T cycles and swelling behavior becomes stable. A slight increase in the swelling pressure after the 15<sup>th</sup> F-T cycle observed in the bottom samples. The most quick decrease in swelling pressure was observed at the end of the 1<sup>st</sup> F-T cycle. At the end of the 1<sup>st</sup> F-T cycle, the swelling pressure decreased from 94 kPa to 52 kPa, decreased by 44% for bottom samples.

After 1<sup>st</sup> F-T cycle, bottom swelling behavior follows a steady trend except the 15<sup>th</sup> 20<sup>th</sup> and 25<sup>th</sup> F-T cycles. Top swelling behavior follows a steady trend after 10<sup>th</sup> F-T cycle. In the top sample, it is also observed a decrease by 44 % from 47 kPa to 26 kPa. According to the results obtained after the 25<sup>th</sup> F-T cycle, 44% decrease in swelling

pressure results was observed in bottom results and 67% in top results. In the Figure 4.35, swelling pressure results of CH<sub>5</sub> after F-T cycles are given.

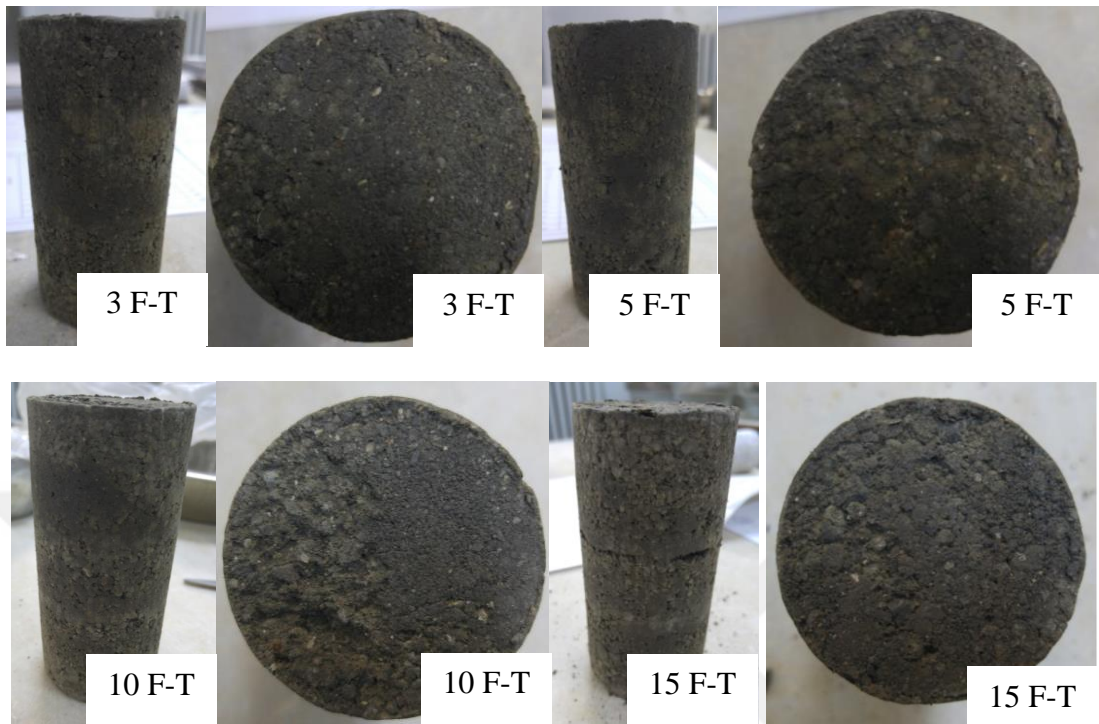


**Figure 4.34** : Physical appearance of CH<sub>5</sub> clay after 3, 5, 10 and 15 F-T cycles.

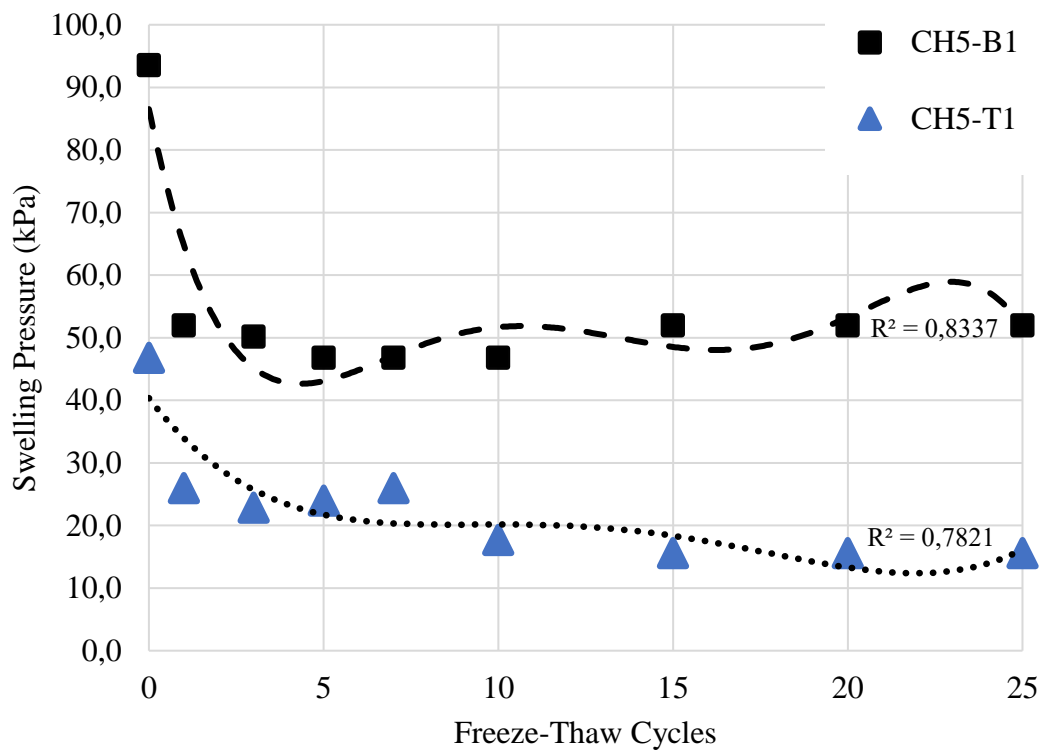


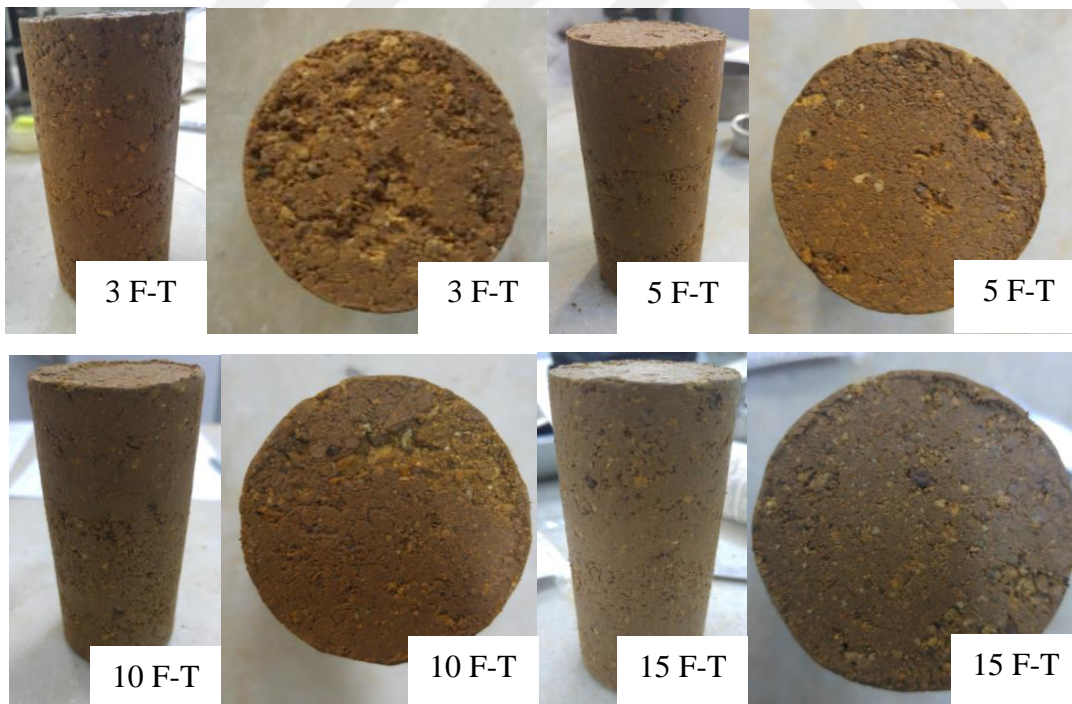
**Figure 4.35** : Swelling pressure results of CH<sub>5</sub> samples after F-T cycles.



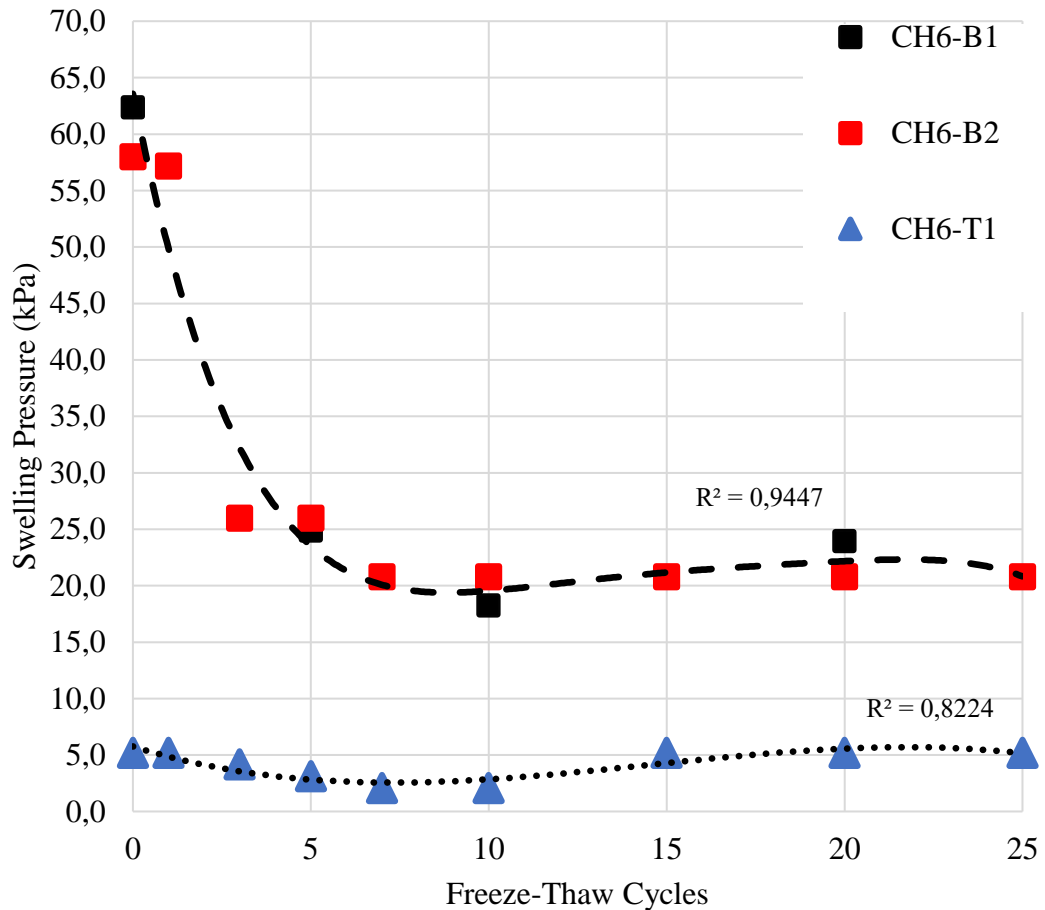
#### 4.4.3.4 CH<sub>6</sub> results

Figure 4.36 shows the visual inspection of CH<sub>6</sub> after 3, 5, 10 and 15 F-T cycles. The results of the CH<sub>6</sub> swelling pressure tests which subjected to the various freeze-thaw cycles are shown in the Figure 4.37. In accordance with previous clay soils, test results show that the bottom swelling pressures are higher than the top swelling pressure results and become stable after numerous F-T cycles.

The most rapid decrease in swelling pressure was observed at the end of the 3<sup>rd</sup> F-T cycle. At the end of the 3<sup>rd</sup> F-T cycle, the swelling pressure decreased from 57 kPa to 26 kPa, decreased by 46% for bottom samples. When the results of the top samples were taken into consideration, it was observed that the changes were not significant enough to be observed due to low swelling pressure values. As a result of freezing-thawing cycles, small decreases were observed until the 10<sup>th</sup> cycle, but these decreases were eliminated. After 10<sup>th</sup> F-T cycle, bottom swelling pressure values follow a steady trend. According to the results obtained after the 25<sup>th</sup> F-T cycle, 67% decrease in swelling pressure results was observed in bottom results. In the Figure 4.37, swelling pressure results of CH<sub>6</sub> after F-T cycles are given.



**Figure 4.36 :** Physical appearance of CH<sub>6</sub> clay after 3, 5, 10 and 15 F-T cycles.



**Figure 4.37 :** Swelling pressure results of CH<sub>6</sub> samples after F-T cycles.

#### 4.4.3.5 CL<sub>1</sub> results

The results of the CL<sub>1</sub> swelling pressure tests which subjected to the F-T cycles are shown in the Figure 4.38. 32% decrease is observed for bottom samples which is the most critical loss of pressure among all F-T cycles. At the end of the 1<sup>st</sup> F-T cycle, the swelling pressure decreased from 57 kPa to 39 kPa. After 10<sup>th</sup> F-T cycle bottom swelling behavior follows a steady trend.

In the top samples, it is also observed a decrease by 50% from 21 kPa to 10 kPa At the end of the 1<sup>st</sup> F-T cycle which is the most significant loss of swelling pressure. After 3<sup>rd</sup> F-T cycle bottom swelling behavior follows a steady trend. According to the results obtained after the 25<sup>th</sup> F-T cycle, 53% decrease in swelling pressure results was observed in bottom results and 80% in top results. In the Figure 4.38, swelling pressure results of CL<sub>1</sub> after F-T cycles are given. Figure 4.39 shows the visual inspection of CL<sub>1</sub> after 3, 5, 7 and 15 F-T cycles.

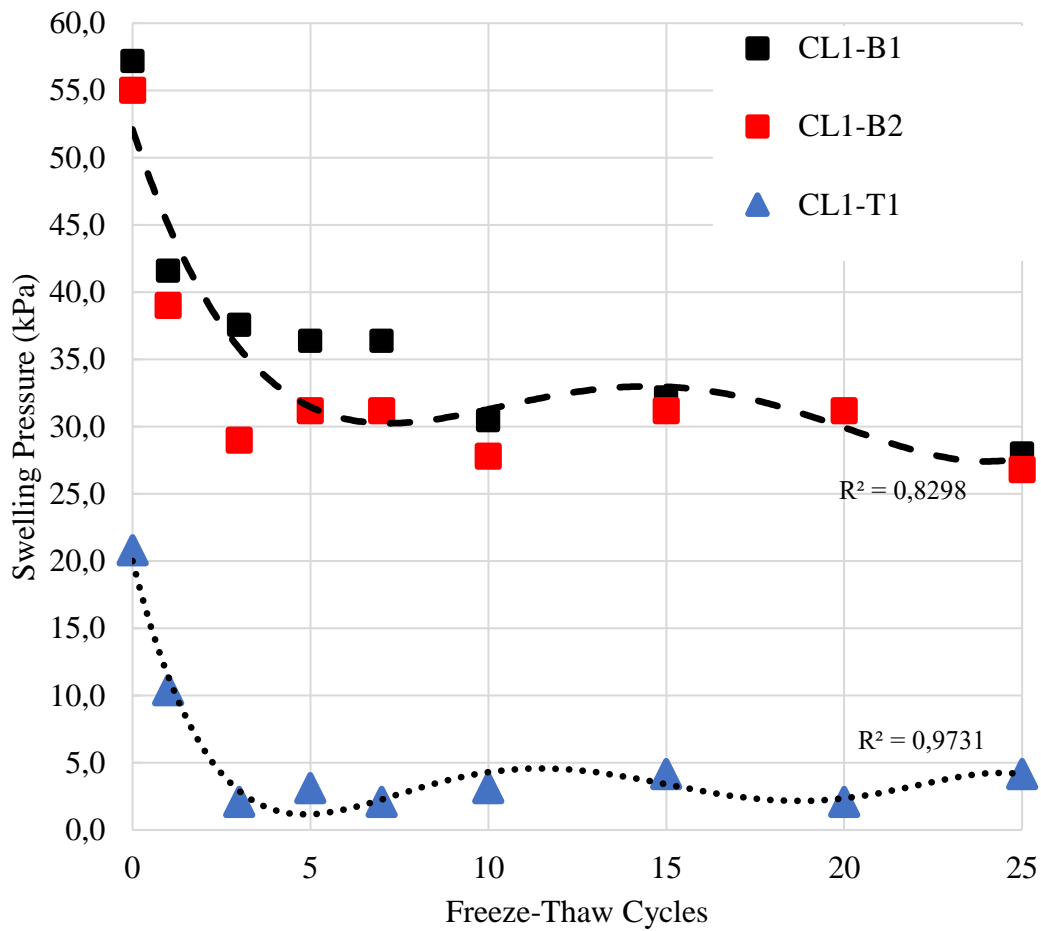


**Figure 4.38 :** Swelling pressure results of CL<sub>1</sub> samples after F-T cycles.

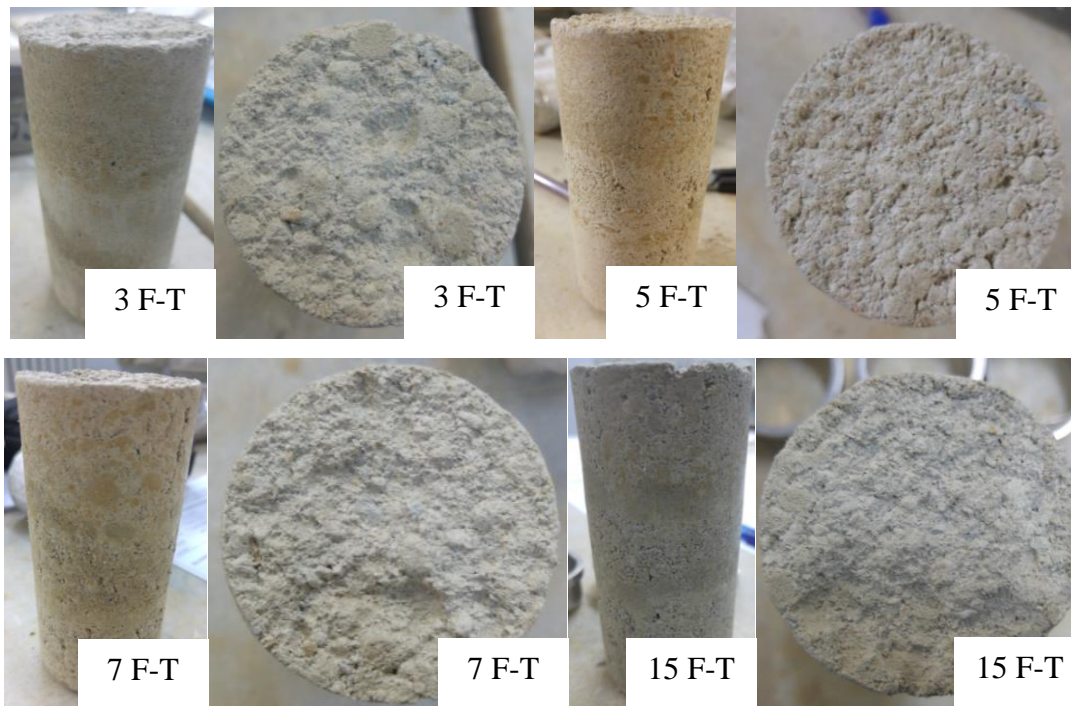


**Figure 4.39 :** Physical appearance of CL<sub>1</sub> clay after 3, 5, 7 and 15 F-T cycles.



#### 4.4.4 Relationships between engineering properties and $\sigma_s$ after F-T cycles

The data obtained from the experimental research were examined. After the F-T cycles, the relationship between the swelling pressures and liquid limit, plasticity index, optimum water content, dry unit weight of soils were investigated. Samples with high liquid limit have more swelling pressures and have decreased with the increasing F-T cycles. Figure 4.40 states that  $\sigma_s$  increases for both bottom and top samples with the increasing liquid limit values. The same swelling pressure behavior was observed with the increasing plasticity index and optimum water content values after the F-T cycles which are shown in the Figure 4.41 and 4.42 respectively. The results of the top and bottom samples were evaluated within themselves in order to establish more accurate relationships. On the other hand, considering the increasing dry unit weights of samples, it was determined that the  $\sigma_s$  followed a decreasing trend. Figure 4.43 indicates the relationship between  $\sigma_s$  and  $\gamma_{dry}$  values of samples. In addition, all swelling pressure test results were evaluated depending on the freeze-thaw cycles by regarding plasticity. As a result of the evaluation, it was observed that the swelling pressures in high plasticity clays decreased and became stable, whereas the observed decreases in low plasticity clay were not as high as the high plasticity clays and were stable with the increasing number of freeze-thaw cycles. This behavior expressed in the Figure 4.44.

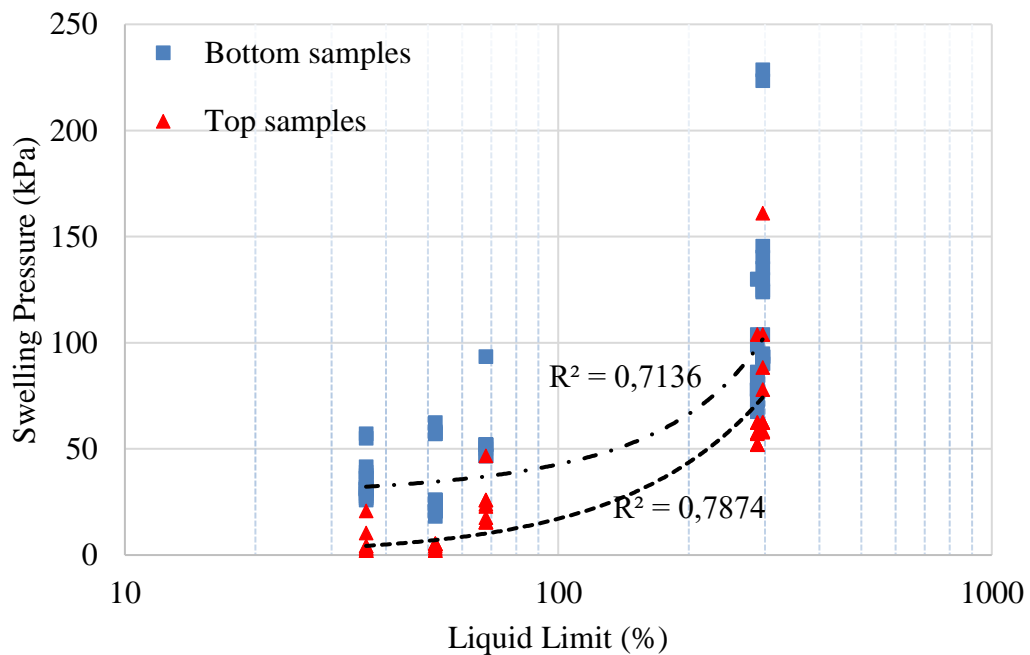


**Figure 4.40 :**  $\sigma_s$  – LL (%) relationships after F-T cycles.

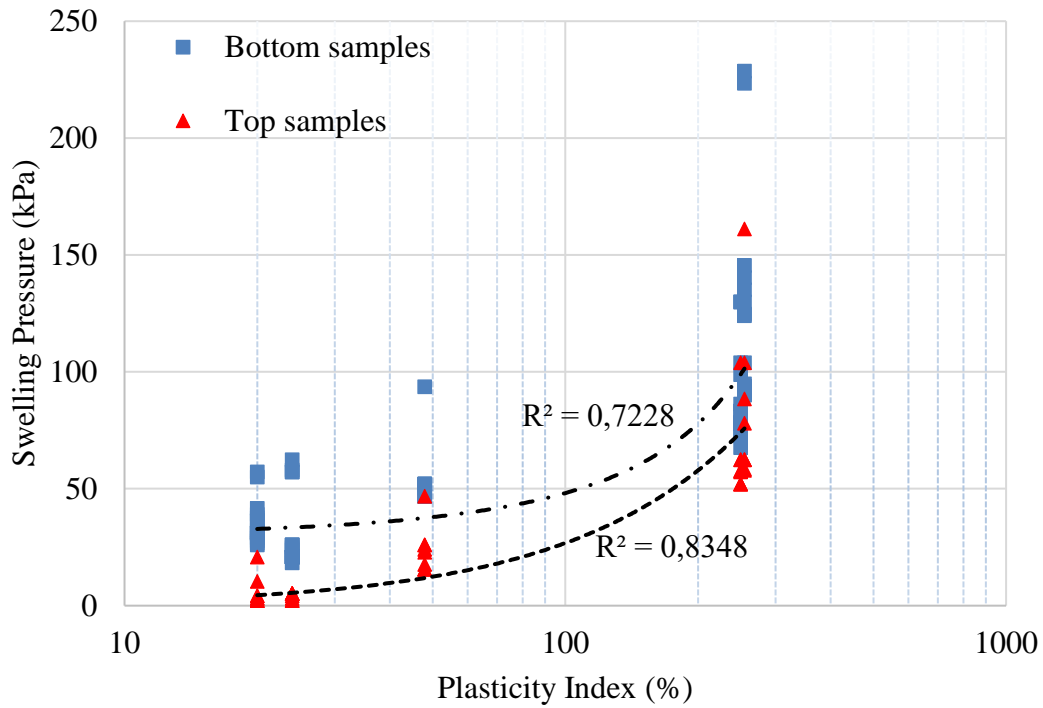


**Figure 4.41** :  $\sigma_s - PI$  (%) relationships after F-T cycles.

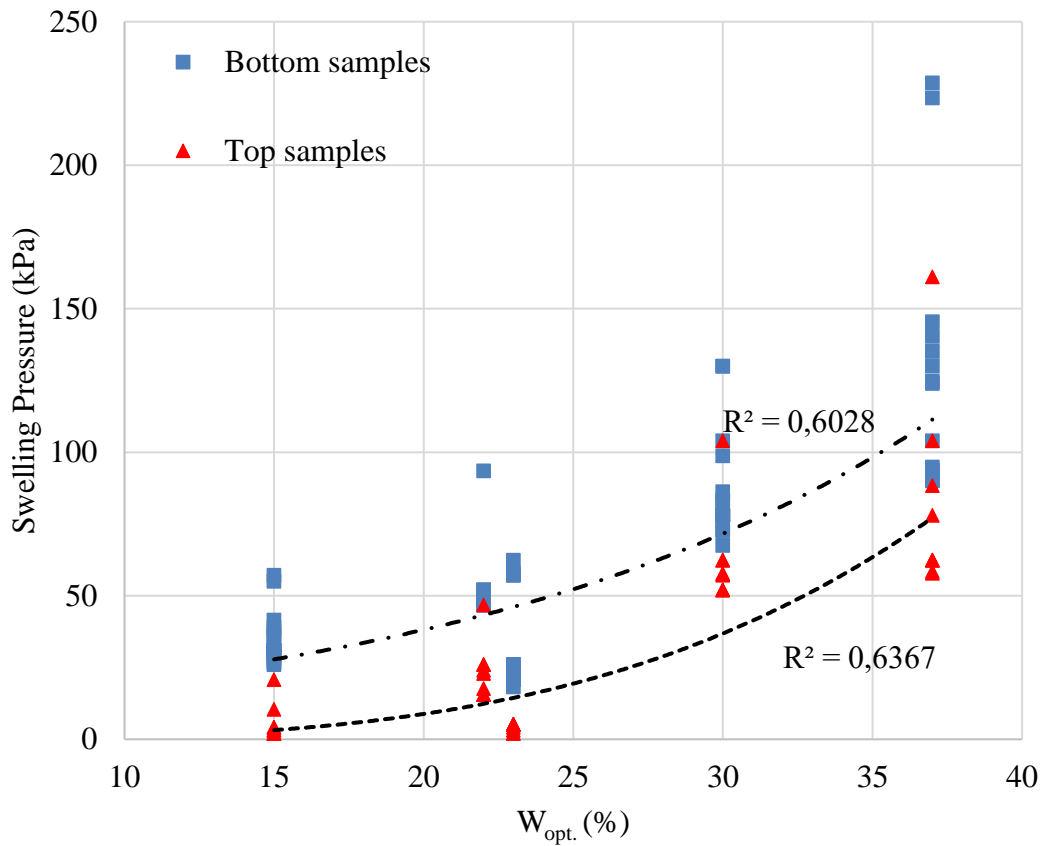


**Figure 4.42** :  $\sigma_s - W_{opt.}$  (%) relationships after F-T cycles.

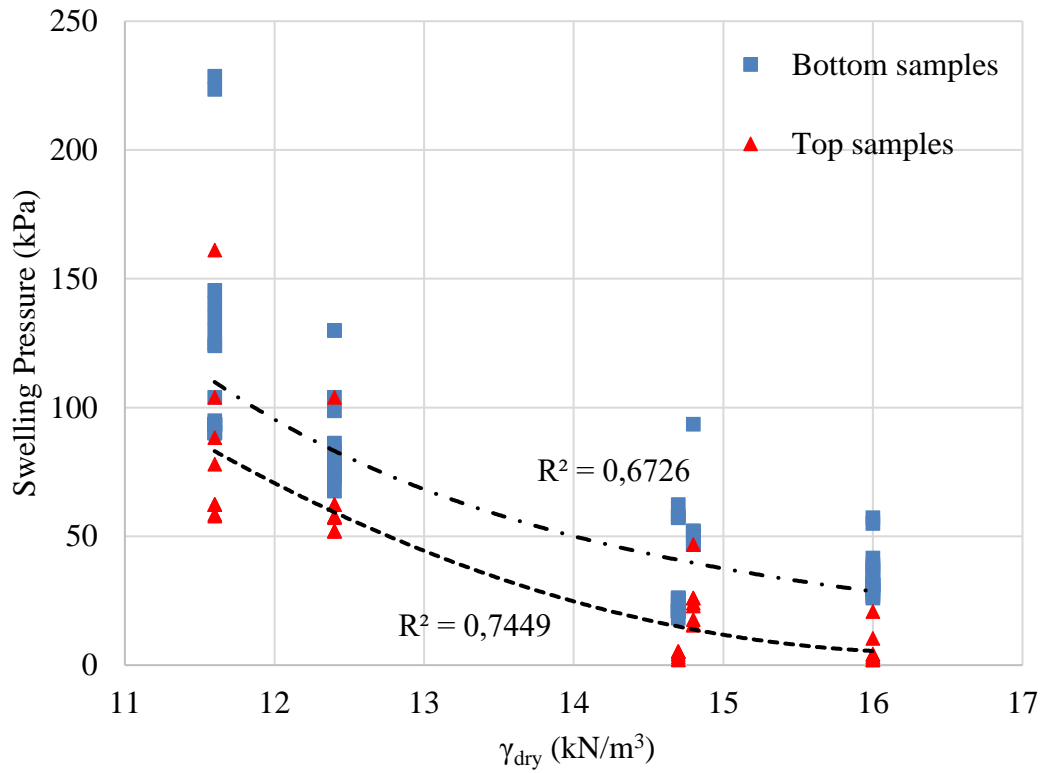


**Figure 4.43 :**  $\sigma_s - \gamma_{dry}$  (kN/m<sup>3</sup>) relationships after F-T cycles.

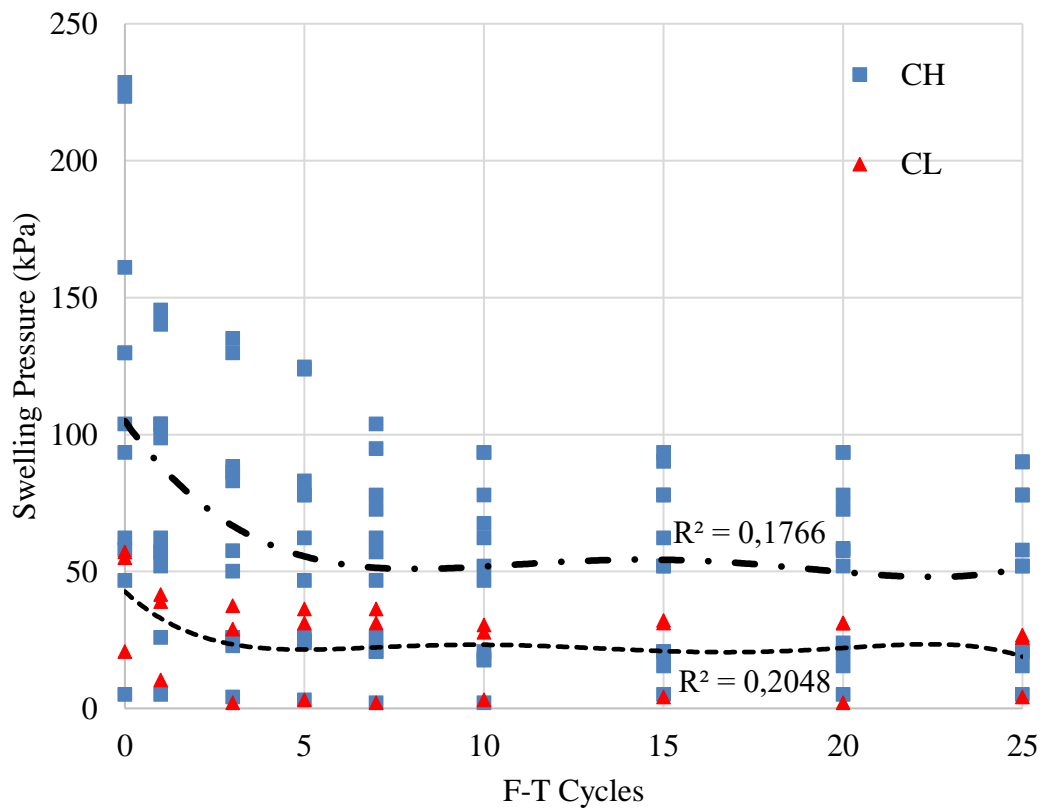


**Figure 4.44 :** All  $\sigma_s$  results according to F-T cycles.

**4.4.5 Relationship between void ratio and swelling pressure after F-T cycles**

The aim of this research is to investigate the reasons of the decrease of the swelling pressures after exposure to the freeze-thaw cycles. Therefore, the void ratios of the prepared soil samples were calculated. The following figures show the void ratios according to the 9 different freeze-thaw cycles. As can be seen from figures, with the increasing number of cycles void ratios increased. After the certain F-T cycle numbers, it was observed that the void ratios did not increase much and reached to the residual values. General behavior that observed from the results, the void ratios did not change much after the 10<sup>th</sup> F-T cycle and the increase in swelling pressures were stabilized accordingly. Figure 4.45, 4.46, 4.47, 4.48 and 4.49 indicates the change in the void ratios (e) according to the F-T cycles of CH<sub>3</sub>, CH<sub>4</sub>, CH<sub>5</sub>, CH<sub>6</sub> and CL<sub>1</sub> respectively.

A 10% increase in the void ratio was observed at the 10<sup>th</sup> F-T cycle for the bottom CH<sub>3</sub> samples which becomes residual after the following cycles. On the other hand, it was observed that for the top samples, at 5<sup>th</sup> cycle reaches to peak level which corresponds to 1,1 times higher than the initial condition. Then, a decrease in the void ratios is evaluated for the last two cycles.

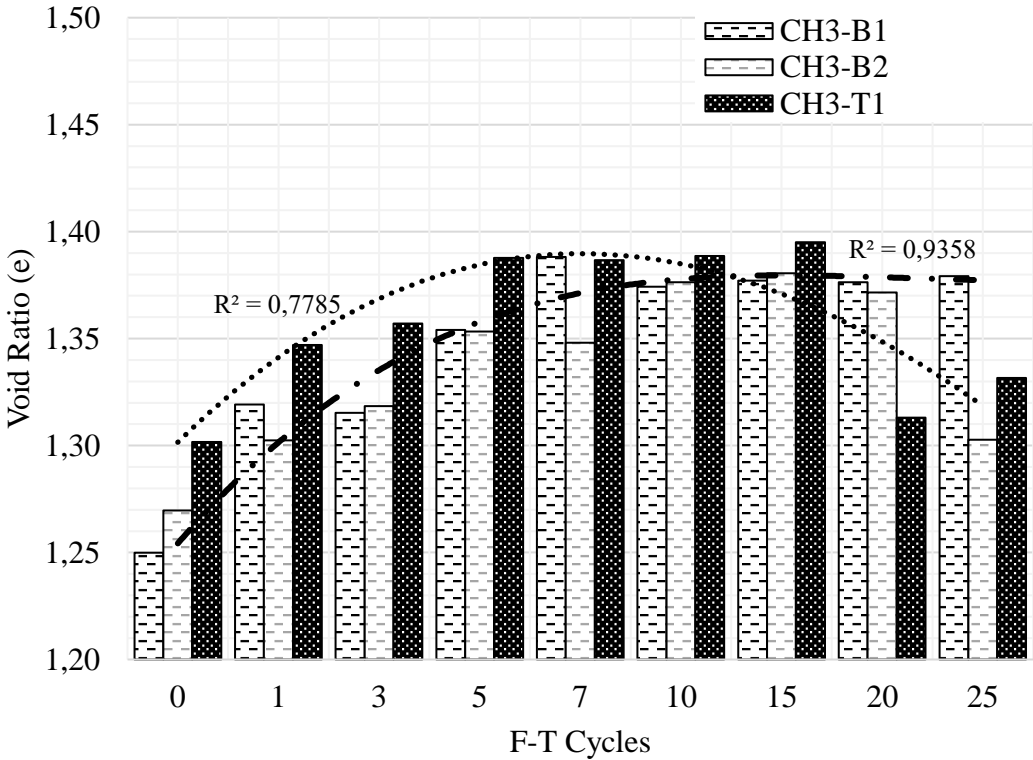


**Figure 4.45 :** Void ratios of CH<sub>3</sub> according to the F-T cycles.

A 18% increase in the void ratio was observed at the 15<sup>th</sup> F-T cycle for the bottom CH<sub>4</sub> samples which becomes residual after the following cycles. On the other hand, it was observed that for the top samples, at 10<sup>th</sup> cycle reaches to a value that corresponds to 12% higher than the initial condition.

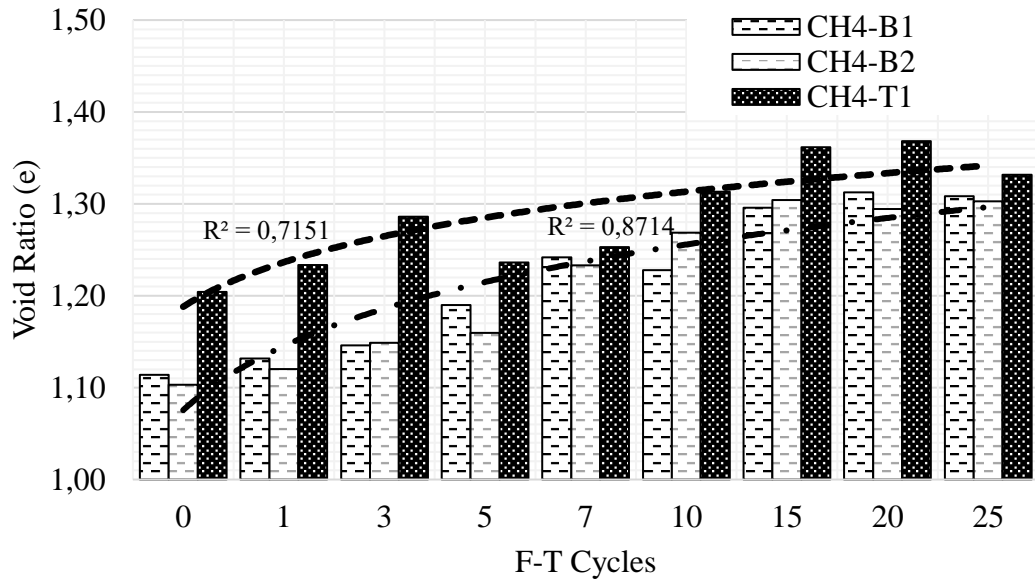


**Figure 4.46 :** Void ratios of CH<sub>4</sub> according to the F-T cycles.

A 11% increase in the void ratio was observed at the 10<sup>th</sup> F-T cycle for the bottom CH<sub>5</sub> samples which becomes residual after the following cycles. It was also observed that for the top samples, at 10<sup>th</sup> cycle void ratios calculated as 16% higher than the first cycle.

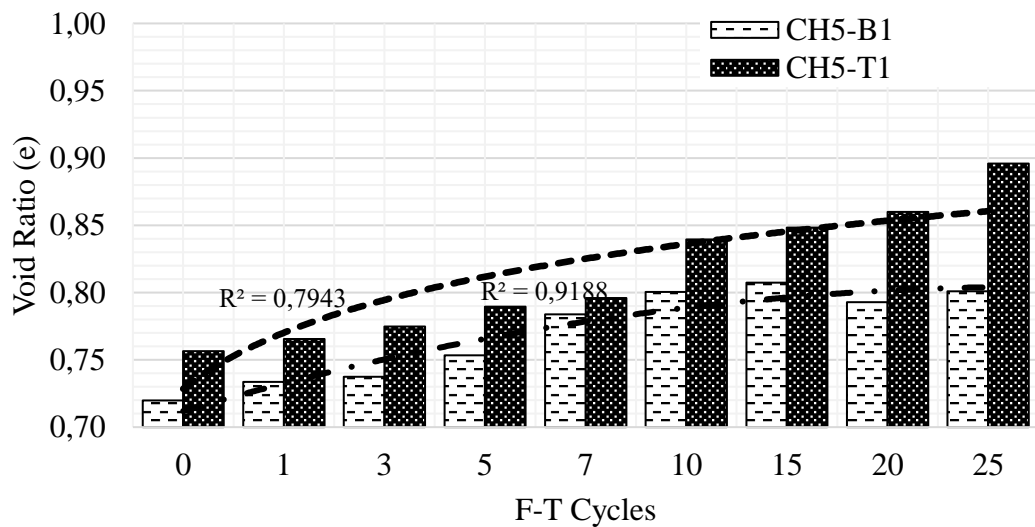


**Figure 4.47 :** Void ratios of CH<sub>5</sub> according to the F-T cycles.

For CH<sub>6</sub> samples, a great amount of increase did not observed comparing to the other specimens. At the 10<sup>th</sup> F-T cycle for the bottom CH<sub>6</sub> samples, 7% increase in the void ratio was observed which becomes residual after the following cycles. It was also observed that for the top samples, at 7<sup>th</sup> cycle void ratios calculated as 14% higher than initial condition.

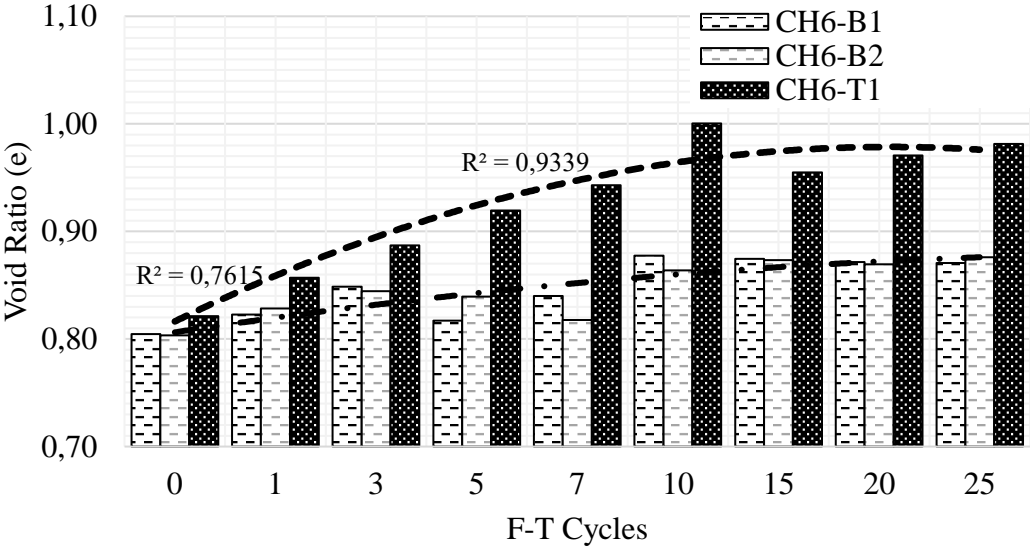


**Figure 4.48 :** Void ratios of CH<sub>6</sub> according to the F-T cycles.

For bottom CL<sub>1</sub> samples, the void ratio results have followed a linear trend which is different behavior comparing to the other specimens. At the 10<sup>th</sup> F-T cycle for the top CL<sub>1</sub> samples, 7% increase in the void ratio was observed which becomes residual after the following cycles.

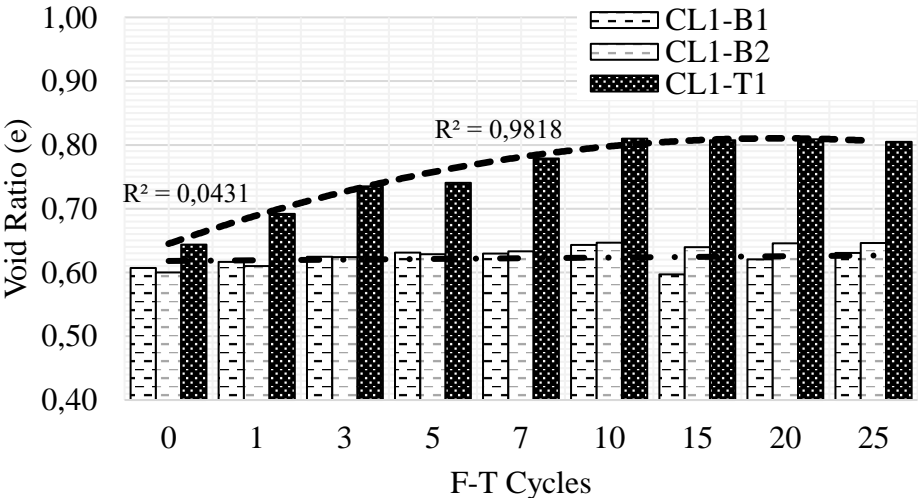


**Figure 4.49 :** Void ratios of CL<sub>1</sub> according to the F-T cycles.

## **5. CONCLUSIONS AND RECOMMENDATIONS**

The soils that located in cold climatic regions are exposed to periodic freeze-thaw cycles. The mechanical properties of the soils in these regions are subject to significant changes due to the ice lenses formed between the soil particles during freezing process and the excess amount of water that occurs during the thawing process. Changes in the geotechnical engineering parameters such as bearing capacity, settlement, and swelling potential of the soils under the effect of freeze-thaw should be considered in the design section of projects. Especially, the deformations occurring on the structures built on clayey soils with high swelling potential constitute an important part. The determination of the potential of swelling on clayey soils that susceptible to swell in cold regions will prevent deformations and damages that may be created on structures, road structures, motorways, sidewalks and substructures to be constructed or to be built on the clay layer. Thereby, the safety will be increased, and the maintenance costs will be reduced in the risk regions where damages may occur.

Within the scope of the master thesis, it is aimed to determine the parameters affecting the swelling pressure of clay soils which are exposed to freezing-thawing cycles. In order to investigate the short and long-term swelling characteristics of soil samples, clayey soils with different plasticity behaviors and different mineralogical characteristics were subjected to varying freeze and thaw cycles, and swelling pressure tests before and after freeze-thawing process were carried out on specimens obtained from these soils. Swelling pressure tests were performed after 0, 1, 3, 5, 7, 10, 15, 20 and 25 F-T cycles of specimens were completed. The relationship between swelling pressures determined by experiments, soil index and mineralogical properties were investigated. The variation of swelling pressure of clay samples was investigated with respect to liquid limit, plastic limit, plasticity index, maximum dry unit volume weight, optimum water content and void ratio. According to the results of the laboratory tests obtained; an increase in swelling pressure was observed as the liquid limit and the plasticity index values of the soils increased. It was also determined that increased

water content values cause increase in the swelling pressures results. After exposed to freeze-thaw, the swelling pressure values of the soils follow the decreasing trend and stabilize after a while. The void ratios of the soils have increased after exposure to freeze-thaw cycles. the volume of water in the sample expands due to freezing process. This physical process may be caused by ice lenses which formed in frozen soils. Ice lenses form through the horizontal lines. In the thawing process, these ice lenses melt and void ratio of the soil increases. The increasing void ratio and the segregation of the soil particles by irregular placement which causes the decomposition of flocculated soil structure may be reason for decrease in swelling pressure results.

In this context, the consistency limits, compaction parameters, swelling pressure values and swelling behavior of the soils after F-T cycles were examined and the results are stated in the below.

The results obtained for Na bentonite (CH<sub>3</sub>) are as follows:

- The Atterberg (consistency) limits of Na bentonite were determined. The liquid limit, LL = 296%, plastic limit, PL = 41%, plasticity index, PI = 255% are determined as a result of the consistency tests. According to the Unified Soil Classification System (USCS), the sodium bentonite was determined as high plasticity clay (CH). As a result of the Harvard compaction test for CH<sub>3</sub>, the  $W_{opt.}$  was determined 37% and  $\gamma_{dmax.}$  was 11.60 kN/m<sup>3</sup>.
- The results of the CH<sub>3</sub> swelling pressure tests indicates that the bottom swelling pressures are higher than the top swelling pressure results. With the increase in the number of freeze-thaw cycles, the loss of swelling pressure rate decreased until the 10<sup>th</sup> cycle and became stable for the bottom samples. For top samples, the results of the swelling pressure were stabilized after the 5<sup>th</sup> F-T cycle. The most rapid decrease in swelling pressure was observed at the end of the 1<sup>st</sup> F-T cycle. The swelling pressure decreased by 36% for bottom samples, by 35% for top samples. After the 25th F-T cycle, an average 59% decrease in swelling pressure results was observed.

The results obtained for Ca Bentonite (CH<sub>4</sub>) are as follows:

- The consistency limits of Ca bentonite were determined. LL = 296%, PL = 41% and PI = 255% are determined as a result of the tests. According to the Unified Soil Classification System (USCS), the calcium bentonite was



determined as high plasticity clay. As a result of the Harvard compaction test for CH<sub>4</sub>, the  $W_{opt.}$  was determined 30% and  $\gamma_{dmax.}$  was 12.40 kN/m<sup>3</sup>.

- The swelling pressure results of the CH<sub>4</sub> are followed by a decrease trend after being exposed to freeze-thaw cycles and become stabilized after the 10<sup>th</sup> F-T cycle for both top and bottom samples. The most rapid decrease in swelling pressure was observed at the end of the 1<sup>st</sup> F-T cycle. A decrease by 22% for bottom samples and a decrease by 40% observed in the swelling pressure results. After the 25<sup>th</sup> F-T cycle, an average 45% decrease in swelling pressure results was determined.

The results obtained for CH<sub>5</sub> are as follows:

- The consistency limits of CH<sub>5</sub> were determined. LL = 68%, PL = 20% and PI = 48% are determined as a result of the tests. According to the Unified Soil Classification System (USCS), determined as high plasticity clay. As a result of the Harvard compaction test for CH<sub>5</sub>, the  $W_{opt.}$  was determined 22% and  $\gamma_{dmax.}$  was 14.80 kN/m<sup>3</sup>.
- In accordance with previous soil samples, the bottom swelling pressures are higher than the top results after F-T cycles and decrease rate of swelling pressure reduced, becomes stable after the 1<sup>st</sup> F-T cycle. The quickest decrease in swelling pressure was observed by 44% for bottom samples, at the end of the 1<sup>st</sup> F-T cycle. Top swelling behavior follows a steady trend after 10<sup>th</sup> F-T cycle. After the 25<sup>th</sup> F-T cycle, 44% decrease in swelling pressure results was observed in bottom results and 67% in top results.

The results obtained for CH<sub>6</sub> are as follows:

- LL = 52%, PL = 28% and PI = 24% are determined as a result of the consistency limit tests. According to the Unified Soil Classification System (USCS), determined as high plasticity clay. As a result of the Harvard compaction test for CH<sub>6</sub>, the  $W_{opt.}$  was determined 23% and  $\gamma_{dmax.}$  was 14.70 kN/m<sup>3</sup>.
- The most rapid decrease in swelling pressure was observed at the end of the 3<sup>rd</sup> F-T cycle. At the end of the 3<sup>rd</sup> F-T cycle, the swelling pressure decreased from 57 kPa to 26 kPa, decreased by 46% for bottom samples. When the results of

the top samples were taken into consideration, it was observed that the changes were not significant enough to be observed due to low amount of swelling pressures. As a result of F-T cycles, small decreases were observed until the 10<sup>th</sup> cycle. After 10<sup>th</sup> F-T cycle, bottom swelling pressure values follow a steady trend. After the 25<sup>th</sup> F-T cycle, 67% decrease in swelling pressure results was observed in bottom results.

The results obtained for CL<sub>1</sub> are as follows:

- LL = 36%, PL = 16% and PI = 20% are determined as a result of the consistency limit tests. According to the Unified Soil Classification System (USCS), determined as low plasticity clay. As a result of the Harvard compaction test for CH<sub>6</sub>, the W<sub>opt.</sub> was determined 15% and  $\gamma_{dmax.}$  was 16 kN/m<sup>3</sup>.
- 32% decrease is observed for bottom samples which is the most critical loss of pressure among all F-T cycles. At the end of the 1<sup>st</sup> F-T cycle, the swelling pressure decreased from 57 kPa to 39 kPa. In the top samples, it is also observed a decrease by 50% from 21 kPa to 10 kPa at the end of the 1<sup>st</sup> F-T cycle. After 10<sup>th</sup> F-T cycle bottom swelling behavior follows a steady trend and for top samples it is determined in the 3<sup>rd</sup> F-T cycle. After the 25<sup>th</sup> F-T cycle, 53% decrease in swelling pressure was observed in bottom results and 80% in top results.

Compared to the Ca and Na bentonite results, sodium bentonite swelling pressures were found to be higher than the calcium bentonite swelling pressures and a greater swelling pressure decrease in sodium bentonite was observed after the freeze-thaw experiments. In addition, the decrease in swelling pressure observed at the end of the 1<sup>st</sup> F-T cycle was more than the calcium bentonite. When these results were examined, the effect of mineralogical properties on swelling pressure behavior was investigated.

After the F-T cycles, the relationship between the swelling pressures and liquid limit, plasticity index, optimum water content, dry unit weight of soils was investigated. Samples with high liquid limit have more swelling pressures and have decreased with the increasing F-T cycles. The same swelling pressure behavior was observed with the increasing plasticity index and optimum water content values after the F-T cycles. On

the contrary, considering the increasing dry unit weights of samples, it was determined that the  $\sigma_s$  followed a decreasing trend.

All swelling pressure test results were evaluated depending on the freeze-thaw cycles by regarding plasticity. It was observed that the swelling pressures in high plasticity clays decreased and became stable, whereas the observed decreases in low plasticity clay were not as high as the high plasticity clays and were stable with the increasing number of freeze-thaw cycles. It was determined that the rate of decrease in swelling pressures for high plasticity clays was higher than low plasticity clay sample.

Lastly, the void ratios of the samples were investigated, and it is stated that with the increasing number of F-T cycles void ratios are increased. After the certain F-T cycle numbers, it was observed that the void ratios did not increase much and reached to the residual values. General behavior that observed from the results, the void ratios did not change much after the 10<sup>th</sup> F-T cycle and the increases in swelling pressures were stabilized accordingly. It was determined that the increase in the void ratio in high plasticity clays was higher than the low plasticity clay. This may be an explanatory reason for the difference in swelling behavior of soils. The effect of plasticity on the change in void ratios was observed.



## REFERENCES

- Al-Ani, T., and Sarapaa, O.** (2008). Clay and clay mineralogy: physical-chemical properties and industrial uses. *Geological Survey of Finland*, 94.
- Altmeyer, W. T.** (1955). Discussion of engineering properties of expansive clays., *Proc. ASCE*, Vol. 81, No. 658, pp. 17-19.
- Andersland, O. B. and Ladanyi, B.** (1994). *An introduction to frozen ground engineering*. Chapman & Hall, Inc.
- Andersland, O. B., and Ladanyi, B.** (2004). *Frozen ground engineering*. John Wiley & Sons.
- ASTM** (2003). *Standart test method for measurement of collapse potential of soils* (ASTM D5333-03).
- ASTM** (2013). *Standart test method for frost heave and thaw weakening susceptibility of soils* (ASTM D5918-13e1).
- ASTM** (2014). *Standart test method for one-dimensional swell or collapse of cohesive soils* (ASTM D4546-14e1).
- ASTM** (2017). *Standard Specification for Coal Fly Ash and Raw or Calcined Natural Pozzolan for Use in Concrete* (ASTM C618-17a).
- Bailey, S. W.** (1980). Summary of recommendations of AIPEA nomenclature committee. *Clay Minerals*, 15(1), 85-93.
- Basma, A. A., Al-Homoud, A. S., and Husein, A.** (1995). Laboratory assessment of swelling pressure of expansive soils. *Applied Clay Science*, 9(5), 355-368.
- Bouma, J., Jongerius, A., Boersma, O., Jager, A., and Schoonderbeek, D.** (1977). The Function of Different Types of Macropores During Saturated Flow through Four Swelling Soil Horizons 1. *Soil Science Society of America Journal*, 41(5), 945-950.
- Boz, A., and Sezer, A.** (2018). Influence of fiber type and content on freeze-thaw resistance of fiber reinforced lime stabilized clay. *Cold Regions Science and Technology*, 151, 359-366.
- Brasher, B. R., Franzmeier, D. P., Valassis, V., and Davidson, S. E.** (1966). Use of saran resin to coat natural soil clods for bulk-density and water-retention measurements. *Soil Science*, 101(2), 108.
- Brekke, T. L., and Selmer-Olsen, R.** (1965). Stability problems in underground constructions caused by montmorillonite-carrying joints and faults. *Engineering Geology*, 1(1), 3-19.
- Brindley, G. W., & Robinson, K.** (1946). The structure of kaolinite. *Mineralogical Magazine and Journal of the Mineralogical Society*, 27(194), 242-253.

- Brindley, G. W., and Brown, G.** (1980). Quantitative X-ray mineral analysis of clays. *Crystal structures of clay minerals and their X-ray identification*, 5, 411-438.
- Brown, R. J. E., & Kupsch, W. O.** (1974). *Permafrost terminology*. National Resource Council of Canada. Technical Memorandum 111.
- Brown, R. J. E., Johnston, G. H., Mackay, J. R., Morgenstern, N. R., and Shilts, W. W.** (1981). Permafrost distribution and terrain characteristics. *Permafrost Engineering Design and Construction*, 31-72.
- Chamberlain, E. J.** (1981). Overconsolidation effects of ground freezing. *Engineering geology*, 18(1-4), 97-110.
- Chamberlain, E. J., and Ayorinde, O. A.** (1991). Freeze-thaw effects on clay covers and liners. In *Cold Regions Engineering*, ASCE, 136-151.
- Chamberlain, E. J., and Blouin, S. E.** (1978). Densification by freezing and thawing of fine material dredged from waterways. In *Proceedings: Permafrost 3rd International Conference*, pp. 623-628.
- Chamberlain, E. J., and Gow, A. J.** (1979). Effect of freezing and thawing on the permeability and structure of soils. *Engineering geology*, 13(1-4), 73-92.
- Chamberlain, E. J., Iskandar, I., and Hunsicker, S. E.** (1990). Effect of freezethaw cycles on the permeability and macrostructure of soils. *Proc. Int. Symp. on Frozen Soil Impacts on Agric., Range, and Forest Lands*, CRREL Special Report 90-1, U. S. Army Corps of Engineers, Cold Regions Research & Engineering Laboratory, Hanover, N.H., 145-155.
- Chapman, D. L.** (1913). LI. A contribution to the theory of electrocapillarity. *The London, Edinburgh, and Dublin philosophical magazine and journal of science*, 25(148), 475-481.
- Chen F.H.** (1965). The use of piers to prevent the uplifting of lightly loaded structure founded on expansive soil. *Concluding proceedings engineering effects of moisture change in soils, international research and engineering conference on expansive clay soils*. Texas, pp 152-171
- Chen, F. H.** (1975). *Foundation on expansive soils*. Elsevier Scientific Publishing Co., New York.
- Chen, F.H.** (1988) *Foundations on Expansive Soils. 2nd Edition*, Elsevier Science Publications, New York.
- Chiappone, A., Mareello, S., Scavia, C., and Setti, M.** (2004). Clay mineral characterization through the methylene blue test: comparison with other experimental techniques and applications of the method. *Canadian Geotechnical Journal*, 41(6), 1168-1178.
- Chittoori, B., and Puppala, A. J.** (2011). Quantitative estimation of clay mineralogy in fine-grained soils. *Journal of Geotechnical and Geoenvironmental engineering*, 137(11), 997-1008.
- Civan, F.** (2015). *Reservoir formation damage*. 3<sup>rd</sup> edition, Gulf Professional Publishing.

- Code, U. B.** (1997). Uniform building code. In *International Conference of Building Officials, Whittier, CA*.
- Ciftliklioglu, K.** (2018). *Effect of freeze-thaw cycles on the stress-strain behavior of clays treated with fly ash and lime*, (Master's Thesis). Istanbul Technical University, Graduate School of Science Engineering and Technology, Istanbul
- Cokca, E., and Birand, A.** (1993). Determination of cation exchange capacity of clayey soils by the methylene blue test. *Geotechnical Testing Journal*, 16(4), 518-524.
- Cokca, E.** (2002). Relationship between methylene blue value, initial soil suction and swell percent of expansive soils. *Turkish Journal of Engineering and Environmental Sciences*, 26(6), 521-530.
- Dagesse, D. F.** (2015). Cyclic freezing and thawing effects on Atterberg limits of clay soils. *Proceedings of the 68th Canadian Geotechnical Conference and 7th Canadian Permafrost Conference*.
- Dakshanamurthy, V., and Raman, V.** (1973). A simple method of identifying an expansive soil. *Soils and Foundations*, 13(1), 97-104.
- Das, B. M.** (2015). *Principles of foundation engineering*. Cengage learning.
- Dawson, R. F.** (1953). *The Movement of Small Houses Erected on an Expansive Clay Soil*. University of Texas at Austin.
- Day, R. W., and Hager, L.** (1999). *Geotechnical and foundation engineering: design and construction*. New York: McGraw-Hill.
- Dayioglu, M.** (2015). *Improving the engineering properties of expansive belle fourche clay by using chemical additives*. (Master's Thesis). South Dakota School of Mines and Technology, Rapid City.
- Eigenbrod, K. D.** (1996). Effects of cyclic freezing and thawing on volume changes and permeabilities of soft fine-grained soils. *Canadian Geotechnical Journal*, Vol. 33(4), Sf. 529-537.
- El- Sohby, M.A. and El-Sayed A. R.** (1981). Some factors affecting swelling of clayey soils. *Geotechnical Engineering*, Vol. 12, pp. 19-39.
- Firoozi, A. A., Taha, M. R., Firoozi, A. A., and Khan, T. A.** (2015). The influence of freeze–thaw cycles on unconfined compressive strength of clay soils treated with lime. *Jurnal Teknologi*, 76(1).
- Flury, M., and Flühler, H.** (1994). Brilliant Blue FCF as a dye tracer for solute transport studies a toxicological overview. *Journal of Environmental Quality*, 23(5), 1108-1112.
- Ghazavi, M., and Roustaei, M.** (2010). The influence of freeze–thaw cycles on the unconfined compressive strength of fiber-reinforced clay. *Cold regions science and technology*, 61(2-3), 125-131.
- Gouy, M.** (1910). Sur la constitution de la charge électrique à la surface d'un électrolyte. *J. Phys. Theor. Appl.*, 9(1), 457-468.

- Greathouse, J. A., Feller, S. E., and McQuarrie, D. A.** (1994). The modified Gouy-Chapman theory: comparisons between electrical double layer models of clay swelling. *Langmuir*, *10*(7), 2125-2130.
- Grim R. E.** (1962). *Applied clay mineralogy*, McGraw-Hill, New York
- Grim, R. E.** (1942). Modern concepts of clay materials. *The Journal of Geology*, *50*(3), 225-275.
- Grim, R. E.** (1953). *Clay mineralogy*. McGraw-Hill, New York
- Grim, R. E.** (1968). *Clay mineralogy 2<sup>nd</sup> Edition*, McGraw-Hill, New York
- Grim, R. E., Bray, R. H., and Bradley, W. F.** (1937). The mica in argillaceous sediments. *American Mineralogist: Journal of Earth and Planetary Materials*, *22*(7), 813-829.
- Hamberg, D. J.** (1985). A simplified method for predicting heave in expansive soils (MS Thesis). *Fort Collins: Colorado State University*, 275.
- Holts, W. G., and Gibbs, H. J.** (1956). Engineering properties of expansive clays. *Transact, ACSE* 121:641 – 677.
- Holtz, R. D., Kovacs, W. D., & Sheahan, T. C. (2011).** *An introduction to geotechnical engineering*, Pearson Education Inc., Upper Saddle River, NJ.
- Holtz, W.G.** (1970). Suggested method for test for one-dimensional expansion and uplift pressure of clay soils. *Special procedures for testing soil and rock for engineering purposes*, ASTM STP 479.
- Hotineanu, A., Bouasker, M., Aldaood, A. and Al-Mukhtar, M.** (2015). Effect of freeze-thaw cycling on the mechanical properties of lime-stabilized expansive clays. *Cold Regions Science and Technology*, Vol. 119, Sf. 151-157.
- Hughes, R. V.** (1951). The application of modern clay concepts to oilfield development. *Drilling and Production Practice*. American Petroleum Institute.
- Isik, A.** (2014). *Experimental investigation of freeze and thaw on compacted soils* (Master's Thesis). Istanbul Technical University, Graduate School of Science Engineering and Technology, Istanbul.
- Jennings, J. E. B., and Knight, K.** (1957). *The Prediction Of total heave from the double oedometer test*, Proc. Symp. Expansive Clays (South Africa Inst. Of Civil Engineers, Johannesburg), Vol. 7, No. 9, pp. 13-19. 1957.
- Johnson, T. C., Berg, R. L., and Dimillio, A.** (1986). Frost action predictive techniques: an overview of research results. *Transportation Research Record*, *1089*, 147-161.
- Khilar, K. C., and Fogler, H. S.** (1998). *Migrations of fines in porous media* (Vol. 12). Springer Science & Business Media.
- Kia, S. F., Fogler, H. S., and Reed, M. G.** (1987). Effect of pH on colloiddally induced fines migration. *Journal of colloid and interface science*, *118*(1), 158-168.



- Konrad, J. M.** (1989). Physical processes during freeze-thaw cycles in clayey silts. *Cold Regions Science and Technology*, 16(3), 291-303.
- Konrad, J. M., and Samson, M.** (2000). Hydraulic conductivity of kaolinite-silt mixtures subjected to closed-system freezing and thaw consolidation. *Canadian Geotechnical Journal*, 37(4), 857-869.
- Lachenbruch, A. H.** (1963). Contraction theory of ice-wedge polygons: a qualitative discussion. *Nat. Acad. Sci., Natl. Res. Counc. Publ.*, 1287, 63-71.
- Lambe, T. W.** (1960). The character and identification of expansive soils, soil PVC meter. *Federal Housing Administration, Technical Studies Program*, FHA 701.
- Lambe, T. W., and Whitman, R. V.** (1969). *Soil mechanics*. John Wiley & Sons, 553 pp.
- Likos, W. J.** (2004). Measurement of crystalline swelling in expansive clay. *Geotechnical Testing Journal*, 27(6), 540-546.
- Mackay, J. R.** (1973). A frost tube for the determination of freezing in the active layer above permafrost. *Canadian Geotechnical Journal*, 10(3), 392-396.
- Marshall, C. E.** (1965). The Physical Chemistry and Mineralogy of Soils. Volume 1: Soil Materials. *Soil Science*, 99(5), 355.
- McKeen, R. G., and Hamberg, D. J.** (1981). Characterization of expansive soils. *Transportation Research Record*, (790).
- Mitchell, J. K., and Soga, K.** (2005). *Fundamentals of soil behavior (Vol. 3)*. Hoboken, NJ: John Wiley & Sons.
- Moore, D. M., and Reynolds, R. C.** (1989). *X-ray diffraction and the identification and analysis of clay minerals* (Vol. 322, p. 321). Oxford: Oxford university press.
- Mungan, N.** (1965). Permeability reduction through changes in pH and salinity. *Journal of Petroleum Technology*, 17(12), 1-449.
- Mungan, N.** (1989). Discussion of an overview of formation damage. *Journal of petroleum technology*, 41(11).
- Nelson, J. D., Chao, K. C., Overton, D. D., and Nelson, E. J.** (2015). *Foundation engineering for expansive soils*. John Wiley & Sons.
- Nelson, J., and Miller, D. J.** (1992). *Expansive soils: problems and practice in foundation and pavement engineering*, John Wiley & Sons, New York, 1992.
- Omoti, U., and Wild, A.** (1979). Use of fluorescent dyes to mark the pathways of solute movement through soils under leaching conditions: 2. Field experiments. *Soil Science*, 128(2), 98-104.
- Othman, M. A., and Benson, C. H.** (1993). Effect of freeze-thaw on the hydraulic conductivity and morphology of compacted clay. *Canadian Geotechnical Journal*, 30(2), 236-246.
- Oweis, I. and Khera, R.** (1998) *Geotechnology of waste management. 2nd Edition*, PWS Publishing, Boston.

- Ozgan, E., Serin, S., Erturk, S. and Vural, I.** (2015). Effect of freezing and thawing on the consolidation settlement of soils. *Soil Mechanics and Foundation Engineering*, Vol. 52(5).
- Parker, J. C., Amos, D. F., & Kaster, D. L.** (1977). An Evaluation of Several Methods of Estimating Soil Volume Change 1. *Soil Science Society of America Journal*, 41(6), 1059-1064.
- Patrick, D. M., and Snethen, D. R.** (1976). *An occurrence and distribution survey of expansive materials in the United States by physiographic areas* (No. FHWA-RD-76-82 Intrm Rpt.).
- Paudel, B., & Wang, B.** (2010). Freeze-thaw effect on consolidation properties of fine grained soils from the Mackenzie Valley. *63<sup>rd</sup> Canadian Geotechnical Conference*, Alberta, Canada.
- Pauling, L.** (1930). The structure of the chlorites. *Proceedings of the National Academy of Sciences of the United States of America*, 16(9), 578.
- Price, L. W.** (1972). *The periglacial environment, permafrost and man*. Washington, D.C.: Association of American Geographers, Committee on College Geography.
- Ravina, I.** (1973). Swelling of clays, mineralogical composition and microstructure, *Proceedings of the Third International Conference on Expansive Soils, Haifa*.
- Reed, M. G.** (1977). Formation permeability damage by mica alteration and carbonate dissolution. *Journal of Petroleum Technology*, 29(09), 1-56.
- Rhoades, J. D.** (1982). Cation Exchange Capacity 1. *Methods of soil analysis. Part 2. Chemical and microbiological properties*, 149-157.
- Rieder, M., Cavazzini, G., D'yakonov, Y. S., Frank-Kamenetskii, V. A., Gottardi, G., Guggenheim, S., ... Robert, J. L.** (1998). Nomenclature of the micas. *Clays and clay minerals*, 46(5), 586-595.
- Schafer, W. M., & Singer, M. J.** (1976). A New Method of Measuring Shrink-Swell Potential Using Soil Pastes 1. *Soil Science Society of America Journal*, 40(5), 805-806.
- Schatz, T., and Martikainen, J.** (2010). *Laboratory studies on the effect of freezing and thawing exposure on bentonite buffer performance: closed-system tests* (No. POSIVA--10-06). Finland.
- Schulze, D. G.** (2002). An introduction to soil mineralogy. *Soil mineralogy with environmental applications*, 1-35.
- Schulze, D. G.** (2005). Encyclopedia of soils in the environment. *Clay Miner*, 1, 246-254.
- Seed, H. B., Woodward J. R., and Lundgren, R.** (1962). Prediction of swelling potential for compacted clays. *Journal of the soil mechanics and foundations division*, 88(3), 53-88.
- Shamburger, J. H., Patrick, D. M., and Lutton, R. J.** (1975). *Design and construction of compacted shale embankments, Volume 2*, Survey of problem areas and current practices. Final Report, No. FHWA-RD-75, 61.

- Skempton, A. W.** (1953). The colloidal activity of clays. *Selected papers on soil mechanics*, 106-118.
- Smart, P. L., and Laidlaw, I. M. S.** (1977). An evaluation of some fluorescent dyes for water tracing. *Water Resources Research*, 13(1), 15-33.
- Snethen, D. R., Johnson, L. D., and Patrick, D. M.** (1977). *An evaluation of expedient methodology for identification of potentially expansive soils* (No. FHWA-RD-77-94). United States. Federal Highway Administration Office of Research and Development.
- Snethen, D. R., Townsend, F. C., Johnson, L. D., Patrick, D. M., and Vedros, P. J.** (1975). *A Review of Engineering Experiences with Expansive Soils in Highway Subgrades*. Army Engineer Waterways Experiment Station Vicksburg Miss.
- Sposito, G.** (1989). Surface-reactions in natural aqueous colloidal systems. *Chimia*, 43(6), 169-176.
- Sridharan, A., and Jayadeva, M. S.** (1982). Double layer theory and compressibility of clays. *Geotechnique*, 32(2), 133-144.
- Sridharan, A., and Prakash, K.** (2000). Classification procedures for expansive soils. *Proceedings of the Institution of Civil Engineers-Geotechnical Engineering*, 143(4), 235-240.
- Sridharan, A., Rao, S. M., and Murthy, N. S.** (1986). A rapid method to identify clay type in soils by the free-swell technique. *Geotechnical Testing Journal*, 9(4), 198-203.
- Stalder, P. J.** (1973). Influence of crystallographic habit and aggregate structure of authigenic clay minerals on sandstone permeability. *Geologie en Mijnbouw*, 52(4), 217-220.
- Stavridakis, E. I.** (2006). Stabilization of problematic soils using cement and lime. *Expansive Soils: Recent Advances in Characterization and Treatment*, Taylor & Francis Group, 385-397.
- Swan, C. and Greene, C.** (1998). Freeze-thaw effects on Boston blue clay. *Soil improvement for big digs*. Geotechnical Special Publications No. 81, ASCE. 161-176.
- Swan, C. W., Grant, A., and Kody, A.** (2013). Characteristics of Chicago Blue Clay Subjected to a Freeze–Thaw Cycle. In *Mechanical Properties of Frozen Soil*. ASTM International.
- Terzaghi, K.** (1952). *Permafrost*. Boston Society of Civil Engineers, pp. 319-368.
- Terzaghi, K., and Peck, R. B.** (1948). *Soil mechanics in engineering practice, 1*.
- Tovey, N. K.** (1971). Soil structure analysis using optical techniques on scanning electron micrographs, 4<sup>th</sup> *International Symposium on Scanning Electron Microscopy*, IIT Research Institute, Chicago (pp. 49-56).
- Tripathy, S., Sridharan, A., and Schanz, T.** (2004). Swelling pressures of compacted bentonites from diffuse double layer theory. *Canadian Geotechnical Journal*, 41(3), 437-450.

- Trudgill, S. T.** (1987). Soil water dye tracing, with special reference to the use of Rhodamine WT, Lissamine FF and Amino G acid. *Hydrological processes*, 1(2), 149-170.
- Van der Merwe, D. H.** (1964). The prediction of heave from the plasticity index and percentage clay fraction of soils. *Civil Engineering*, 103-107.
- Velasco, E.** (2013). Scanning Electron Microscope (SEM) as a means to determine dispersibility (Master's Thesis). Iowa State University, Ames, Iowa.
- Verwey, E. J. W., Overbeek, J. T. G., and Van Nes, K.** (1948). *Theory of the stability of lyophobic colloids: the interaction of sol particles having an electric double layer*. Elsevier Publishing Company.
- Viklander, P.** (1998). Permeability and volume changes in till due to cyclic freeze-thaw. *Canadian Geotechnical Journal*, Vol. 35(3), 471-477.
- Viklander, P., and Eigenbrod, D.** (2000). Stone movements and permeability changes in till caused by freezing and thawing. *Cold Regions Science and Technology*, 31(2), 151-162.
- Wang, J. L., and Peters, D. B.** (1985). Overview of artificial island design and construction in the Arctic. *Civil Engineering in the Arctic Offshore*, pp. 28-38.
- Weaver, C. E., and Pollard, L. D.** (1973). Developments in sedimentology, 15. *The chemistry of clay minerals*.
- Whittig, L. D., and Allardice, W. R.** (1986). X-ray diffraction techniques. *Methods of soil analysis. Part 1. Physical and mineralogical methods*, 331-362.
- Xie SB, Qu JJ, Lai YM et. al.** (2015). Effects of freeze-thaw cycles on soil mechanical and physical properties in the Qinghai-Tibet Plateau. *Journal of Mountain Science*, Vol. 12(4).
- Yao, H. L., Yang, Y., Cheng, P., and WU, W. P.** (2004). Standard moisture absorption water content of soil and its testing standard. *Rock and Soil Mechanics. Wuhan*, 25, 856-859.
- Yıldız, M., & Soğancı, A. S.** (2012). Effect of freezing and thawing on strength and permeability of lime-stabilized clays. *Scientia Iranica*, 19(4), 1013-1017.
- Yukselen, Y., and Kaya, A.** (2008). Suitability of the methylene blue test for surface area, cation exchange capacity and swell potential determination of clayey soils. *Engineering Geology*, 102(1-2), 38-45.
- Url-1** <<http://www.geology.arkansas.gov>>, data retrieved 10.09.2017.

## **APPENDICES**

### **APPENDIX A: Swelling pressure and normalized $\sigma_s/\sigma_0$ results**



## APPENDIX A

**Table A.1** : Swelling pressure and normalized  $\sigma_s/\sigma_0$  results of CH<sub>3</sub> after F-T cycles.

Freeze-Thaw Cycles	CH <sub>3</sub> (Na bentonite)	$\sigma_s$ (kPa)	Normalized $\sigma_s/\sigma_0$
<b>0</b>	T1	161,10	1,00
	B1	223,47	0,98
	B2	228,66	1,00
<b>1</b>	T1	103,94	0,65
	B1	145,51	0,64
	B2	140,32	0,61
<b>3</b>	T1	88,35	0,55
	B1	129,92	0,57
	B2	135,12	0,59
<b>5</b>	T1	77,95	0,48
	B1	124,72	0,55
	B2	123,94	0,54
<b>7</b>	T1	62,36	0,39
	B1	94,87	0,41
	B2	103,94	0,45
<b>10</b>	T1	62,36	0,39
	B1	93,54	0,41
	B2	93,54	0,41
<b>15</b>	T1	62,36	0,39
	B1	93,54	0,41
	B2	90,14	0,40
<b>20</b>	T1	59,45	0,37
	B1	93,54	0,41
	B2	93,54	0,41
<b>25</b>	T1	59,45	0,32
	B1	93,54	0,41
	B2	93,54	0,41

**Table A.2** : Swelling pressure and normalized  $\sigma_s/\sigma_0$  results of CH<sub>4</sub> after F-T cycles.

Freeze-Thaw Cycles	CH <sub>4</sub> (Ca bentonite)	$\sigma_s$ (kPa)	Normalized $\sigma_s/\sigma_0$
0	T1	103,94	1,00
	B1	129,92	1,00
	B2	129,92	1,00
1	T1	62,36	0,60
	B1	98,74	0,76
	B2	103,94	0,80
3	T1	57,62	0,44
	B1	83,15	0,64
	B2	86,24	0,56
5	T1	62,36	0,60
	B1	77,95	0,60
	B2	83,15	0,64
7	T1	57,17	0,55
	B1	72,76	0,56
	B2	77,95	0,60
10	T1	51,97	0,50
	B1	77,95	0,60
	B2	67,56	0,52
15	T1	51,97	0,50
	B1	77,95	0,60
	B2	77,95	0,60
20	T1	57,68	0,60
	B1	72,76	0,56
	B2	77,95	0,60
25	T1	51,97	0,50
	B1	77,95	0,60
	B2	77,95	0,60

**Table A.3** : Swelling pressure and normalized  $\sigma_s/\sigma_0$  results of CH<sub>5</sub> after F-T cycles.

Freeze-Thaw Cycles	CH <sub>5</sub>	$\sigma_s$ (kPa)	Normalized $\sigma_s/\sigma_0$
<b>0</b>	T1	46,77	1,00
	B1	93,54	1,00
<b>1</b>	T1	25,98	0,56
	B1	51,97	0,56
<b>3</b>	T1	22,87	0,49
	B1	50,17	0,54
<b>5</b>	T1	23,98	0,51
	B1	46,77	0,50
<b>7</b>	T1	25,98	0,56
	B1	46,77	0,50
<b>10</b>	T1	17,67	0,38
	B1	46,77	0,50
<b>15</b>	T1	15,59	0,33
	B1	51,97	0,56
<b>20</b>	T1	15,59	0,33
	B1	51,56	0,72
<b>25</b>	T1	15,59	0,33
	B1	51,97	0,56



**Table A.4** : Swelling pressure and normalized  $\sigma_s/\sigma_0$  results of CH<sub>6</sub> after F-T cycles.

Freeze-Thaw Cycles	CH <sub>6</sub>	$\sigma_s$ (kPa)	Normalized $\sigma_s/\sigma_0$
<b>0</b>	T1	5,20	1,00
	B1	62,36	1,09
	B2	58	0,92
<b>1</b>	T1	5,20	1,00
	B1	57,17	0,92
	B2	57,17	0,92
<b>3</b>	T1	4,16	0,80
	B1	25,98	0,42
	B2	25,98	0,42
<b>5</b>	T1	3,12	0,60
	B1	24,87	0,40
	B2	25,98	0,42
<b>7</b>	T1	2,08	0,40
	B1	20,79	0,33
	B2	20,79	0,33
<b>10</b>	T1	2,08	0,40
	B1	18,24	0,29
	B2	20,79	0,33
<b>15</b>	T1	5,20	1,00
	B1	20,79	0,33
	B2	20,79	0,33
<b>20</b>	T1	5,20	1,00
	B1	23,94	0,38
	B2	20,79	0,33
<b>25</b>	T1	5,20	1,00
	B1	20,79	0,33
	B2	20,79	0,33

**Table A.5** : Swelling pressure and normalized  $\sigma_s/\sigma_0$  results of CL<sub>1</sub> after F-T cycles.

<b>Freeze-Thaw Cycles</b>	<b>CL<sub>1</sub></b>	<b><math>\sigma_s</math> (kPa)</b>	<b>Normalized <math>\sigma_s/\sigma_0</math></b>
<b>0</b>	T1	20,79	1,00
	B1	57,17	1,00
	B2	55,00	0,96
<b>1</b>	T1	10,39	0,50
	B1	41,58	0,73
	B2	39,00	0,68
<b>3</b>	T1	2,08	0,10
	B1	37,55	0,66
	B2	28,98	0,51
<b>5</b>	T1	3,12	0,15
	B1	36,38	0,64
	B2	31,18	0,55
<b>7</b>	T1	2,08	0,10
	B1	36,38	0,64
	B2	31,18	0,55
<b>10</b>	T1	3,12	0,15
	B1	30,46	0,53
	B2	27,79	0,49
<b>15</b>	T1	4,16	0,20
	B1	32,16	0,56
	B2	31,18	0,55
<b>20</b>	T1	2,08	0,10
	B1	31,20	0,55
	B2	31,20	0,55
<b>25</b>	T1	4,16	0,20
	B1	25,98	0,45
	B2	26,80	0,47

## CURRICULUM VITAE



**Name Surname** : Efe ASLAN  
**Place and Date of Birth** : 23/07/1993  
**E-Mail** : efe468@gmail.com

### EDUCATION :

- **B.Sc.** : 2016, Istanbul Technical University, Civil Engineering Faculty, Civil Engineering Department

### PROFESSIONAL EXPERIENCE AND REWARDS:

- 2018- Research Assistant at the Istanbul Technical University, Civil Engineering Faculty, Soil Mechanics and Geotechnical Engineering Department.

### PUBLICATIONS, PRESENTATIONS AND PATENTS ON THE THESIS:

- **Aslan E., Dayioglu A., Senol A.** 2018. Determination Of Changes In Swelling Pressure Characteristics Of Clays Exposed To Freeze-Thaw Cycles, 17<sup>th</sup> National Soil Mechanics And Geotechnical Engineering Conference, September 26-28 2018, Istanbul, Turkey.

### OTHER PUBLICATIONS, PRESENTATIONS AND PATENTS:

- **Ciftliklioglu K., Aslan E., Senol A.** 2019. Effect Of Freeze-Thaw Cycles On The Strength Behavior Of Bentonite By Use Lime, International Civil Engineering And Architecture Conference, April 17-20 2019, Trabzon, Turkey.